Trace elements and Sr-Nd-Pb isotopes of K-rich, shoshonitic, and calc-alkaline magmatism of the Western Mediterranean Region:

Lithos 107 (2009) 68–92

Contents lists available at ScienceDirect

Lithos

journal homepage: www.elsevier.com/locate/lithos

Trace elements and Sr–Nd–Pb isotopes of K-rich, shoshonitic, and calc-alkaline magmatism of the Western Mediterranean Region: Genesis of ultrapotassic to calc-alkaline magmatic associations in a post-collisional geodynamic setting

Sandro Conticelli [a,b,*], Luisa Guarnieri [a], Alice Farinelli [a], Massimo Mattei [c], Riccardo Avanzinelli [a,1], Gianluca Bianchini [d], Elena Boari [a], Simone Tommasini [a], Massimo Tiepolo [e], Dejan Prelević [f], Giampiero Venturelli [g]

[a] Dipartimento di Scienze della Terra, Università degli Studi di Firenze, Via Giorgio La Pira, 4, I-50121, Firenze, Italy
[b] Istituto di Geoscienze e Georisorse, U.O. Firenze, C.N.R., Via Giorgio La Pira, 4, I-50121, Firenze, Italy
[c] Dipartimento di Scienze Geologiche, Università degli Studi di Roma Tre, Largo S. Gesualdo Murialdo, 1, 00146, Roma, Italy
[d] Dipartimento di Scienze della Terra, Università degli Studi di Ferrara, Campo Universitario, Via Giuseppe Saragat, 1, Ferrara, Italy
[e] C.N.R. — Istituto di Geoscienze e Georisorse — U.O. di Pavia, via Ferrata 1, Pavia, Italy
[f] Geowißenshaften Institut, Johannes Gütemberg Universität, Becherweg, 7, Mainz, Germany
[g] Dipartimento di Scienze della Terra, Università degli Studi di Parma, Campus Universitario, Parma, Italy

ARTICLE INFO

Article history:
Received 15 October 2007
Accepted 25 July 2008
Available online 8 August 2008

Keywords:
Sr–Nd–Pb isotopes
Trace elements
Lamproite
Shoshonite
Calc-alkaline rocks
Western Alps
Corsica
Murcia-Almeria
Tuscany
Western Mediterranean Basin
Geodynamics

ABSTRACT

High-MgO ultrapotassic rocks are found in four different areas of the Western Mediterranean basin associated in space and time with shoshonitic and calc-alkaline rocks. They represent different magmatic events at the active continental plate margin from Oligocene to Pleistocene. These rocks are found within the Western Alps (Northern Italy), in Corsica (France), in Murcia-Almeria (South-Eastern Spain), and in Southern Tuscany (Central Italy). Ultrapotassic terms are mostly lamprophyres, but olivine latitic lavas with a clear lamproitic affinity are also found. Lamproite-like rocks range from slightly silica under-saturated to silica over-saturated, and they are characterised by low Al_2O_3, CaO, and Na_2O contents. They are plagioclase-free rocks, but K-feldspar is abundant beside other K-bearing phases. Shoshonitic and calc-alkaline rocks are invariably space associated to lamproites, and they either precede or follow them. High-Mg ultrapotassic rocks are characterised by strong enrichment of incompatible elements, which prevent further enrichment due to shallow level crustal contamination. K_2O and incompatible element contents decrease passing from high-Mg ultrapotassic to high-Mg shoshonitic and calc-alkaline rocks suggesting that K and incompatible trace elements enrichments are a primary characteristic. Ultrapotassic to calc-alkaline rocks from Western Mediterranean regions, in spite of their different age of emplacement, are characterised by similar incompatible trace elements distribution. Depletion of High Field Strength elements with respect to Large Ion Lithophile elements is observed. Positive spikes at Th, U, and Pb, with negative spikes at Ba, Nb, Ta, Sr, P, and Ti, are common characteristics of ultrapotassic (lamproitic) to high-K calc-alkaline rocks. Ultrapotassic rocks are extremely enriched in radiogenic Sr and unradiogenic Nd with respect to the associated shoshonitic and calc-alkaline rocks. Different isotopic values are distinctive of the different magmatic provinces irrespective of magmatic affinities. $^{87}Sr/^{86}Sr_i$ ranges between 0.71645 and 0.71759 for Western Alps lamproites, between 0.71226 and 0.71230 for Corsica lamproite, between 0.71642 and 0.72259 for Murcia-Almeria lamproites, and between 0.71578 and 0.71672 for Tuscany lamproites. Radiogenic Sr decreases along with K_2O through shoshonitic to calc-alkaline rocks. Conversely $^{143}Nd/^{144}Nd_i$ values increase with decreasing K_2O, with the highest value of 0.51243 found for the one samples from Murcia-Almeria. Contrasting trends are observed among initial values of lead isotopes, but all falling well within the field of upper crustal rocks. Different trends of $^{207}Pb/^{204}Pb_i$ and $^{208}Pb/^{204}Pb_i$ vs. $^{206}Pb/^{204}Pb_i$ for samples from the different provinces are observed. Several evidences indicate that most of the magmas of the different provinces have been generated in a depleted upper mantle (i.e., lithospheric) modified by metasomatism, but an asthenospheric component is also recognised in Corsica. At least two different subduction-related metasomatic agents re-fertilised the depleted original upper mantle source. Carbonate-free siliciclastic sediments and carbonate-rich sediments have been recycled within the upper mantle through subduction and partial melting. Assuming that metasomatic component is concentrated in a vein network, in Tuscany and Corsica, time relationships

* Corresponding author. Dipartimento di Scienze della Terra, Università degli Studi di Firenze, Via Giorgio La Pira, 4, I-50121, Firenze, Italy.
E-mail address: sandro.conticelli@unifi.it (S. Conticelli).
[1] Now at: Department of Earth Sciences, University of Bristol, Bristol, UK.

0024-4937/$ – see front matter
doi:10.1016/j.lithos.2008.07.016

indicate that low degree of partial melting of the pure vein produced lamproitic-like magmas, whereas an increase in the partial melting involve the surrounding upper mantle, then diluting the alkaline component and produced the entire spectra of magma observed. In South-Eastern Spain calc-alkaline magmatism preceded lamproitic ones, and might be generated by partial melting of mantle wedge metasomatised by fluids from oceanic slab prior to collision. Lamproitic magmas followed after melt-dominated metasomatic agents invaded the lithospheric upper mantle domain. Migration of the magmatism with time is the result of eastward migration of subduction with subsequent opening of Balearic, Ligure-Provençal, and Tyrrhenian basins.

1. Introduction

K_2O enrichment is one of the most striking features of the mostly Mio–Pliocene to present time subduction-related volcanic rocks in the Western Mediterranean (Savelli, 2002, and references therein), with few Oligocene volcanic rocks in the Western Alps (Venturelli et al., 1984a). The increase in K in orogenic magmatic associations is a common characteristic of Mediterranean volcanic rocks. Indeed it is also found in the Aeolian Arc (Francalanci et al., 2007, Tommasini et al., 2007 and references therein), in the Balkan Peninsula (e.g., Altherr et al., 2004; Cvetković et al., 2004a; Prelević et al., 2008, and references therein), in Anatolia (e.g., Francalanci et al., 2000; Agostini et al., 2005; Innocenti et al., 2005) and at a minor extent in the South Aegean Volcanic Arc (e.g., Francalanci et al., 2005). Ultrapotassic rocks in the Mediterranean area are silica saturated, lamproites, and silica under-saturated, kamafugites/leucitites. Sometimes leucite-bearing lamproites are also found (Venturelli et al., 1991a).

It is generally accepted that alkaline K-rich magmas in the Mediterranean have been produced by partial melting of a depleted peridotite modified by metasomatism (e.g., Thompson, 1977; Dal Piaz et al., 1979; Venturelli et al., 1984a; Peccerillo et al., 1988; Foley and Venturelli, 1989; Conticelli and Peccerillo, 1992; Conticelli, 1998; Peccerillo, 1999; Prelević and Foley, 2007; Prelević et al., 2008). K-rich metasomatising agents permeating and reacting with depleted peridotitic mantle may cause local refertilisation, thus producing veins of clinopyroxene/amphibole/phlogopite minerals at the expense of olivine and orthopyroxene (e.g., Sekine and Wyllie, 1982; Foley, 1990, 1992; Conceição and Green, 2004). Partial melting of the diverse vein mineralogy produces high-Mg K-rich magmas with different degrees of silica saturation/under saturation. Magmatic rocks of mantle origin generated during continental collision are common in the Western Mediterranean Basin (Fig. 1). Among ultrapotassic rocks Barton (1979) and Foley et al. (1987) recognised at least three different groups of rocks characterised by different contents of CaO, Na_2O, and Al_2O_3, which are reflected in a different mineralogy. In the Western Mediterranean all the different types of ultrapotassic rocks crop out. Kamafugitic and leucititic ultrapotassic rocks, however, are confined in the Roman Magmatic Province and in very recent times, from the Pleistocene to Holocene (Conticelli et al., 2004, and references therein), and their possible genesis and relationships with calc-alkaline rocks are extensively discussed by Avanzinelli et al. (2008).

Ultrapotassic rocks from Western Mediterranean are generally interpreted as subduction-related: Alpine subduction, "south-south-eastward". Dipping beneath Africa–Adriatic plates (e.g., Doglioni et al., 1999; Peccerillo and Martinotti, 2006) and Apennine subduction, north-north-westward dipping beneath the Eurasian plate (Peccerillo and Turco, 2004). Alternatively, a plume-related genesis is suggested to account for the isotopic characteristics of the overall magmatic rocks found in the Central Mediterranean region (Gasperini et al., 2002; Bell et al., 2004). In detail in Central-Southern Italy the spatial isotopic variations have been variously interpreted (e.g., Hawkesworth and Vollmer, 1979; Conticelli et al., 2002; Bell et al., 2004; Martelli et al., 2004; Avanzinelli et al., 2008) causing scientific debate about some major issues: 1) the genesis of the high-Mg variably K-enriched silica-saturated magmas; 2) the processes involved in diluting the alkaline component passing from high-Mg ultrapotassic to high-K calc-alkaline and calc-alkaline s.s. associated magmas; 3) the geodynamics of the Western Mediterranean that may account for the mechanism for mantle metasomatism and magma generation.

To shed some light on these issues we focus attention on four magmatic provinces of the Western Mediterranean area. In this region ultrapotassic rocks with lamproitic affinity are associated, spatially and temporally, to shoshonitic, high-K calc-alkaline and calc-alkaline rocks. Samples from Western Alps (Northwestern Italy), Corsica (France), Murcia-Almeria (South-Eastern Spain), and Tuscany (Central Italy) (Fig. 1) have been collected. New high precision trace elements and Sr, Nd, and Pb isotopic data have been performed to compare a homogeneous data set to avoid possible laboratory bias. The geochemical and isotopic data are supplemented with petrology and discussed in the frame of the structural geological, seismic tomography and palaeomagnetic data pertinent to constraint the geodynamics of the Region.

2. Geodynamic framework of the Western Mediterranean

The geologic setting of the Mediterranean region is the result of a complex geodynamic history due to the different velocities of movement of Africa and Eurasia plates. This brought to the convergence of the two plates with formation in the Western Mediterranean of arcuate mountain belts and extensional back-arc basins (Horvath and Berckheimer, 1982; Dewey et al., 1989). Since 35 Ma, convergence has been achieved by continuous subduction processes (Doglioni et al., 1999; Rosembaum et al., 2002; Faccenna et al., 2004), whose slabs are well imaged by seismic tomography and deep seismicity (Wortel and Spakman, 2000).

Geodynamic models indicate that about 30–35 Ma ago, the subduction plane was located along the Iberian margin, between the Apennines and Gibraltar. Since that time, the tectonic evolution of the area has been characterised by the differential backward motion of the subduction trench. This backward motion induced the formation of the Liguro-Provençal (30–16 Ma) and Tyrrhenian (12–1 Ma) back-arc basins on the top of the Ionian slab, and of the Alboran basin (Lower Miocene) on the rear of the Gibraltar arc. The back-arcs opening has been coeval with the progressive bending of the Gibraltar and Calabrian arcs and with the formation of the northern Apenninic arc, on the front of the northern Tyrrhenian Sea basin. The bending processes of such arcs has been proved in detail by a large amount of paleomagnetic data, which show systematic, opposite, vertical axis rotations along the two arms of the arcs (e.g., Lonergan and White, 1997; Platt et al., 2003; Mattei et al., 2004, 2006, 2007; Cifelli et al., 2007, 2008).

The Gibraltar Arc represents the westernmost segment of the Alpine–Mediterranean Belt. The arc is formed by the Rif (North Africa) and the Betic Cordillera (Southern Spain) fold-and-thrust belt, with his associated foredeep and foreland basins along its outer margin (Guadalquivir Basin and Gharb basin in Spain and Morocco respectively). Extensional tectonics started during early Miocene times forming sedimentary basins in the internal part of the Betics and Rif, and in the Alboran Sea (Watts et al., 1993; Comas et al., 1999). During

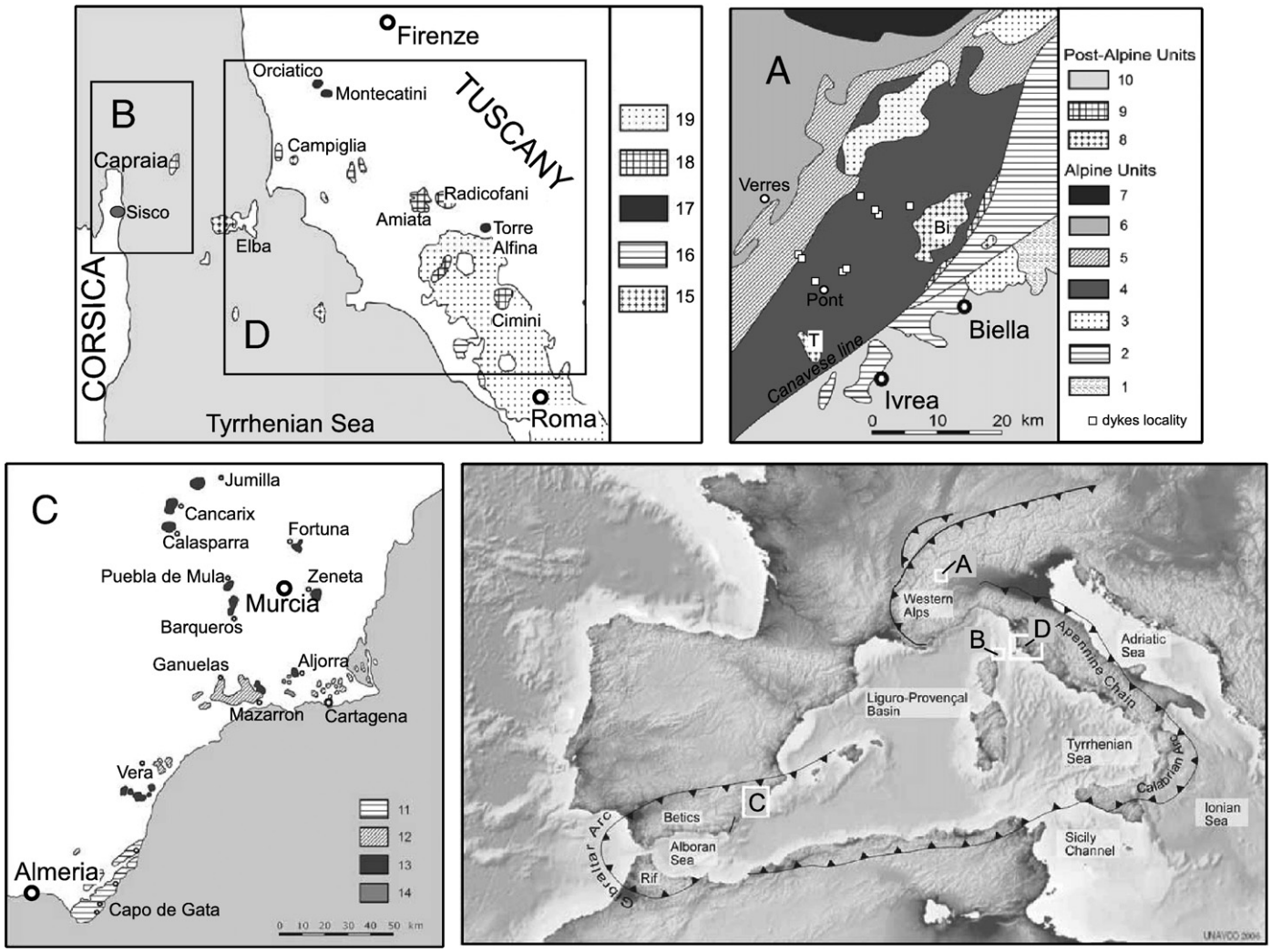

Fig. 1. Sketch map of the Western Mediterranean region with reported major tectonic features and areas of occurrence of ultrapotassic to calc-alkaline orogenic rocks. A) Western Alps, Oligocene magmatism: 1) low grade Permian granite and granodiorite; 2) Ivrea zone mafic complex; 3) Ivrea zone kinzigitic rocks; 4) internal Sesia-Lanzo zone (eclogitic micashists); 5) external Sesia-Lanzo zone (gneiss complex); 6) Schistes Lustres and ophiolitic complex; 7) Monte Rosa and Gran Paradiso nappe (orthogneiss); 8) Oligocene Plutonic rocks, Traversella (T) and Biella plutons (Bi); 9) Oligocene volcanoclastic cover series; 10) Pleistocene–Holocene covers; note that small open squares indicates samples localities. B) Corsica, Miocene–Pliocene. C) Murcia-Almeria, Miocene–Pliocene Magmatism: 11) calc-alkaline to high-K calc-alkaline volcanic rocks; 12) high-K to shoshonitic volcanic rocks; 13) ultrapotassic lamproitic volcanic rocks; 14) Na-alkali basalts. D) Tuscany, Pliocene–Pleistocene: 15) Pliocene intrusive granites and granodiorites of Tuscan Anatectic Province; 16) Pliocene rhyolites and rhyodacites of the Tuscan Anatectic Province; 17) lamproitic volcanic rocks; 18) shoshonites to high-K calc-alkaline volcanic rocks; 19) Leucite-bearing ultrapotassic to shoshonitic rocks of the Roman Magmatic Province (Pleistocene). Redrawn after Dal Piaz et al. (1979), Venturelli et al. (1984a), Peccerillo et al. (1987), Benito et al. (1999), Callegari et al. (2004), Chelazzi et al. (2006), and Owen (2008).

the Late Miocene, the Gibraltar region experienced a drastic modification of the tectonic regime, probably related with the reduced efficiency of the roll-back processes in the Gibraltar Arc subduction system (Faccenna et al., 2004; Duggen et al., 2004). As a consequence, the whole Betics–Rif and the Alboran Sea Basin underwent a complex pattern of compressional and strike-slip tectonics which, in some cases, inverted previous extensional structures (Watts et al., 1993; Comas et al., 1999). Volcanism accompanied and postdated Neogene extension, with arc-tholeiitic, calc-alkaline, shoshonitic and ultrapotassic volcanism scattered across the eastern sector of Alboran Sea and Betic–Rif chain.

The Africa–Eurasia convergence and the consequent subduction of the Adriatic–Ionian lithosphere resulted in the formation of the Apennine chain, and in the coeval opening of the Liguro-Provençal and Tyrrhenian back-arc basins. Subduction slabs are present beneath the Calabrian arc where deep seismicity is detected along a narrow (roughly 200 km) and steep (70°) Benioff plane, dipping to northwest down to about 500 km (e.g., Anderson and Jackson, 1987; Giardini and Velonà, 1991; Selvaggi and Chiarabba, 1995), and possibly in the Northern Apennines, where subcrustal earthquakes occur down to 90 km (Selvaggi and Amato, 1992).

The tectonic history of the Apennines was mainly controlled by slab retreat, shown by the migration of the orogenic front and by the onset of siliciclastic deposits, which get progressively younger toward the Adriatic–Ionian foreland (Royden et al., 1987). The onset of siliciclastic deposition occurred in Northern Apennines in the oceanic Ligurian domain, which was deformed during late Cretaceous to early Eocene, and formed a double vergent accretionary wedge, now outcropping from Corsica to Italian peninsula (Treves, 1984; Carmignani et al., 1994). Since Oligocene, foredeep basin migrated eastward and formed on the top of continental sequences of the Apulia margin. Their incorporation into the Apenninic orogenic wedge marked the subduction of Adriatic continental lithosphere underneath Europe. During the Neogene, the foredeep basin further migrated toward the Apulia foreland in front of the Apennines thrust front, to reach the site of the Quaternary deposition in the Adriatic foreland, where the foredeep deposition is no more active (Patacca et al., 1992; Cipollari and Cosentino, 1995).

Table 1
List of samples studied, provenance, ages, and petrography

Region	Age Ma	Locality	Affinity	Sample	Body	Rock type	Petrography
Western Alps	33–29	*Lower Gressonney Valley — Rio Rechantez, 2.5 km NE Verres*	LMP	MEC 242	Dyke	*Minette*	**Phl**(Ol)+**Cpx**+**Kfs**+Ol+Ap+Kfs+*Ser*+*Cal*
Western Alps	33–29	*Lower Gressonney Valley — Rio Rechantez, 2.5 km NE Verres*	LMP	VdA 17	Dyke	*Minette*	**Phl**(Ol)+**Cpx**+**Kfs**+Ol+Ap+Kfs+*Ser*+*Cal*
Western Alps	33–29	*Lower Gressonney Valley — Rio Rechantez, 2.5 km NE Verres*	LMP	VdA 15	Dyke	*Minette*	**Phl**(Ol)+**Cpx**+**Kfs**+Ol+Ap+Kfs+*Ser*+*Cal*
Western Alps	33–29	*Aosta Valley — Plan d'Albard*	LMP	VDA 03	Dyke	*Minette*	**Phl**(Ol)+**Cpx**+**Kfs**+Ol+Ap+Kfs+*Ser*+*Cal*
Western Alps	33–29	*Aosta Valley — Plan d'Albard*	LMP	MEC 247	Dyke	*Minette*	**Phl**+**Cpx**+Krh+Kfs+Ap+Opaques+*Cal*
Western Alps	33–29	*Gressonney Valley — Cora Road*	SHO	VDA 14	Dyke	*Shoshonite*	
Western Alps	33–29	*Cervo Valley — between Piedicavallo and Issime, near Vecchia Lake*	SHO	MEC 241	Dyke	*Latite*	**Phl**+**Pl**+Kfs+Qtz+Opaques
Western Alps	33–29	*Stolen Valley (Issime, Gressoney Valley) — below Alpe Muntuschuz*	SHO	MEC 216	Dyke	*Latite*	**Bt**+**Pl**+**Hbl**+Kfs+Ap+Qtz+Opaques+*Chl*+*Spn*+*Ep*+*Ab*+*Ser*
Western Alps	33–29	*Gressonney Valley — Niel*	HKCA	VDA 08	Dyke	*Bas andesite*	
Western Alps	33–29	*Oropa Valley (Biella) — Favaro, "Sesia Lanzo" Nappe*	HKCA	KAW 697a	Lava	*Bas andesite*	**Pl**+**Cpx**+**Hbl**+Bt+Ap+Opaque+*Cal*
Western Alps	33–29	*Gressonney Valley — Issime Dam*	HKCA	VDA 10	Dyke	*Bas andesite*	**Pl**+**Cpx**+**Hbl**+Bt+Ap+Opaque+*Cal*
Western Alps	33–29	*Aosta valley — 1.3 km from Pont Saint Martin, "Niou" ore deposit*	HKCA	MEC 251	Dyke	*Andesite*	**Pl**+**Hbl**+Kfs+Ap+Opaque+*Ep*+*Chl*+*Cal*
Western Alps	33–29	*Ayas Valley — Upper Chasten Valley, Alpe Pera Piccola*	HKCA	MEC 240	Dyke	*Dacite*	Pl+Bt+Qtz+Opaques+*Cal*+*Ser*+*Chl*
Corsica	14.5	*Corsica Island — Sisco*	LMP	SIS 07	Dyke	*Lamproite*	**Ol**(Chr)+**Phl**+Cpx+Kfs+Krh+Ap+Chr
Corsica	14.5	*Corsica Island — Sisco*	LMP	SIS 04	Dyke	*Lamproite*	**Ol**(Chr)+**Phl**+Cpx+Kfs+Krh+Ap+Chr
Corsica	7.15	*Capraia Island, Ferraione Cape*	HKCA	CP 101	Lava	*Bas andesite*	**Pl**+**Ol**+Cpx+Kfs+Opx+Mag+Glass
Corsica	7.55	*Capraia Island, Peraiola lookout*	HKCA	CP 110	Lava	*Andesite*	**Plg**+**Cpx**+Mag+Chr+Glass
Corsica	4.63	*Capraia Island, Zenobito Cape*	SHO	CP 54	Scoria	*Basalt*	**Ol**(Chr)+Cpx+Pl+Mag+Chr+Glass
Corsica	4.63	*Capraia Island, Zenobito Plane*	SHO	CP 105	Lava	*Basalt*	**Ol**(Chr)+Cpx+Pl+Mag+Chr+Glass
Murcia-Almeria	9.18	*Capo de Gata, Calas Barronal*	CA	Alm 13	Lava	*Andesite*	**Pl**+**Cpx**+**Ol**+**Opx**+Mag+Glass
Murcia-Almeria	9.18	*Capo de Gata, Calas Barronal*	HKCA	Alm 14	Lava	*hK andesite*	**Pl**+**Cpx**+**Ol**+**Opx**+Mag+Glass
Murcia-Almeria	9.18	*Capo de Gata, Cerro Barronal*	HKCA	Alm 17	Lava	*hK andesite*	**Pl**+**Cpx**+**Opx**+**Ol**+Mag+Glass
Murcia-Almeria	9.18	*Capo de Gata, Cortiijo Sotijlio*	SHO	Alm 21	Lava	*Ol-latite*	**Pl**+**Cpx**+**Opx**+**Ol**+Mag+Glass
Murcia-Almeria	9.18	*Capo de Gata, Las Negras, Cerro Negro*	CA	Alm 25	Lava	*Andesite*	**Cpx**+**Pl**+**Ol**+**Opx**+Mag+Glass
Murcia-Almeria	9.18	*Capo de Gata, Mesa Roldan*	SHO	Alm 27	Dome	*Ol-latite*	**Pl**+**Cpx**+**Opx**+**Ol**+Mag+Glass
Murcia-Almeria	9.18	*Capo de Gata, Cerro Gallinaza*	SHO	Alm 28	Dome	*Trachydacite*	**Bt**+**Qtz**+**Hbl**+**Opx**+**Cpx**+Pl+Opaque+Glass
Murcia-Almeria	9.18	*Capo de gata, Isleta del Moro*	CA	Alm 29	Lavas	*Andesite*	**Pl**+**Cpx**+**Opx**+Mag+Glass
Murcia-Almeria	9.18	*Capo de Gata, El Pozo del Capitan*	CA	Alm 32	Lavas	*Andesite*	**Pl**+**Cpx**+**Opx**+Mag+Glass
Murcia-Almeria	9.18	*Capo de Gata, Fernan Perez*	HKCA	Alm 34	Lavas	*hK dacite*	**Pl**+**Hbl**+**Bio**+Qtz+Cpx+Opaque+Glass
Murcia-Almeria	9.18	*Capo de Gata, Cerro Vela Blanca*	SHO	Alm 39	Lavas	*Trachyte*	**Pl**+**Cpx**+**Opx**+Mag+Glass
Murcia-Almeria	9.18	*Capo de Gata, Monsul P. Peneita*	HKCA	Aml 31	Dyke	*hK dacite*	**Pl**+**Hbl**+**Opx**+Cpx+Mag+Glass
Murcia-Almeria	8.08	*Zeneta, Murcia, Cabezo Negro*	LMP	SP 035	Dyke	*Fortunite*	**Ol**+**Phl**±**Ap**±**Cpx**+Kfs+Ap+Opaques± Phl±Bt±*Qtz*+*Cal*
Murcia-Almeria	8.08	*Zeneta, Murcia, Cabezo Negro*	LMP	SP 040	Lava	*Fortunite*	**Ol**+**Phl**±**Ap**±**Cpx**+Kfs+Ap+Opaques± Phl±Bt±*Qtz*+*Cal*
Murcia-Almeria	7.13	*Fortuna, Murcia, Cabezitos Negros*	LMP	SP 044	Lava	*Fortunite*	**Ol**+**Phl**+**Cpx**+**Ap**+*Kfs*+Opx+Opaques+ Pri+Glass
Murcia-Almeria	7.13	*Fortuna, Murcia, Cabezitos Negros*	LMP	SP 049	Lava	*Fortunite*	**Ol**+**Phl**+**Cpx**+**Ap**+Kfs+Opx+Opaques+ Pri+Glass
Murcia-Almeria	7.13	*Fortuna, Murcia, Cabezitos Negros*	LMP	SP 050	Lava	*Fortunite*	**Ol**+**Phl**+**Cpx**+**Ap**+Kfs+Opx+Opaques+ Pri+Glass
Murcia-Almeria	7.06	*Calasparra, Murcia, Cerro Negro quarry*	LMP	SP 077	Lava	*Fortunite*	**Ol**+**Phl**+**Cpx**+**Ap**+Kfs+Krh+Opaques
Murcia-Almeria	7.06	*Calasparra, Murcia, Cerro Negro quarry*	LMP	SP 078	Lava	*Fortunite*	**Ol**+**Phl**+**Cpx**+**Ap**+Kfs+Krh+Opaques
Murcia-Almeria	7.06	*Cancarix, Murcia, Sierra de las Cabras*	LMP	SP 723	Lava	*Cancalite*	**Ol**+**Phl**+Kfs+Krh+Opaques+Ap
Murcia-Almeria	7.06	*Cancarix, Murcia, Sierra de las Cabras*	LMP	SP 725	Lava	*Cancalite*	**Ol**+**Phl**+Opx+Kfs+Krh+Cpx+Opaques+Ap
Murcia-Almeria	6.76	*Jumilla, Murcia, Jumilla road to Hellin, km 14*	LMP	SP 055	Lava	*Jumillite*	**Ol**+**Phl**+Kfs+Opx+Cpx+Ap+Opaques+ Glass
Murcia-Almeria	6.76	*Jumilla, Murcia, Jumilla road to Hellin, km 14*	LMP	SP 452	Lava	*Jumillite*	**Ol**+**Cpx**+**Phl**+Kfs+Krh+Ap+Opaques+Cal
Murcia-Almeria	6.37	*Vera, Quarry*	LMP	Alm 01	Lopolith	*Verite*	Ol(Chr)+Phl+Glass
Murcia-Almeria	6.37	*Vera, Quarry*	LMP	Alm 02	Lopolith	*Verite*	**Ol**(Chr)+**Phl**+Glass
Murcia-Almeria	6.37	*Vera, Bridge on the river*	LMP	SP 011	Laccolith	*Verite*	**Ol**+**Phl**+Glass
Tuscany	4.1	*Orciatico, Soccer Field*	LMP	ORC 01	Laccolith	*Lamproite*	**Ol**(Chr)+Phl+Cpx+Sa+Ap+Ilm+Chr+Krh
Tuscany	4.1	*Orciatico, Uccelliera*	LMP	OR 12	Dyke	*Lamproite*	**Ol**(Chr)+Phl+Cpx+Sa+Ap+Ilm+Chr+Krh
Tuscany	4.1	*Montecatini, Quarry beneath the village*	LMP	MVC100	Plug	*Minette*	**Phl**+**Cpx**+Sa+Ap+Ol+Ilm+Mag
Tuscany	1.35	*Radicofani, Ghino di Tacco Castle, scoria cone*	SHO	VS 184	Scoria	*Shoshonite*	**Ol**(Chr)+**Cpx**+Sa+Mag+Glass
Tuscany	1.35	*Radicofani, Cassia Road, lava flow north tongue*	SHO	VS 106	Lava	*Shoshonite*	**Ol**(Chr)+**Cpx**+Sa+Mag+Glass
Tuscany	1.35	*Radicofani, Upper portion of the Neck*	SHO	VS 150	Neck	*Shoshonite*	**Ol**(Chr)+**Cpx**+Pl+Mag+Glass
Tuscany	1.35	*Radicofani, Cemetery, middle portion of the neck*	SHO	VS 151	Neck	*Bas andesite*	**Ol**(Chr)+**Cpx**+Pl+Mag+Glass
Tuscany	1.35	*Radicofani, Cemetery, middle portion of the neck*	SHO	VS 123	Neck	*Bas andesite*	**Ol**(Chr)+**Cpx**+Pl+Mag+Glass
Tuscany	1.35	*Radicofani, Village, bottom of the neck*	HKCA	VS 122	Neck	*Bas andesite*	**Ol**(Chr)+**Plg**+**Cpx**+Mag+Glass
Tuscany	1.19	*Cimini Mounts, Viterbo town*	SHO	VS 193	Pumice	*Latite*	**Cpx**+**Sa**+Bt+Mag+Plg+Glass
Tuscany	1.01	*Cimini Mounts, intersection road to Faggeta peak*	SHO	VS 200	Lava	*Latite*	**Cpx**+**Ol**(Chr)+**Sa**+Mag+Bt+Glass
Tuscany	0.94	*Cimini Mounts, Piagge Quarry*	SHO	VS 159	Lava	*Shoshonite*	**Ol**(Chr)+**Cpx**+**Sa**+Mag+Glass
Tuscany	0.94	*Cimini Mounts, Faggeta Scoria Cone*	SHO	VS 202	Scoria	*Shoshonite*	**Ol**(Chr)+Cpx+Glass
Tuscany	0.94	*Cimini Mounts, Cimino East of Grottone*	SHO	VS 204	Lava	*Olivin latite*	**Ol**(Chr)+**Cpx**+Sa+Pl+Mag+Glass
Tuscany	0.94	*Cimini Mounts, intersection with provincial road*	SHO	VS 148	Lava	*Olivin latite*	**Ol**(Chr)+**Cpx**+Sa+Pl+Mag+Glass
Tuscany	0.88	*Torre Alfina, lava flow south tongue*	LMP	VS 29	Lava	*Olivin latite*	**Ol**(Chr)+Cpx+Sa+Phl+Ilm+Chr+Glass
Tuscany	0.88	*Torre Alfina, lava flow south tongue*	LMP	VS 28	Lava	*Olivin latite*	**Ol**(Chr)+Cpx+Sa+Phl+Ilm+Chr+Glass
Sedimentary and metasedimentary rocks							
Apennine		*Umbria, Polino Village, limestone*		AM 07		*Limestone*	
Betic		*Garrucha, limestone*		Alm10b		*Limestone*	
Apennine		*Tuscany, Boccheggiano*, Ligurian Units		SD 33		*Limestone*	

(continued on next page)

Table 1 (*continued*)

Region	Age Ma	Locality	Affinity	Sample	Body	Rock type	Petrography
Sedimentary and metasedimentary rocks							
Apennine		*Lepini Mounts, Morolo Hill*		ERN57		*Limestone*	
Apennine		*Elba Island, Monte Castello*		ST135/26		*Marlstone*	
Apennine		*Tuscany, Chianti, Sugame pass*		SD 49		*Marlstone*	
Betic		*Garrucha*		Alm 07		*Marlstone*	
Apennine		*Tuscany, Chianti, San Polo Village*		SD 53		*Marlstone*	
Apennine		*Southern Tuscany, Seggiano village, Pietraforte*		SD 45		*Sandstone*	
Tuscan-Basement		*Poggio Nibbio drill 8, 2817–2818 m*		SD 63		*Phyllites*	
Tuscan-Basement		*Paglia drill 1, 3104.4–3106.6 m*		SD 59		*Phyllites*	
Tuscan-Basement		*Sasso drill 22, 2242 m*		SS 2242		*Phyllites*	
Tuscan-Basement		*Sasso drill 22, 2076 m*		SS 2076		*Ga-micashist*	
Tuscan-Basement		*Montecerboli drill, 2916 m*		M2916		*Ga-micashist*	
Tuscan-Basement		*Torre Alfina, xenolith in lava flow B*		VS 41i		*Granulite*	
Tuscan-Basement		*Torre Alfina, xenolith in lava flow B*		SD 75		*Gneiss*	
Tuscan-Basement		*Torre Alfina, xenolith in lava flow B*		VS 44		*Gneiss*	

Age data sources are: Western Alps = Dal Piaz et al. (1977), Venturelli et al. (1984a) and references therein; Corsica and Capraia = Civetta et al. (1976), Barberi et al. (1986), Aldighieri et al. (2004); Murcia and Almeria = Turner et al. (1999), Duggen et al. (2004, 2005), and references therein; Tuscany = Ferrara and Tonarini (1986), Conticelli et al. (2004) and references therein. Legend for mineral abbreviations: Phl = phlogopite; Ol = olivine; Kfs = K-feldspar; Ap = apatite; Ser = sericite; cal = calcite; Krh = K-richterite; Pl = plagioclase; Hbl = amphibole; Qtz = quartz; Chl = chlorite; Spn = spinel; Ep = epidote; Ab = albite; Bt = biotite; Chr = chromite; Opx = orthopyroxene; Mag = magnetite; Pri = priderite; Ilm = ilmenite. The mineral when in bold is a phenocryst; within brackets it is enclosed in the preceeding phase; when italic it is a secondary mineral. Bas andesite = Basaltic andesite; hk-dacite = high-K dacite; hK andesite = high-K andesite.

The Miocene-to-Present formation of the Apenninic orogen was coeval with the fast opening of the Liguro-Provençal, first, and Tyrrhenian back-arc, later, basins. Basin spreading was related to the south-eastward retreat of a NW-W dipping Ionian/Adriatic slab, and was progressively accompanied by formation of new oceanic crust, and drifting and rotation of the Corsica–Sardinia and Calabria blocks (Cifelli et al., 2007; Mattei et al., 2007). After the end of the Corsica–Sardinia drifting, back-arc extension continued in the Southern Tyrrhenian Sea (Fig. 1). In this basin rifting started along the western margin of the Southern Tyrrhenian Sea (Sardinian margin) during Serravallian, and progressively migrated south-eastward in the Vavilov (late Messinian–early Pliocene) and Marsili (late Pliocene–early Pleistocene) basins. Rifting and basin subsidence were followed by a drifting stage, with the emplacement of oceanic crust in the Vavilov and Marsili seamounts (Mattei et al., 2002; Nicolosi et al., 2006, and references therein). Calc-alkaline, shoshonitic, and ultrapotassic magmatism invariantly accompanied the westward subduction of the Adriatic–Ionian lithosphere. Orogenic volcanism started during the Oligocene in the Provençal and Sardinia regions, then migrates during the Quaternary along the Tyrrhenian coast of the Italian peninsula and in the Aeolian islands, following the progressive retreat of the subducting slab toward east and south-east (Savelli, 2002, and references therein).

The western Alps are a continuation of the same subduction system but with an opposite polarity of the subducted plate, the direction of which reversed in the Ligurian area. They also originated from Africa and Eurasia convergence, from the late Cretaceous onward, causing the closure of the Ligurian–Piedmont and Valais oceans and the subsequent collision between the Apulian and Eurasian plates (Dercourt et al., 1986; Stampfli et al., 2001). Collision was accommodated by crustal imbrications and subduction of continental material as attested by the presence of UHP rocks in the Dora Maira massif (Chopin, 1984; Schreyer et al., 1987). The western termination of the Alpine belt is a tight arc formed during the late Tertiary (Schmid and Kissling, 2000; Collombet et al., 2002) without any back-arc extension. The deep geometry of the western Alps is well documented by seismic reflection, seismic tomography and geological data, which show the Alpine orogeny is dominated by Europe-vergent tectonic structures, which formed during Cretaceous–Neogene times. Southeastward subduction of the European lithosphere is proved by the presence of well defined East-Southeastern dipping seismic reflectors, which image the deep geometry of crustal and upper mantle bodies. Tomographic images of the western Alps are consistent and show a high velocity body down to 200–300 km, which is interpreted as the Eurasian lithosphere subducted southeastward below the Adriatic promontory with a shallow dip angle (Spakman et al., 1993; Piromallo and Morelli, 2003; Lippitsch et al., 2003). Subduction and continental collision have been also responsible for the main metamorphic events, including the formation of blue schist and coesite-bearing, eclogite-facies rocks, formed at pressures of up to 3 GPa (i.e., at depths which may have reached 100 km). UHP metamorphism involves continental units confirming that pieces of continental European lithosphere were involved in subduction processes (Chopin, 1984; Schreyer et al., 1987).

3. Samples and analytical methods

The studied samples represent the overall compositional spectra of ultrapotassic to sub-alkaline rocks from the four different regions of the Western Mediterranean in which lamproites occurs (Fig. 1). In addition crustal sedimentary and metamorphic rocks from the Apennine Chain have been also investigated (Table 1). Petrography and major elements data from literature have been used, whereas trace elements and isotopes have been either determined or re-determined using up-to-date analytical methods in order to gather an internally consistent and finely precise dataset with comparable errors.

In few cases, only on new samples, major elements have been determined by XRF and AAS. Trace element concentrations (Table 2) were determined on fused disks with laser ablation-inductively coupled plasma mass spectrometry (LA-ICPMS) at the CNR–IGG-Pavia using a 266 nm laser microprobe (model Brilliant, Quantel) coupled with a quadrupole ICPMS (model DRCe, PerkinElmer). The laser was operated at 10 Hz of repetition rate, the power on the sample was 5.5 mW and spot size was set at 80 μm. ICPMS gas flows were set to have the maximum sensitivity in the middle of the mass spectrum (^{139}La) and the minimum oxide production ($ThO^+/Th^+ < 1\%$). Single analyses consisted in the acquisition of 60 s of background and 60 s of ablation signals. Acquisition was carried out in peak hopping mode with a dwell time of 10 ms. NIST SRM 610 and ^{43}Ca were adopted as external and internal standards, respectively. Data reduction was carried out with the software package "Glitter" (van Achtenberg et al., 2001). Precision and accuracy were evaluated on the USGS-BCR-2 reference material and are estimated to be better than 5 and 10% relative, respectively. Some duplicate analyses have been performed at ActLabs (Ontario) using lithoresearch schedule, analytical techniques and errors can be found at http://www.actlabs.com/gg_rock_litho_usa.htm. Bias between the two methods has been checked though the

Table 2
Major (wt.%) and trace elements (ppm) compositions for lamprophyres, lamproites, shoshonites and calc-alkalic rocks from Western Mediterranean

Region	Affinity	Sample	SiO_2	TiO_2	Al_2O_3	Fe_2O_3	FeO	MnO	MgO	CaO	Na_2O	K_2O	P_2O_5	LOI	Sum	Mg-#	A.I.	Li	F	S	Cl	Sc	V	Cr
Western Alps	LMP	MEC 242	49.3	1.05	11.3	1.63	4.60	0.10	13.6	7.65	1.60	5.94	1.10	2.30	100.17	82.46	0.80	32	–	–	–	30.8	149	922
Western Alps	LMP	VDA 17	50.3	1.15	10.2	6.95	–	0.12	11.5	6.64	0.85	7.39	1.27	2.75	99.18	79.44	0.00	41	–	–	–	25.0	155	640
Western Alps	LMP	VDA 15	48.8	1.19	10.9	7.10	–	0.12	11.3	7.78	1.41	6.47	1.33	2.04	98.48	78.83	0.00	41	–	–	–	29.0	181	560
Western Alps	LMP	VDA 03	55.1	1.31	10.2	4.68	–	0.08	8.94	4.02	1.13	9.24	1.13	3.53	99.36	81.66	0.00	93	–	–	–	13.0	83	470
Western Alps	LMP	MEC 247	56.0	1.24	11.0	2.21	2.65	0.09	9.27	3.11	1.29	9.07	1.09	1.80	98.82	80.74	1.09	42	–	–	–	16.6	95	571
Western Alps	SHO	VDA 14	52.2	0.94	13.9	7.25	–	0.13	7.31	7.40	2.47	3.75	0.92	3.24	99.50	70.15	0.58	21	–	–	–	27.0	182	310
Western Alps	SHO	MEC 241	60.0	0.53	17.3	2.14	3.39	0.10	2.10	3.76	3.37	4.38	0.37	2.30	99.74	45.31	0.59	23	–	–	–	11.7	89	23.4
Western Alps	SHO	MEC 216	60.4	0.54	17.4	2.06	3.12	0.11	2.04	4.34	3.59	4.09	0.37	2.10	100.16	46.24	0.59	14	–	–	–	11.2	85	21.1
Western Alps	HKCA	VDA 08	54.2	0.98	17.2	7.57	–	0.143	4.52	8.08	2.82	1.82	0.41	2.47	100.19	58.19	0.00	–	–	–	–	23.0	177	80.0
Western Alps	HKCA	KAW 697a	53.7	0.86	17.6	2.96	3.50	0.15	2.55	7.77	3.09	1.89	0.37	5.24	99.67	46.46	0.41	–	–	–	–	16.7	142	–
Western Alps	HKCA	VDA 10	54.8	0.64	14.7	7.36	–	0.14	6.83	8.45	2.20	2.34	0.29	2.20	100.02	68.38	0.00	19	–	–	–	34.0	202	250
Western Alps	HKCA	MEC 251	59.3	0.63	17.5	1.64	3.48	0.11	2.85	5.08	3.27	2.89	0.18	2.90	99.83	54.67	0.49	19	–	–	–	15.1	109	33.0
Western Alps	HKCA	MEC 240	63.1	0.42	17.1	0.69	3.97	0.11	1.08	3.23	3.63	3.18	0.22	3.56	100.22	33.04	0.55	–	–	–	–	2.26	16	–
Corsica	LMP	SIS 07	58.3	2.31	10.8	1.74	3.26	0.07	7.05	2.93	1.01	10.4	0.76	2.14	100.73	75.39	1.19	35	–	–	–	13.0	92	411
Corsica	LMP	SIS 04	58.5	2.27	10.8	0.81	2.42	0.06	6.63	3.12	1.02	10.7	0.67	2.09	99.16	81.54	0.00	22	–	–	–	11.5	84	340
Corsica	HKCA	CP 101	61.9	0.69	15.3	2.67	2.45	0.07	3.48	5.48	3.14	3.33	0.18	1.36	100.00	60.08	0.57	–	–	–	–	–	128	177
Corsica	HKCA	CP 110	62.3	0.68	15.2	3.27	1.45	0.07	2.88	4.59	3.14	3.90	0.29	2.19	100.00	57.87	0.62	–	–	–	–	–	137	132
Corsica	SHO	CP 54	50.6	1.650	15.5	9.31	0.80	0.125	6.41	7.92	2.83	2.42	0.48	1.13	99.10	59.41	0.47	12	170	–	559	22.8	166	400
Corsica	SHO	CP 105	51.5	1.52	15.4	3.97	5.18	0.14	8.18	7.33	2.99	2.57	0.37	0.87	100.00	66.22	0.50	–	–	–	–	–	168	428
Murcia-Almeria	LMP	SP 452	50.3	1.35	8.80	6.12	–	0.01	14.5	5.94	1.09	7.04	1.62	2.51	99.21	84.62	1.07	–	–	–	–	16.8	82	908
Murcia-Almeria	LMP	SP 055	52.7	1.34	9.53	5.36	–	0.03	13.1	4.87	1.75	6.97	1.15	2.63	99.40	85.04	1.09	–	–	–	–	15.0	94	941
Murcia-Almeria	LMP	SP 078	53.1	1.71	9.41	5.74	–	0.07	14.6	2.90	0.64	8.58	1.13	1.62	99.46	85.57	1.10	39	–	–	–	12.8	86	897
Murcia-Almeria	LMP	SP 077	54.6	1.75	9.52	5.66	–	0.07	13.3	2.87	0.05	8.86	0.95	1.60	99.23	84.56	1.02	38	–	–	–	12.6	86	891
Murcia-Almeria	LMP	SP 725	55.9	1.49	9.30	4.67	–	0.08	11.8	4.12	1.08	8.93	1.24	1.22	99.84	85.47	1.23	–	3700	–	229	12.7	82	810
Murcia-Almeria	LMP	SP 723	57.8	1.58	9.84	4.75	–	0.07	10.2	3.19	1.02	9.20	1.18	0.79	99.66	83.39	1.18	–	3900	–	189	15.9	107	757
Murcia-Almeria	LMP	SP 044	56.4	1.38	11.0	5.60	–	0.07	8.93	2.60	0.87	8.34	0.86	3.26	99.26	78.80	0.95	–	–	–	–	16.9	113	582
Murcia-Almeria	LMP	SP 050	56.8	1.54	11.7	5.98	–	0.07	9.23	2.69	1.04	8.48	0.86	1.84	100.15	78.25	0.93	42	–	–	–	18.7	131	567
Murcia-Almeria	LMP	SP 049	57.1	1.35	11.5	5.58	–	0.07	9.06	2.78	1.16	7.84	0.75	2.26	99.44	79.10	0.91	41	–	–	–	20.2	142	543
Murcia-Almeria	LMP	SP 035	64.7	1.06	12.5	2.75	–	0.04	2.38	3.69	1.98	7.18	0.89	2.79	99.96	66.86	0.88	59	–	–	–	9.8	76	399
Murcia-Almeria	LMP	SP 040	68.5	1.01	12.3	3.13	–	0.03	1.73	2.32	2.01	7.28	0.91	1.63	100.85	56.30	0.91	53	–	–	–	10.4	82	342
Murcia-Almeria	LMP	Alm 02	54.7	1.54	10.8	0.50	4.10	0.07	7.58	4.99	2.84	3.47	0.60	8.81	99.99	77.75	0.78	–	–	–	–	14	93	550
Murcia-Almeria	LMP	Alm 01	58.1	1.71	10.9	1.11	2.82	0.07	3.52	6.70	1.89	6.82	0.76	5.54	99.99	65.91	0.96	–	–	–	–	15	97	610
Murcia-Almeria	LMP	SP 011	66.5	1.45	9.82	3.59	–	0.03	2.68	2.25	1.11	7.34	0.54	4.53	99.84	63.50	0.99	39	–	–	–	9.2	92	581
Murcia-Almeria	SHO	Alm 27	56.3	0.42	19.2	3.94	1.79	0.10	3.41	4.69	2.90	3.24	0.07	3.90	99.99	57.27	0.43	–	–	–	–	23	122	18
Murcia-Almeria	SHO	Alm 39	59.4	0.53	16.7	5.24	0.44	1.01	4.04	0.45	0.55	9.87	0.11	2.60	100.98	62.17	0.69	–	–	–	–	21	136	23
Murcia-Almeria	SHO	Alm 21	59.9	0.55	16.8	3.64	1.77	0.17	3.04	0.50	2.91	7.15	0.11	2.52	98.99	55.82	0.75	–	–	–	–	21	160	30
Murcia-Almeria	SHO	Alm 28	65.9	0.38	16.2	1.73	1.61	0.04	2.16	2.58	2.48	4.36	0.06	2.50	100.01	58.86	0.54	–	–	–	–	12	75	28
Murcia-Almeria	SHO	Alm 40	69.2	0.36	15.7	2.29	0.21	0.10	1.31	0.59	1.63	6.11	0.06	2.44	99.99	54.75	0.59	–	–	–	–	9	38	10
Murcia-Almeria	HKCA	Alm 17	61.5	0.53	16.9	0.65	4.19	0.08	3.34	5.84	3.08	2.33	0.12	1.41	99.99	59.46	0.45	–	–	–	–	21	158	21
Murcia-Almeria	HKCA	Alm 34	62.2	0.42	15.4	3.35	1.60	0.07	3.22	5.44	2.26	2.66	0.10	3.30	100.00	59.41	0.43	–	–	–	–	21	133	30
Murcia-Almeria	HKCA	Alm 14	62.3	0.57	16.9	0.47	4.48	0.08	3.07	5.94	3.10	2.46	0.13	1.44	100.93	56.77	0.46	–	–	–	–	20	150	18

Sample	Co	Ni	Cu	Zn	Ga	Rb	Sr	Y	Zr	Nb	Cs	Ba	La	Ce	Pr	Nd	Sm	Eu	Gd	Tb	Dy	Ho	Er	Tm	Yb	Lu	Hf	Ta	Pb	Th	U
MEC 242	57.4	303	14	70	–	379	825	29	463	36.1	10.8	3950	86.7	219	31.5	142	29.0	4.82	17.1	1.61	6.2	0.97	2.36	0.29	1.68	0.24	11.3	2.38	28	135	23.1
VDA 17	33	300	60	80	17	395	829	32	593	34.1	17.1	4293	117	273	38.2	174	34.2	6.15	19.4	1.99	7.6	1.22	2.93	0.37	2.04	0.27	16.1	2.43	36	155	28.3
VDA 15	34	270	20	80	16	321	756	32	472	28.3	10.4	4213	107	256	35.7	159	32.4	6.07	18.8	2.00	7.7	1.21	2.97	0.38	2.19	0.28	13.0	1.97	34	127	22.6
VDA 03	25	280	30	90	19	555	799	31	665	34.4	28.4	3797	106	260	37.1	169	33.6	5.88	19.0	1.85	7.3	1.18	2.77	0.34	1.93	0.25	18.1	2.73	105	134	22.4
MEC 247	41.1	260	40	80	–	646	550	29	638	36.4	13.2	3533	97.6	256	36.8	168	34.0	5.24	18.7	1.77	6.6	1.00	2.34	0.28	1.58	0.22	16.6	2.28	132	135	24.2
VDA 14	26	140	50	90	19	172	882	29	334	24.2	6.00	2592	55.7	127	16.9	75.0	16.2	3.32	10.4	1.28	5.9	1.03	2.89	0.40	2.46	0.36	9.2	1.74	36	72.3	22.0
MEC 241	52.9	46.3	3.8	54.1	–	222	555	26	370	38.6	3.75	2400	63.9	131	16.1	57.1	10.2	1.80	7.3	0.90	4.8	0.91	2.64	0.39	2.61	0.42	9.1	2.92	28	137	29.0
MEC 216	64.9	59.4	6.7	46.6	–	193	587	26	353	35.4	5.48	2388	62.2	130	15.9	57.1	10.1	1.79	7.3	0.90	4.7	0.92	2.67	0.39	2.61	0.41	9.3	2.39	26	135	30.0
VDA 08	16	40	<10	90	20	63	560	28	167	13.5	0.60	1046	40.9	77.8	8.87	35.1	6.80	1.86	5.7	0.90	4.9	0.93	2.73	0.40	2.61	0.39	4.3	0.99	20	19.6	4.91
KAW 697a	–	55.4	12.7	73.2	–	58	563	23	187	12.8	1.39	1622	36.5	72.5	8.57	32.8	6.37	1.51	5.5	0.75	4.3	0.86	2.45	0.35	2.32	0.37	3.7	0.83	17	21.3	6.11
VDA 10	25	60.0	60	70	16	79	468	20	97	6.20	0.80	778.0	23.4	46.7	5.43	21.9	4.67	1.24	4.1	0.64	3.6	0.71	2.08	0.31	2.02	0.31	2.8	0.50	18	11.2	2.60
MEC 251	23.3	36.0	8.5	65.0	–	83	666	18	133	9.24	1.71	1007	30.2	59.3	6.84	25.5	4.78	1.12	4.1	0.57	3.3	0.68	1.95	0.29	1.87	0.29	2.9	0.70	11	10.5	3.26

(continued on next page)

Table 2 (*continued*)

Sample	Co	Ni	Cu	Zn	Ga	Rb	Sr	Y	Zr	Nb	Cs	Ba	La	Ce	Pr	Nd	Sm	Eu	Gd	Tb	Dy	Ho	Er	Tm	Yb	Lu	Hf	Ta	Pb	Th	U
MEC 240	–	12.8	3.2	58.3	–	103	605	19	199	12.4	0.86	1315	54.4	101	10.4	34.7	5.35	1.23	4.3	0.55	3.1	0.64	1.92	0.29	2.01	0.33	4.4	0.79	16	20.1	5.69
SIS 07	27.0	272	–	–	–	317	681	16	996	57.8	2.63	925	135	302	33.4	125	16.3	2.65	8.2	1.0	4.0	0.75	1.47	0.21	1.26	0.18	26.6	4.10	14	36.8	4.29
SIS 04	19.0	230	30	100	23	318	640	19	1040	54.8	2.00	1450	183	367	41.6	146	19.1	3.50	11.3	1.1	4.6	0.79	2.10	0.28	1.59	0.21	32.1	3.96	12	37.9	4.61
CP 101	11.9	29	12	73	21	116	733	19	185	11.9	9.16	711	58.5	109	11.5	43.6	8.01	1.76	5.3	0.77	3.6	0.70	2.05	0.29	1.84	0.276	5.4	0.90	61	23.1	6.43
CP 110	15.2	–	11	79	23	161	933	31	234	14.3	15.2	1410	165	297	28.9	105	16.4	3.00	9.5	1.24	5.6	1.01	2.85	0.40	2.49	0.358	6.3	1.11	82	49.4	11.7
CP 54	30.0	69	25	87	18	115	399	20	221	15.0	4.00	540	29.3	68.4	10.9	51.9	9.60	2.09	6.2	1.00	4.9	0.99	2.70	0.40	2.30	0.35	5.6	1.20	12	24.0	3.80
CP 105	40.6	88	30	88	19	148	343	22	209	19.9	6.20	484	30.8	74.0	8.96	39.6	8.24	1.92	6.1	0.88	4.3	0.84	2.31	0.32	1.97	0.285	5.6	1.22	14	22.1	4.47
SP 452	43.5	558	18.9	104	22	322	1617	34	749	32.3	10.5	3776	105	272	38.2	167	32.0	5.18	18.8	1.81	7.3	1.17	2.84	0.35	2.12	0.30	19.2	2.69	68	114	30.1
SP 055	39.6	464	24.7	69.8	–	736	842	27	671	29.5	91.5	2593	80.5	223	33.0	146	27.9	4.32	15.2	1.45	5.7	0.92	2.26	0.28	1.70	0.25	18.7	2.81	64	91.2	16.0
SP 078	40.4	574	53.0	85.6	–	716	579	22	746	28.2	21.0	1823	80.7	233	35.4	157	30.6	4.62	15.9	1.46	5.3	0.81	1.94	0.24	1.37	0.20	21.0	2.22	66	93.0	25.3
SP 077	36.7	523	42.2	79.6	–	733	600	24	802	32.5	18.5	1846	79.9	232	34.8	155	29.8	4.56	15.5	1.39	5.1	0.79	1.87	0.23	1.33	0.19	21.4	2.26	68	96.9	26.7
SP 725	32.1	470	28.5	83.3	21	696	962	30	872	38.9	26.6	1815	109	295	43.1	188	35.9	5.46	18.6	1.72	6.5	1.04	2.53	0.32	1.90	0.28	23.9	2.59	110	117	24.1
SP 723	40.5	601	37.7	99.3	22	746	978	33	860	35.7	78.0	1893	118	328	48.9	214	40.2	6.09	21.3	1.91	7.2	1.15	2.93	0.36	2.14	0.31	23.7	2.41	111	129	32.4
SP 044	32.4	371	37.7	113.8	23	765	586	31	620	38.5	33.2	2096	73.0	195	28.8	127	25.2	4.04	14.9	1.52	6.5	1.08	2.84	0.37	2.23	0.33	17.9	2.61	90	75.2	21.9
SP 050	38.3	479	57.5	110.9	–	753	649	34	594	28.5	21.8	1766	85.6	228	33.8	149	29.0	4.60	16.8	1.67	7.2	1.21	3.19	0.41	2.52	0.37	15.6	2.03	73	101	24.3
SP 049	41.5	430	87.5	138.7	–	903	703	36	687	33.3	18.1	1841	87.4	235	34.8	152	30.0	4.74	17.4	1.74	7.4	1.25	3.27	0.42	2.58	0.38	16.6	2.49	83	106	26.5
SP 035	15.4	179	27.8	73.2	–	311	549	22	323	25.7	15.1	1881	50.6	137	18.5	82.6	17.8	2.91	10.6	1.11	4.8	0.76	1.89	0.24	1.46	0.21	9.4	2.56	114	64.5	13.0
SP 040	10.6	89	19.9	68.7	–	314	492	21	355	25.2	16.1	1920	47.6	132	17.4	76.0	16.6	2.78	10.4	1.09	4.7	0.75	1.86	0.23	1.41	0.20	7.0	2.13	111	63.0	12.5
Alm 02	23	290	20	60	18	389	467	21	672	32	63.4	1550	93.8	252	33.4	149	26.8	4.49	13.4	1.3	5.3	0.90	2.20	0.29	1.70	0.21	18.4	3.30	54	78.7	19.3
Alm 01	23	300	30	50	20	444	484	22	693	35	67.6	1580	99.0	267	35.3	155	28.1	4.79	14.3	1.4	5.5	0.90	2.30	0.31	1.80	0.23	18.9	3.40	52	83.0	20.5
SP 011	16.9	157	39.5	65.3	–	514	448	19	624	42.2	27.8	1384	74.6	236	30.3	128	23.7	3.69	13.0	1.17	4.4	0.71	1.79	0.22	1.28	0.18	16.6	2.42	38	73.4	19.0
Alm 27	12	10	20	40	15	72	229	12	67	3	1.5	314	9.60	19.0	2.16	8.80	2.0	0.68	2.0	0.4	2.3	0.50	1.40	0.22	1.50	0.24	1.9	0.40	7	3.0	1.2
Alm 39	12	<20	<10	160	19	453	81	14	120	6	4.0	553	15.7	39.5	3.84	15.5	3.5	0.81	2.9	0.5	3.0	0.50	1.60	0.26	1.70	0.25	3.5	2.60	28	6.5	3.1
Alm 21	11	20	10	90	18	335	104	15	116	4	3.9	552	15.4	33.3	3.88	15.6	3.5	0.83	3.0	0.5	2.8	0.50	1.60	0.24	1.50	0.23	3.2	0.50	24	6.2	2.9
Alm 28	6	<20	20	30	15	147	93	10	115	5	5.9	298	21.5	42.7	4.18	14.5	2.5	0.59	2.0	0.3	1.9	0.40	1.10	0.17	1.10	0.16	3.2	0.70	24	9.4	2.6
Alm 40	3	<20	<10	60	18	278	41	22	185	7	7.4	411	25.7	55.8	6.08	23.8	5.0	0.95	4.2	0.7	4.3	0.80	2.50	0.38	2.40	0.38	5.1	0.70	14	9.7	8.1
Alm 17	10	6	<10	40	18	126	241	16	128	4	12.2	273	17.7	38.2	4.33	17.3	3.9	1.04	3.4	0.6	3.2	0.60	1.80	0.27	1.70	0.24	3.5	0.50	31	6.7	3.7
Alm 34	11	9	20	40	16	115	144	14	101	5	4.5	243	18.5	39.8	4.11	16.4	3.3	0.80	2.7	0.5	3.0	0.60	1.60	0.26	1.70	0.25	2.8	0.50	16	5.5	2.2
Alm 14	13	4	<10	60	21	135	221	16	113	4	11.2	253	18.6	38.7	4.51	17.6	3.9	0.97	3.4	0.6	3.2	0.60	1.80	0.26	1.60	0.24	3.1	0.40	35	6.3	3.6

Region	Affinity	Sample	SiO_2	TiO_2	Al_2O_3	Fe_2O_3	FeO	MnO	MgO	CaO	Na_2O	K_2O	P_2O_5	LOI	Sum	Mg-#	A.I.	Li	F	S	Cl	Sc	V	Cr	Co
Murcia-Almeria	HKCA	Aml 31	62.8	0.52	16.4	0.46	3.84	0.07	3.19	5.22	3.13	2.43	0.12	1.85	99.99	61.13	0.48	–	–	–	–	17	115	30	13
Murcia-Almeria	CA	Alm 25	59.0	0.54	15.9	2.18	5.11	0.12	5.25	8.05	2.18	1.31	0.09	0.30	99.99	60.89	0.32	–	–	–	–	38	256	60	18
Murcia-Almeria	CA	Alm 13	60.0	0.62	16.9	0.47	5.28	0.06	3.97	6.72	3.15	1.83	0.11	0.92	99.95	59.35	0.42	–	–	–	–	25	174	70	13
Murcia-Almeria	CA	Alm 29	62.4	0.70	16.5	1.88	2.42	0.05	2.90	7.61	3.03	1.70	0.08	0.70	100.00	59.66	0.41	–	–	–	–	31	180	60	9
Murcia-Almeria	CA	Alm 32	62.6	0.45	15.2	2.22	2.05	0.10	2.41	8.76	2.69	1.62	0.09	1.77	99.99	55.53	0.41	–	–	–	–	32	215	80	13
Tuscany	LMP	ORC 01	57.8	1.51	11.8	2.24	3.12	0.08	8.2	3.46	1.31	8.06	0.85	1.55	99.99	76.96	0.00	30	4007	–	199	19	116	500	28
Tuscany	LMP	OR 12	58.1	1.42	11.8	1.52	3.38	0.07	8.70	3.56	1.35	7.92	0.69	1.46	100.00	79.35	0.91	–	–	–	–	17.0	100	449	31.0
Tuscany	LMP	MVC100	56.9	1.37	12.6	3.25	2.84	0.10	7.15	3.47	1.20	7.91	0.92	2.43	100.11	72.11	0.00	39	–	558	–	20.2	137	380	27.0
Tuscany	LMP	VS 29	55.5	1.36	13.4	0.78	5.08	0.10	9.36	4.70	1.18	7.46	0.54	0.58	100.00	77.14	0.00	39	4070	131	205	17.0	122	520	28.0
Tuscany	LMP	VS 28	56.0	1.27	13.9	1.38	4.08	0.09	8.72	4.94	1.13	7.49	0.53	0.47	100.05	77.35	0.00	–	–	–	–	–	125	642	26.0
Tuscany	SHO	VS 184	56.4	1.17	14.9	1.26	4.25	0.11	9.48	5.37	1.44	4.96	0.29	0.41	100.01	78.69	0.00	41	–	–	–	20.4	131	494	35.7
Tuscany	SHO	VS 106	55.0	0.96	16.1	1.86	4.15	0.10	8.32	6.86	2.00	3.87	0.23	0.55	100.00	74.86	0.00	31	–	–	–	21.7	150	481	39.0
Tuscany	SHO	VS 150	54.5	1.01	16.2	2.80	3.77	0.11	8.03	7.31	1.82	3.62	0.27	0.39	99.80	72.69	0.00	–	–	–	–	25.0	167	458	30.0
Tuscany	SHO	VS 151	53.8	0.87	16.9	2.87	4.13	0.11	7.97	7.58	2.23	3.02	0.22	0.39	100.01	71.22	0.00	–	–	–	–	26.0	176	407	33.0
Tuscany	SHO	VS 123	53.6	0.89	17.0	2.63	3.84	0.11	7.82	7.84	2.32	2.95	0.20	0.80	100.00	73.72	0	32	–	–	–	24.1	195	380	27
Tuscany	SHO	VS 202	52.9	1.19	14.7	5.03	1.20	0.10	9.58	6.50	1.15	5.89	0.28	1.47	100.00	77.72	0.00	–	–	–	–	19.4	111	580	29
Tuscany	SHO	VS 204	54.1	1.01	15.9	0.92	4.50	0.09	8.82	6.19	1.42	5.84	0.29	0.91	100.00	77.65	0.54	–	–	–	–	20.4	115	490	29
Tuscany	SHO	VS 159	56.9	1.10	15.4	1.02	3.92	0.10	7.65	5.50	1.33	5.77	0.27	1.01	100.00	76.84	0.55	–	–	–	–	–	103	390	26
Tuscany	SHO	VS 148	57.6	0.94	15.3	1.89	3.11	0.11	7.49	5.43	1.98	5.45	0.29	0.42	100.00	76.55	0.60	–	–	–	–	18.2	112	422	28
Tuscany	SHO	VS 200	60.4	0.82	15.5	1.56	3.28	0.09	4.41	5.39	2.10	5.62	0.25	0.62	100.00	66.36	0.62	–	–	–	–	17.5	111	164	17
Tuscany	SHO	VS 193	63.1	0.85	16.5	1.07	3.14	0.06	2.07	3.83	2.34	5.49	0.23	1.30	100.00	51.41	0.59	–	–	–	–	10.6	75	49	10.0
Tuscany	HKCA	VS 122	54.5	0.89	17.0	0.93	5.07	0.11	8.09	7.54	1.95	3.26	0.20	0.49	100.00	74.06	0.00	27	–	–	–	23.2	170	409	25.2
Sedimentary and metasedimentary rocks																									
Umbria	Limestone	AM 07	0.2	bdl	0.0	0.03	–	bdl	0.41	56.03	0.05	bdl	bdl	43.20	99.99	–	–	–	–	–	–	1.0	–	21	1
Murcia-Almeria	Limestone	Alm10b	2.1	bdl	0.1	0.14	1.32	0.09	0.37	54.10	0.01	0.02	0.02	41.76	100.00	–	–	–	–	–	–	<1	12	4	<1
Tuscany	Limestone	SD 33	6.7	0.09	2.1	1.21	–	0.13	0.70	50.20	0.61	0.14	bdl	38.20	100.04	–	–	–	–	–	–	3.2	–	21	6

Southern latium	Limestone	ERN57	7.7	0.07	2.1	0.76	–	0.03	1.05	47.59	0.55	0.28	0.08	39.85	100.00	–	–	4	–	–	–	1.2	17	–	2
Tuscany	Marlstone	ST135/26	10.8	bdl	0.9	1.06	–	0.31	0.52	48.30	0.01	0.09	0.02	38.10	100.07	–	–	–	–	–	–	–	12	1	<3
Tuscany	Marlstone	SD 49	18.8	0.28	6.7	2.80	–	0.11	1.24	37.82	0.28	1.28	0.04	30.70	100.05	–	–	–	–	–	–	6.9	–	64	13
Murcia-Almeria	Marlstone	Alm 07	28.5	0.22	5.0	1.38	0.60	0.05	2.26	34.18	0.33	0.89	0.96	25.61	100.02	–	–	–	–	–	–	4.0	40	28	2
Tuscany	Marlstone	SD 53	43.9	0.60	13.8	5.99	–	0.20	3.06	14.42	1.35	2.09	0.05	14.60	100.06	–	–	–	–	–	–	14.5	–	240	20
Tuscany	Sandstone	SD 45	47.9	0.47	8.2	2.58	–	0.06	2.58	18.07	0.60	1.50	0.02	17.72	99.63	–	–	–	–	–	–	6.1	–	54	8
Tuscan-Basement	Phyllites	SD 63	51.7	0.44	24.4	9.31	–	0.20	2.43	0.22	1.47	5.34	0.12	4.97	100.63	–	–	–	–	–	–	23.1	–	180	34
Tuscan-Basement	Phyllites	SD 59	59.1	0.92	17.6	8.82	–	0.07	3.30	1.30	1.20	2.70	0.14	5.20	100.30	–	–	–	–	–	–	17.0	–	114	17
Tuscan-Basement	Phyllites	SS 2242	59.4	0.94	20.4	0.83	5.68	0.04	2.35	0.86	1.39	4.28	0.13	3.05	99.36	–	–	–	–	–	–	–	130	90	16
Tuscan-Basement	Ga-micashist	SS 2076	61.4	0.85	20.1	0.94	4.53	0.05	1.95	0.63	1.35	4.10	0.13	3.47	99.49	–	–	–	–	–	–	17.8	120	80	15
Tuscan-Basement	Ga-micashist	M2916	63.8	0.76	18.6	0.85	5.03	0.04	1.85	0.36	1.05	3.72	0.12	3.27	99.44	–	–	–	–	–	–	15.1	128	124	16
Tuscan-Basement	Granulite	VS 41i	64.0	0.44	8.3	0.30	5.60	0.12	10.03	10.02	0.26	0.29	0.53	0.06	100.00	–	–	–	–	–	–	56.0	–	1163	35
Tuscan-Basement	Gneiss	SD 75	64.1	0.93	16.7	6.38	–	0.05	1.91	1.93	2.00	3.96	0.10	1.91	100.01	–	–	–	–	–	–	14.7	–	130	16
Tuscan-Basement	Gneiss	VS 44	66.7	0.95	16.1	6.74	–	0.09	1.82	3.30	1.49	1.90	0.12	0.80	99.99	–	–	–	–	–	–	18.0	–	138	20

Sample	Ni	Cu	Zn	Ga	Rb	Sr	Y	Zr	Nb	Cs	Ba	La	Ce	Pr	Nd	Sm	Eu	Gd	Tb	Dy	Ho	Er	Tm	Yb	Lu	Hf	Ta	Pb	Th	U
Aml 31	<20	<10	90	18	128	221	17	129	4	11.4	298	21.6	44.5	5.08	19.6	4.3	1.07	3.6	0.6	3.3	0.60	1.90	0.28	1.70	0.25	3.6	0.50	43	6.9	3.9
Alm 25	<20	20	50	14	57	194	15	60	3	6.6	129	9.2	19	2.38	10.0	2.5	0.77	2.5	0.5	2.9	0.50	1.60	0.25	1.60	0.24	1.8	0.30	8	2.9	1.2
Alm 13	20	<10	40	17	101	242	17	126	4	9.6	266	17.0	36.4	4.27	17.2	3.8	1.06	3.5	0.6	3.4	0.70	1.90	0.29	1.80	0.28	3.4	0.50	25	6.0	3.0
Alm 29	<20	<10	40	16	73	218	21	130	6	2.5	248	22.3	45	5.08	20.2	4.2	1.02	3.8	0.7	4.0	0.80	2.30	0.34	2.10	0.31	3.6	0.50	31	6.6	2.0
Alm 32	20	10	40	16	83	155	16	71	3	3.6	192	12.0	24.1	2.74	11.0	2.6	0.71	2.6	0.5	2.9	0.60	1.70	0.27	1.70	0.27	2.1	0.40	10	3.8	2.5
ORC 01	280	50	80	21	612	577	24	749	39	25.2	1400	148.0	352	47.4	193	26.9	4.32	14.4	1.27	5.2	0.89	2.42	0.32	1.85	0.25	21.4	2.93	30	119	14.9
OR 12	274	–	–	–	609	613	32	797	41.0	18.0	1224	141.0	338	–	178	28.0	3.80	–	1.20	–	–	–	–	1.40	0.33	18.9	3.10	41	121	17.8
MVC100	140	340	90	21	768	408	28	491	30	14.0	1370	79.8	206	29.8	133	23.5	4.02	13.6	1.3	5.9	0.99	2.67	0.36	2.19	0.30	13.4	2.17	19	112	18.2
VS 29	310	40	90	19	399	579	27	532	28.5	35.5	1390	110.0	249	31.1	120	20.0	3.80	12.9	1.44	6.3	1.07	2.81	0.38	2.31	0.32	15.7	2.47	53	50.4	10.7
VS 28	301	41.0	85.0	22	418	637	30	555	30.1	33.3	1292	94.0	247	29.80	116.0	18.4	3.68	12.4	1.39	6.0	1.05	2.67	0.37	2.39	0.34	16.2	2.53	55	53.0	11.7
VS 184	267	34	77	21	379	391	27	495	26.3	22.0	839	77.0	179	21.7	88.0	15.2	2.33	6.2	0.96	5.0	1.04	2.60	0.36	1.90	0.29	12.2	1.79	43	58.3	10.3
VS 106	181	39	69	14	297	354	23	389	18.1	22.0	691	60.0	133	15.7	65.0	11.7	2.60	8.0	1.25	6.0	1.15	3.11	0.40	2.60	0.40	9.0	1.44	37	40.0	8.01
VS 150	151	30	64	18	224	346	27	279	16.2	14.1	681	56.3	126	17.0	67.0	10.9	2.00	5.8	0.87	4.9	0.96	2.63	0.36	2.16	0.34	7.9	1.10	31	36.0	7.10
VS 151	107	30	61	17	201	335	23	211	12.9	13.3	625	46.0	105	12.2	44.0	7.22	1.74	5.2	0.78	4.4	0.92	2.31	0.33	1.94	0.31	7.2	1.00	21	23.2	3.81
VS 123	97	30	60	16	161	325	22	197	12.3	14.1	612	47.8	103	12.5	47.1	7.87	1.85	6.2	0.86	4.5	0.87	2.48	0.35	2.15	0.32	6.5	0.99	20	21.0	3.94
VS 202	230	50	70	18	345	454	19	473	27	26.1	938	99.6	229	28	105	16.5	2.91	9.8	1.0	4.7	0.81	2.22	0.31	1.79	0.26	14.3	2.05	45	47.1	8.52
VS 204	243	37	64	–	353	506	29	415	31	–	918	86.0	197	–	99	17.7	2.49	–	1.0	–	–	–	–	2.09	0.35	11.3	2.13	54	50.0	7.41
VS 159	154	26	72	20	382	409	23	429	24	–	756	93.1	193	–	–	15.9	2.32	–	1.1	–	–	–	–	1.96	0.34	10.9	1.90	49	58.0	8.50
VS 148	149	29	65	20	375	669	27	375	21	–	998	97.0	189	–	86	15.1	2.19	–	1.3	–	–	–	–	2.30	0.40	9.4	1.80	82	59.0	8.00
VS 200	65	31	60	–	337	588	25	302	16	–	947	97.0	179	–	79	14.8	2.32	–	1.3	–	–	–	–	3.00	0.45	8.9	1.50	66	55.0	7.00
VS 193	20	15	49	–	276	514	27	239	15.0	–	920	92.0	156	–	54.0	12.8	1.92	–	1.1	–	–	–	–	2.80	0.38	7.0	1.80	74	49.0	7.00
VS 122	137	33	66	14	214	343	24	211	14.5	18.0	666	49.5	111	13.5	50.0	8.30	1.83	6.1	0.82	4.7	0.95	2.51	0.35	2.10	0.36	6.6	1.00	32	29.8	4.20
Sedimentary and metasedimentary rocks																														
AM 07	10	–	–	–	3	645	9	<10	3	–	35	7.5	11	–	9	1.6	0.37	–	0.2	–	–	–	–	0.89	0.09	0.5	0.09	–	1.7	–
Alm10b	1	10	11	<1	2	694	<2	12	2	1.1	8	5.5	7	1	2	0.3	<0.05	0.2	<0.1	<0.1	<0.1	<0.1	<0.05	<0.1	<0.04	<0.2	<0.1	<5	0.4	0.80
SD 33	19	–	–	–	3	564	11	<5	6	–	36	9.0	12	–	9	1.7	0.38	–	0.2	–	–	–	–	0.92	0.10	0.5	0.10	–	1.7	–
ERN57	–	3	15	–	15	386	5	10	2	0.6	56	4.3	7	1	4	0.8	0.19	0.8	0.1	0.7	0.15	0.42	0.06	0.36	0.06	0.3	0.10	0	1.0	2.26
ST135/26	<3	8	23	–	4	243	20	26	<3	–	11	14.0	13	–	14	–	–	–	–	–	–	–	–	–	–	–	–	10	5.0	
SD 49	45	–	–	–	51	642	19	52	10	–	526	20.0	31	–	16	3.2	0.76	–	0.5	–	–	–	–	1.49	0.20	1.3	0.51	–	5.4	–
Alm 07	20	10	35	4	37	574	11	110	4	13.1	134	14.4	27	3	13	2.5	0.54	2.2	0.4	2.1	0.40	1.20	0.18	1.10	0.17	2.8	0.40	7	3.7	2.60
SD 53	102	–	–	–	93	339	24	102	15	–	358	28.0	61	–	29	6.7	1.50	–	1.1	–	–	–	–	2.70	0.43	2.6	1.02	12	10.9	2.33
SD 45	23	–	–	–	45	182	24	158	12	–	210	23.0	46	–	18	3.8	0.74	–	0.5	–	–	–	–	1.60	0.27	3.2	0.75	–	5.4	–
SD 63	–	–	–	–	261	159	38	154	23	–	673	62.0	133	–	53	10.0	2.39	–	1.1	–	–	–	–	3.88	0.77	4.6	1.70	53	20.0	2.01
SD 59	102	–	–	–	139	99	21	162	25	–	423	47.0	90	–	39	9.3	1.51	–	0.9	–	–	–	–	3.55	0.66	5.3	1.40	–	15.0	–
SS 2242	40	30	70	25	159	171	37	205	20	9.0	804	59.1	115	13	47	9.0	2.01	8.0	1.3	7.3	1.37	3.97	0.60	3.93	0.56	5.8	1.81	19	14.6	3.18
SS 2076	50	30	60	26	149	150	36	228	17	6.3	717	52.2	104	12	45	8.1	1.74	7.0	1.2	6.6	1.25	3.74	0.56	3.50	0.51	6.4	1.55	14	14.8	3.12
M2916	36	30	80	21	133	101	28	206	14	5.1	548	46.9	92	10	36	6.7	1.44	5.8	1.0	5.5	1.06	3.17	0.47	3.05	0.45	5.7	1.29	14	13.8	2.23
VS 41i	62	–	–	–	27	253	21	75	15	–	293	69.7	197	–	129	21.8	2.00	–	0.9	–	–	–	–	0.98	0.35	2.1	0.77	20	14.2	1.77
SD 75	42	–	–	–	133	177	42	251	19	–	632	41.3	80	–	37	7.2	1.25	–	0.9	–	–	–	–	3.70	0.43	6.4	1.10	24	13.9	1.10
VS 44	57	–	–	–	55	216	27	337	19	–	375	49.0	91	–	37	6.7	1.76	–	0.7	–	–	–	–	3.01	0.67	8.1	0.97	23	14.1	0.81

Table 3
Sr and Nd isotopes for lamprophyres, lamproites, shoshonites, and calc-alkalic from Western Mediterranean

Region	Affinity	Sample	$^{87}Sr/^{86}Sr$	2σ	$(^{87}Sr/^{86}Sr)_i$	$^{143}Nd/^{144}Nd$	2σ	$(^{143}Nd/^{144}Nd)_i$
Western Alps	LMP	MEC 242	0.717024	±0.000005	0.716459	0.512032	±0.000006	0.512008
Western Alps	LMP	VDA 17	0.718180	±0.000007	0.717592	0.512014	±0.000005	0.511991
Western Alps	LMP	VDA 15	0.717280	±0.000007	0.716756	0.512020	±0.000005	0.511996
Western Alps	LMP	VDA 03	0.718024	±0.000007	0.717168	0.512026	±0.000005	0.512002
Western Alps	LMP	MEC 247	0.717894	±0.000008	0.716446	0.512034	±0.000006	0.512010
Western Alps	SHO	VDA 14	0.712412	±0.000007	0.712156	0.512125	±0.000005	0.512098
Western Alps	SHO	MEC 241	0.712135	±0.000007	0.711642	0.512118	±0.000007	0.512097
Western Alps	SHO	MEC 216	0.711099	±0.000007	0.710694	0.512118	±0.000005	0.512097
Western Alps	HKCA	VDA 08	0.711397	±0.000007	0.711258	0.512265	±0.000005	0.512242
Western Alps	HKCA	KAW 697a	0.710258	±0.000007	0.710131	0.512325	±0.000004	0.512302
Western Alps	HKCA	VDA 10	0.708096	±0.000006	0.707888	0.512241	±0.000005	0.512216
Western Alps	HKCA	MEC 251	0.711673	±0.000007	0.711519	0.512263	±0.000004	0.512241
Western Alps	HKCA	MEC 240	0.709197	±0.000006	0.708987	0.512313	±0.000006	0.512295
Corsica	LMP	SIS 07	0.712575	±0.000006	0.712298	0.512169	±0.000004	0.512162
Corsica	LMP	SIS 04	0.712560	±0.000020	0.712264	0.512156	±0.000006	0.512149
Corsica	HKCA	CP 101	0.708765	±0.000006	0.708719	0.512351	±0.000005	0.512346
Corsica	HKCA	CP 110	0.710266	±0.000005	0.710213	0.512244	±0.000003	0.512239
Corsica	SHO	CP 54	0.708190	±0.000010	0.708135	0.512257	±0.000008	0.512254
Corsica	SHO	CP 105	0.708159	±0.000008	0.708077	0.512277	±0.000004	0.512273
Murcia-Almeria	LMP	SP 452	0.716470	±0.000006	0.716415	0.512051	±0.000005	0.512046
Murcia-Almeria	LMP	SP 055	0.716908	±0.000008	0.716666	0.512019	±0.000005	0.512014
Murcia-Almeria	LMP	SP 078	0.720358	±0.000007	0.719999	0.512031	±0.000005	0.512026
Murcia-Almeria	LMP	SP 077	0.720812	±0.000007	0.720458	0.512031	±0.000006	0.512025
Murcia-Almeria	LMP	SP 725	0.717521	±0.000008	0.717311	0.512019	±0.000005	0.512014
Murcia-Almeria	LMP	SP 723	0.717647	±0.000008	0.717426	0.512028	±0.000005	0.512023
Murcia-Almeria	LMP	SP 044	0.718071	±0.000008	0.717689	0.512044	±0.000006	0.512039
Murcia-Almeria	LMP	SP 050	0.718268	±0.000007	0.717928	0.512040	±0.000005	0.512035
Murcia-Almeria	LMP	SP 049	0.718196	±0.000008	0.717820	0.512051	±0.000005	0.512045
Murcia-Almeria	LMP	SP 035	0.720365	±0.000008	0.720177	0.512036	±0.000006	0.512029
Murcia-Almeria	LMP	SP 040	0.721627	±0.000007	0.721415	0.512050	±0.000004	0.512043
Murcia-Almeria	LMP	Alm 02	0.722728	±0.000007	0.722510	0.512013	±0.000005	0.512009
Murcia-Almeria	LMP	Alm 01	0.722831	±0.000008	0.722591	0.512024	±0.000005	0.512019
Murcia-Almeria	LMP	SP 011	0.721029	±0.000007	0.720729	0.512018	±0.000004	0.512013
Murcia-Almeria	SHO	Alm 27	0.710361	±0.000008	0.710243	0.512440	±0.000005	0.512432
Murcia-Almeria	SHO	Alm 39	0.715409	±0.000006	0.713300	0.512208	±0.000005	0.512200
Murcia-Almeria	SHO	Alm 21	0.714860	±0.000008	0.713646	0.512168	±0.000005	0.512160
Murcia-Almeria	SHO	Alm 28	0.713720	±0.000008	0.713124	0.512189	±0.000005	0.512182
Murcia-Almeria	SHO	Alm 40	0.716011	±0.000007	0.713454	0.512234	±0.000005	0.512227
Murcia-Almeria	HKCA	Alm 17	0.714010	±0.000007	0.713813	0.512185	±0.000005	0.512177
Murcia-Almeria	HKCA	Alm 34	0.716403	±0.000008	0.716102	0.512172	±0.000005	0.512165
Murcia-Almeria	HKCA	Alm 14	0.713900	±0.000007	0.713670	0.512184	±0.000004	0.512176
Murcia-Almeria	HKCA	Aml 31	0.715803	±0.000007	0.715584	0.512125	±0.000005	0.512117
Murcia-Almeria	CA	Alm 25	0.709967	±0.000006	0.709856	0.512393	±0.000006	0.512384
Murcia-Almeria	CA	Alm 13	0.713011	±0.000007	0.712853	0.512229	±0.000004	0.512221
Murcia-Almeria	CA	Alm 29	0.711354	±0.000007	0.711228	0.512252	±0.000005	0.512245
Murcia-Almeria	CA	Alm 32	0.710631	±0.000007	0.710429	0.512392	±0.000005	0.512383
Tuscany	LMP	ORC 01	0.715970	±0.000010	0.715791	0.512096	±0.000004	0.512094
Tuscany	LMP	OR 12	0.716150	±0.000010	0.715983	0.512091	±0.000006	0.512088
Tuscany	LMP	MVC100	0.717040	±0.000010	0.716723	0.512089	±0.000010	0.512086
Tuscany	LMP	VS 29	0.715809	±0.000010	0.715784	0.512118	±0.000007	0.512117
Tuscany	LMP	VS 28	0.715967	±0.000005	0.715943	0.512116	±0.000004	0.512115
Tuscany	SHO	VS 184	0.715934	±0.000009	0.715880	0.512051	±0.000005	0.512050
Tuscany	SHO	VS 106	0.714906	±0.000008	0.714859	0.512109	±0.000005	0.512108
Tuscany	SHO	VS 150	0.714120	±0.000011	0.714084	0.512139	±0.000005	0.512138
Tuscany	SHO	VS 151	0.713520	±0.000014	0.713487	0.512171	±0.000005	0.512170
Tuscany	SHO	VS 123	0.713496	±0.000007	0.713469	0.512194	±0.000003	0.512193
Tuscany	SHO	VS 202	0.714009	±0.000005	0.713980	0.512084	±0.000006	0.512083
Tuscany	SHO	VS 204	0.714896	±0.000007	0.714869	0.512075	±0.000004	0.512074
Tuscany	SHO	VS 159	0.715648	±0.000010	0.715612	0.512084	±0.000005	0.512083
Tuscany	SHO	VS 148	0.713385	±0.000008	0.713363	0.512091	±0.000003	0.512090
Tuscany	SHO	VS 200	0.713270	±0.000006	0.713246	0.512096	±0.000003	0.512095
Tuscany	SHO	VS 193	0.713657	±0.000008	0.713630	0.512116	±0.000004	0.512115
Tuscany	HKCA	VS 122	0.713860	±0.000010	0.713825	0.512180	±0.000006	0.512179
Sedimentary and metasedimentary rocks								
Umbria	Limestone	AM 07	0.707460	±0.000009	0.707453	0.511824	±0.000019	0.511798
Murcia-Almeria	Limestone	Alm10b	0.710440	±0.000008	0.710436	0.512046	±0.000004	0.512027
Tuscany	Limestone	SD 33	0.707551	±0.000006	0.707543	–	–	–
Southern latium	Limestone	ERN57	0.708841	±0.000007	0.708785	0.512151	±0.000004	0.512123
Tuscany	Marlstone	ST135/26	0.707669	±0.000007	0.707645	–	–	–
Tuscany	Marlstone	SD 49	0.708797	±0.000006	0.708683	–	–	–
Murcia-Almeria	Marlstone	Alm 07	0.709399	±0.000007	0.709307	0.512109	±0.000006	0.512081
Tuscany	Marlstone	SD 53	0.711234	±0.000007	0.710839	–	–	–
Tuscany	Shale	SD 50	0.729473	±0.000007	0.728156	–	–	–
Tuscan-Basement	Phyllites	SD 63	0.728423	±0.000007	0.726062	–	–	–

Table 3 (*continued*)

Region	Affinity	Sample	$^{87}Sr/^{86}Sr$	2σ	$(^{87}Sr/^{86}Sr)_i$	$^{143}Nd/^{144}Nd$	2σ	$(^{143}Nd/^{144}Nd)_i$
Sedimentary and metasedimentary rocks								
Tuscan-Basement	Phyllites	SD 59	0.724882	±0.000007	0.722862	–	–	–
Tuscan-Basement	Phyllites	SS 2242	0.736265	±0.000008	0.734927	–	–	–
Tuscan-Basement	Ga-micashist	SS 2076	0.726264	±0.000007	0.724835	–	–	–
Tuscan-Basement	Ga-micashist	M2916	0.738229	±0.000012	0.736335	0.511893	±0.000007	0.511867
Tuscan-Basement	Granulite	VS 41i	0.717663	±0.000008	0.717509	0.512066	±0.000008	0.512043
Tuscan-Basement	Gneiss	SD 75	0.721555	±0.000009	0.720474	0.512039	±0.000008	0.512012
Tuscan-Basement	Gneiss	VS 44	0.713971	±0.000010	0.713605	0.512108	±0.000007	0.512083

analysis of international and internal reference sample as unknown, and it has been found within the error levels of the two procedures.

Isotopic analyses Sr, Nd, and Pb (Tables 3 and 4) were performed at the Dipartimento di Scienze della Terra, University of Firenze (Avanzinelli et al., 2005). Acid wash with 6 N HCl+8 N HNO_3 has been prevently performed on the overall samples before digestion and Sr, Nd, and Pb purification. Then two splits of residual sample powder (20–30 mg each) were dissolved in a HF–HNO_3–HCl mixture (supra-pure quality for Sr and Nd, and ultra-pure quality for Pb). Sr and Nd fractions were separated following standard chromatographic techniques using AG50x8 and PTFE–HDEHP resins with HCl as eluent, whilst Pb fraction was separated using 150 μl of Sr-SPEC with HNO_3 and HCl as eluents (Deniel and Pin, 2001). The total procedural blanks were <200, <100, <300 pg for Sr, Nd, and Pb, respectively, resulting in negligible correction to the samples. Mass spectrometric analyses were performed on a Thermo Finnigan Triton-Ti thermal ionization mass spectrometer equipped with nine movable collectors. Sr and Nd isotope compositions were measured in dynamic mode and are reported normalised to $^{86}Sr/^{88}Sr=0.1194$ and $^{146}Nd/^{144}Nd=0.7219$ (Thirlwall, 1991), respectively. Exponential-

Table 4
Lead isotopes for Lamproites and lamprophyres, shoshonites, and calc-alkalic rocks from Western Mediterranean

Region	Affinity	Sample	$^{206}Pb/^{204}Pb$	$^{207}Pb/^{204}Pb$	$^{208}Pb/^{204}Pb$	μ	*k*	$(^{206}Pb/^{204}Pb)_i$	$(^{207}Pb/^{204}Pb)_i$	$(^{208}Pb/^{204}Pb)_i$
Western Alps	LMP	MEC 242	18.910	15.702	39.511	52.85	6.05	18.664	15.691	39.036
Western Alps	LMP	VDA 15	18.879	15.719	39.351	43.05	5.81	18.678	15.710	38.980
Western Alps	LMP	VDA 03	18.690	15.717	39.093	13.74	6.18	18.626	15.714	38.967
Western Alps	LMP	MEC 247	18.724	15.719	39.095	11.81	5.78	18.669	15.716	38.993
Western Alps	SHO	VDA 14	18.847	15.681	39.031	39.38	3.40	18.663	15.672	38.832
Western Alps	SHO	MEC 241	18.993	15.693	39.278	67.06	4.88	18.680	15.679	38.792
Western Alps	SHO	MEC 216	19.037	15.694	39.490	75.01	4.64	18.687	15.678	38.973
Western Alps	HKCA	VDA 08	18.727	15.671	38.918	15.77	4.12	18.653	15.667	38.822
Western Alps	HKCA	KAW 697a	18.706	15.672	38.909	23.46	3.60	18.597	15.666	38.783
Western Alps	HKCA	VDA 10	18.688	15.670	38.916	9.27	4.45	18.645	15.668	38.855
Western Alps	HKCA	MEC 240	18.723	15.679	38.868	23.25	3.65	18.615	15.674	38.742
Corsica	LMP	SIS 04	18.864	15.698	39.342	24.87	8.50	18.808	15.696	39.190
Corsica	HKCA	CP 101	18.735	15.702	39.086	6.83	3.72	18.727	15.702	39.077
Corsica	SHO	CP 54	18.667	15.664	38.993	20.34	6.53	18.652	15.663	38.963
Corsica	SHO	CP 105	18.678	15.645	38.989	20.80	5.10	18.663	15.644	38.965
Murcia-Almeria	LMP	SP 452	18.813	15.706	39.127	28.42	3.90	18.783	15.705	39.090
Murcia-Almeria	LMP	SP 078	18.815	15.707	39.092	24.69	3.79	18.788	15.705	39.059
Murcia-Almeria	LMP	SP 725	18.803	15.711	39.111	14.12	5.00	18.787	15.710	39.086
Murcia-Almeria	LMP	SP 049	18.786	15.707	39.152	20.49	4.15	18.764	15.706	39.122
Murcia-Almeria	LMP	SP 040	18.752	15.695	39.055	7.28	5.21	18.743	15.695	39.040
Murcia-Almeria	LMP	Alm 02	18.808	15.691	39.029	23.02	4.21	18.786	15.690	38.998
Murcia-Almeria	LMP	Alm 01	18.815	15.697	39.046	25.40	4.18	18.790	15.696	39.012
Murcia-Almeria	LMP	SP 011	18.828	15.694	39.065	31.74	4.00	18.797	15.693	39.025
Murcia-Almeria	SHO	Alm 27	18.854	15.676	38.923	11.03	2.58	18.838	15.676	38.910
Murcia-Almeria	SHO	Alm 39	18.812	15.693	39.035	7.13	2.17	18.802	15.692	39.028
Murcia-Almeria	SHO	Alm 21	18.794	15.684	38.986	7.78	2.21	18.783	15.684	38.978
Murcia-Almeria	SHO	Alm 28	18.869	15.689	38.984	6.98	3.74	18.859	15.688	38.972
Murcia-Almeria	HKCA	Alm 17	18.783	15.684	39.013	7.68	1.87	18.772	15.684	39.006
Murcia-Almeria	HKCA	Alm 34	18.904	15.682	38.972	8.86	2.58	18.891	15.681	38.962
Murcia-Almeria	HKCA	Alm 14	18.782	15.686	39.015	6.62	1.81	18.773	15.685	39.010
Murcia-Almeria	HKCA	Aml 31	18.807	15.687	39.030	5.84	1.83	18.798	15.687	39.025
Murcia-Almeria	CA	Alm 25	18.835	15.689	38.955	9.65	2.50	18.821	15.689	38.944
Murcia-Almeria	CA	Alm 13	18.775	15.684	39.013	7.72	2.07	18.764	15.683	39.006
Murcia-Almeria	CA	Alm 29	18.874	15.671	38.869	4.15	3.41	18.868	15.671	38.863
Murcia-Almeria	CA	Alm 32	18.820	15.694	39.009	16.10	1.57	18.797	15.693	38.997
Tuscany	LMP	ORC 01	18.717	15.699	39.116	31.99	8.25	18.697	15.698	39.062
Tuscany	LMP	OR 12	18.708	15.693	39.117	27.96	7.02	18.690	15.692	39.077
Tuscany	LMP	MVC100	18.774	15.705	39.226	61.84	6.36	18.735	15.703	39.146
Tuscany	LMP	VS 29	18.677	15.678	38.918	12.96	4.87	18.675	15.678	38.915
Tuscany	SHO	VS 184	18.671	15.662	38.984	15.38	5.85	18.668	15.662	38.978
Tuscany	SHO	VS 123	18.710	15.701	39.101	12.69	5.51	18.707	15.701	39.096
Tuscany	SHO	VS 204	18.691	15.662	38.994	8.82	6.97	18.690	15.662	38.991
Tuscany	SHO	VS 159	18.684	15.663	39.022	11.10	7.05	18.683	15.663	39.018
Tuscany	SHO	VS 148	18.731	15.689	39.091	6.31	7.62	18.730	15.689	39.089
Sedimentary and metasedimentary rocks										
Murcia-Almeria	Marlstone	Alm 07	18.779	15.674	38.928	23.88	1.47	18.649	15.668	38.867
Tuscan-Basement	Granulite	VS 41i	18.220	15.626	38.332	5.62	8.29	18.189	15.625	38.251
Tuscan-Basement	Gneiss	SD 75	18.612	15.597	38.755	2.97	13.06	18.596	15.596	38.688
Tuscan-Basement	Gneiss	VS 44	18.507	15.624	38.715	2.30	17.99	18.494	15.623	38.643

law mass fractionation correction was used for all Sr and Nd isotopic data. Pb has been purified following the method described by Deniel and Pin (2001) using 100–150 μl Sr-spec resins in quartz fibres microcolumns. Pb separation efficiency was evaluated to be about 97%. Pb samples were loaded onto zone-refined Re filaments, with addition of 0.5 μl of silica gel and 1 μl of high-purity H_3PO_4 and measured in static mode with a ThermoFinnigan Triton TI©; average runs were measured at 1400 °C and yielded ~1.5 V of ^{208}Pb. Mass bias was monitored with repeated measurements of SRM 981 reference standard and we obtained a mass discrimination factor (ε) of 0.15% per a.m.u. The external reproducibility was: NBS 987 = 0.710251 ± 12 ($^{87}Sr/^{86}Sr_{triple}$; 2σ, n = 120); La Jolla = 0.511845 ± 7 ($^{143}Nd/^{144}Nd_{triple}$; 2$\sigma$, n = 55); SRM 981 = $^{208}Pb/^{204}Pb$ = 36.495 ± 23; $^{207}Pb/^{204}Pb$ = 15.423 ± 7; $^{206}Pb/^{204}Pb$ = 16.888 ± 6; $^{207}Pb/^{206}Pb$ = 0.91328 ± 15; $^{208}Pb/^{207}Pb$ = 2.3662 ± 4; $^{208}Pb/^{206}Pb$ = 2.1610 ± 7 (2σ, n = 45).

4. Lamproite to calc-alkaline magmatic associations of the Western Mediterranean

Lamproite to calc-alkaline volcanism in the Western Mediterranean is found in four restricted areas and it was active at different stages of the tectonic evolution of this region: during Oligocene in the western Alps, North-Western Italy (from 33 to 29 Ma, Venturelli et al., 1984a, and references therein); during Mio–Pliocene in Corsica, France, and nearby Capraia Island (from 14.2 to 4.6 Ma, Civetta et al., 1978; Barberi et al., 1986; Aldighieri et al., 2004); during the Miocene in Murcia and Almeria, South-Eastern Spain (from 11.7 to 6.3 Ma, Turner et al., 1999; Duggen et al., 2004, 2005, and references therein); during the Plio–Pleistocene in Tuscany, Central Italy (from 4.1 to 0.88 Ma, Ferrara and Tonarini, 1985; Conticelli et al., 1992, and references therein).

4.1. Western Alps

Post-Alpine (Oligocene) dykes and small lava flows with lamproitic, shoshonitic and high-K calc-alkaline natures are found within a restricted area in the internal zone of the North-Western Alps. These rocks are found mostly within the Sesia-Lanzo and Combin Units North of the Canavese Line (Fig. 1). They are the hypabissal remnant of a possibly more intense volcanic activity, which is found, close to the Canavese line, in the form of calc-alkaline to shoshonitic volcano-sedimentary unit in the internal portion of the cover series of the Sesia Zone. In addition, coeval intrusive rocks with differentiated compositions and mineralogy are found nearby in the Valle del Cervo and Biella areas, with petrologic affinity ranging from shoshonitic to calc-alkaline (Callegari et al., 2004). Lamproitic-like plagioclase-free ultrapotassic dykes (minette) have a micaceous appearance. They are characterised by intersertal textures with phlogopite (phl), clinopyroxene (cpx), and K-feldspar (kfs), accompanied by minor altered olivine (ol), and riebckite–arfvedsonite amphibole; accessory apatite, sphene, and Fe–Ti oxides are also present. Some carbonate of possible secondary origin is sometimes found (Table 1). Shoshonitic to high-K calc-alkaline plagioclase-bearing rocks (kersantite to spessartite) are found associated in space and time with ultrapotassic rocks. From a strictly classification view-point, lamproite-like rocks are better defined as lamprophyres (Owen, 2008), but we prefer to use the resemblance terminology suggested by Foley et al. (1987). The lamproite-like samples have consistently high MgO contents (8.64–13.6 wt.%; Venturelli et al., 1984a). In the SiO_2–K_2O diagram these samples plot close to the lamproitic samples from Corsica and Murcia-Almeria (Fig. 2). Shoshonitic rocks have strongly variable MgO content (1.88–10.9; Venturelli et al., 1984b; Guarnieri, 2007) overlapping at the low-silica end those from Corsica. High-K calc-alkaline rocks show also fairly variable MgO (1.08–7.52; Venturelli et al., 1984b; Guarnieri,

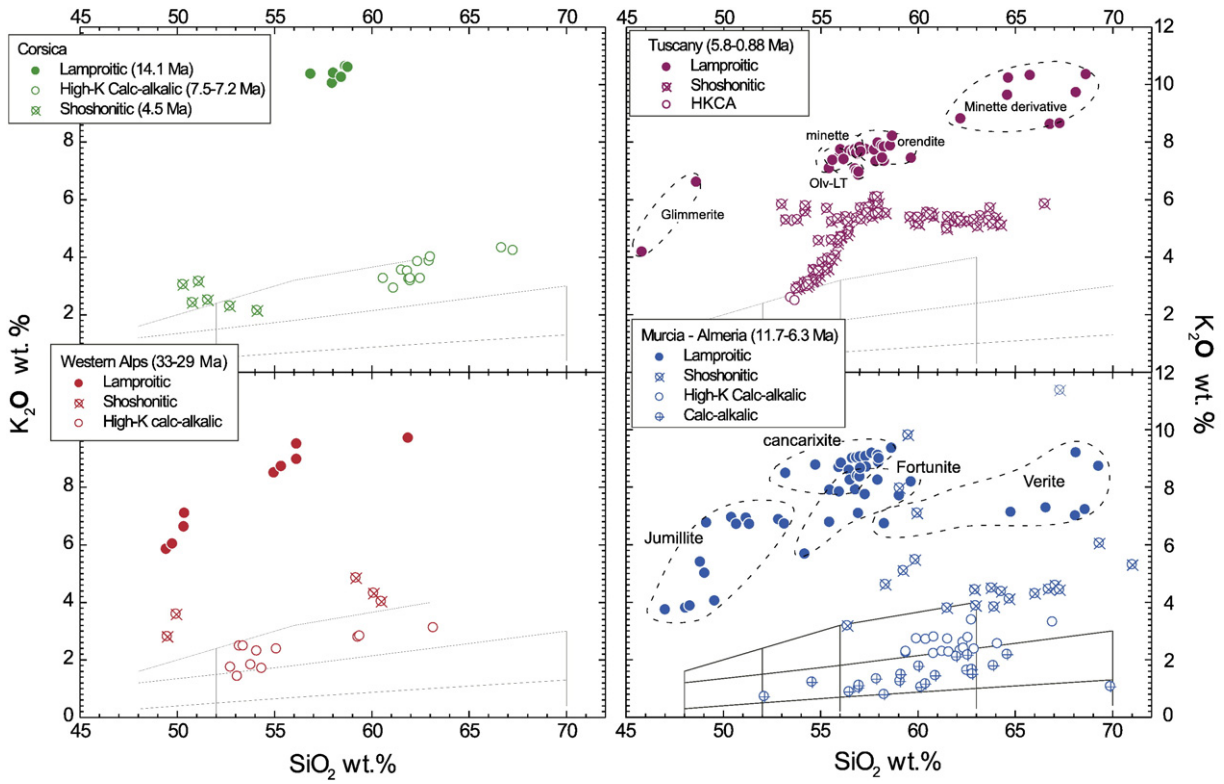

Fig. 2. K_2O (wt.%) vs. SiO_2 classification diagram for orogenic magmatic rocks (Peccerillo and Taylor, 1976) with reported ultrapotassic, shoshonitic and calc-alkaline coeval rocks from Western Alps (Venturelli et al., 1984a), Corsica (Peccerillo et al., 1988), Murcia-Almeria (Venturelli et al., 1984b; Toscani et al., 1990, 1995; Venturelli et al., 1991a, b; Contini et al., 1993; Guarnieri, 2007), and Tuscany (Conticelli and Peccerillo, 1990; Conticelli et al., 1992, 2001; Ferrari et al., 1995; Conticelli, 1998; Perini et al., 2003, 2004; Chelazzi et al., 2006; Conticelli's unpublished data).

2007), with data plotting on the potassium-rich basaltic andesite to rhyolite fields, partially overlapping high-K calc-alkaline rocks from Corsica and Murcia-Almeria (Fig. 2).

4.2. Corsica

Dykes, lava flows, and pyroclastic rocks of Mio–Pliocene ages are found closely associated in the north easternmost sector of Corsica Island (France) and nearby Northern Tyrrhenian Sea (Fig. 1). Sisco dykes are situated on the northeastern edge of Corsica Island, whereas lavas and pyroclastic rocks are found at Capraia Island, a few kilometers east of Sisco. Recent occurrence of submarine shoshonites, with enclaves of ultrapotassic nature, has been reported also at Cornacya Seamount, offshore south east of Sardinia, by Mascle et al. (2001). The Sisco dykes have a peralkaline index >1 and can be classified strictly as lamproite (Velde, 1967; Wagner and Velde, 1986; Peccerillo et al., 1988). Shoshonitic and high-K calc-alkaline rocks are found at Capraia Island. The lamproite samples are restricted to the Corsica Island and show slightly lower MgO contents (6.38–7.13 wt.%, Peccerillo et al., 1987, 1988) with low contents of MgO-rich phenocryst with respect to other Mediterranean lamproites. They have, however, the highest K_2O with intermediate contents of silica plotting on the right edge of an imaginary lamproitic trend (Fig. 2). Lamproites from Sisco are the oldest events (14.2 Ma; Civetta et al., 1978). High-K calc-alkaline rocks are from the oldest volcanic episode of the Capraia Island (i.e., 7.5–7.15 Ma). They are intermediate to felsic in composition (from high-K andesite to rhyolite), with MgO between 1.38 and 3.91 wt.%, overlapping the trend of high-K calc-alkaline rocks from Western Alps and Murcia-Almeria (Fig. 2). Shoshonitic rocks are the youngest episode of the Capraia Island (4.6 Ma) with MgO within the range between 2.63 and 8.18 wt.% (Chelazzi et al., 2006).

4.3. Murcia-Almeria

The Murcia-Almeria is the largest magmatic province among those studied (e.g., Benito et al., 1999). Shallow level submarine lava flows, hyaloclastites, dykes, plugs, cryptodomes, and pyroclastic flow are among the several way of emplacement of magmas in this area during Miocene. No deep sited magma emplacement has been recorded. Lamproite-like ultrapotassic rocks (8.08–6.37 Ma; Turner et al., 1999; Duggen et al., 2004, 2005) display the largest compositional variability among the overall Western Mediterranean ultrapotassic rocks (Fig. 2). MgO ranges from 1.73 to 16.7 wt.% (e.g., Venturelli et al., 1984b, 1991a, 1991b; Contini et al., 1993; Toscani et al., 1995; Guarnieri, 2007), showing a bell shaped differentiation pattern on a K_2O vs. silica diagram (Fig. 2). They have been classified as jumillite, cancarixite, fortunite, and verite, but we still prefer to use the general term lamproite to group all of them under a unique group of rocks following suggestions of Foley et al. (1987). Shoshonites are rare, most of them straddling the field between shoshonitic rocks and high-K calc-alkaline ones, but some plot along a trend connecting with lamproites at very high K_2O contents (Fig. 2). No high MgO rocks are found among shoshonitic ones (MgO = 0.43–4.08 wt.%). Miocene high-K calc-alkaline rocks are widespread along the Murcia-Almeria coast (10.4–6.2 Ma; Turner et al., 1999; Duggen et al., 2004; 2005). Their MgO ranges from 0.98 to 5.34 wt.%. HKCA rocks from Murcia-Almeria overlap those from Corsica (Fig. 2). Typical two pyroxene calc-alkaline rocks are found exclusively at Capo de Gata, Almeria, with a large compositional range (Toscani et al., 1990). They are coeval to shoshonitic and high-K calc-alkaline rocks (13.4–6.8 Ma; Turner et al., 1999; Duggen et al., 2004; 2005) with MgO between 1.47 and 7.03 wt.%: they plot on the lowermost part of the K_2O vs. SiO_2 diagram (Fig. 2).

4.4. Tuscany

Lava flows and pyroclastic rocks, dikes and plugs form the Tuscan Magmatic Province (Peccerillo et al., 1987; Innocenti et al., 1992). They are found within the northernmost portion of the Italian peninsula (Fig. 1). Plagioclase-free ultrapotassic rocks of the Tuscan Magmatic Province have a peralkaline index <1, but their mineralogy is typical of lamproite and of minette (Wagner and Velde, 1986; Conticelli et al., 1992; Cellai et al., 1994; Conticelli, 1998). Olivine is commonly the only phenocryst phase and usually encloses Al-poor/Cr-rich euhedral spinel. Phlogopite and Al-poor clinopyroxene are the most abundant phases in the groundmass; sanidine is ubiquitous. Lamproite-like rocks from Tuscany display a large MgO range from 0.98 to 9.58 wt.% but lower K_2O at comparable SiO_2 contents with respect to other lamproite-like rocks (Fig. 2). Shoshonites are abundant, and they have the most mafic compositions among the overall Mediterranean shoshonites (Conticelli et al., 2007; Perini et al., 2000, 2003, 2004; authors' unpublished data). In addition two divergent trends are also

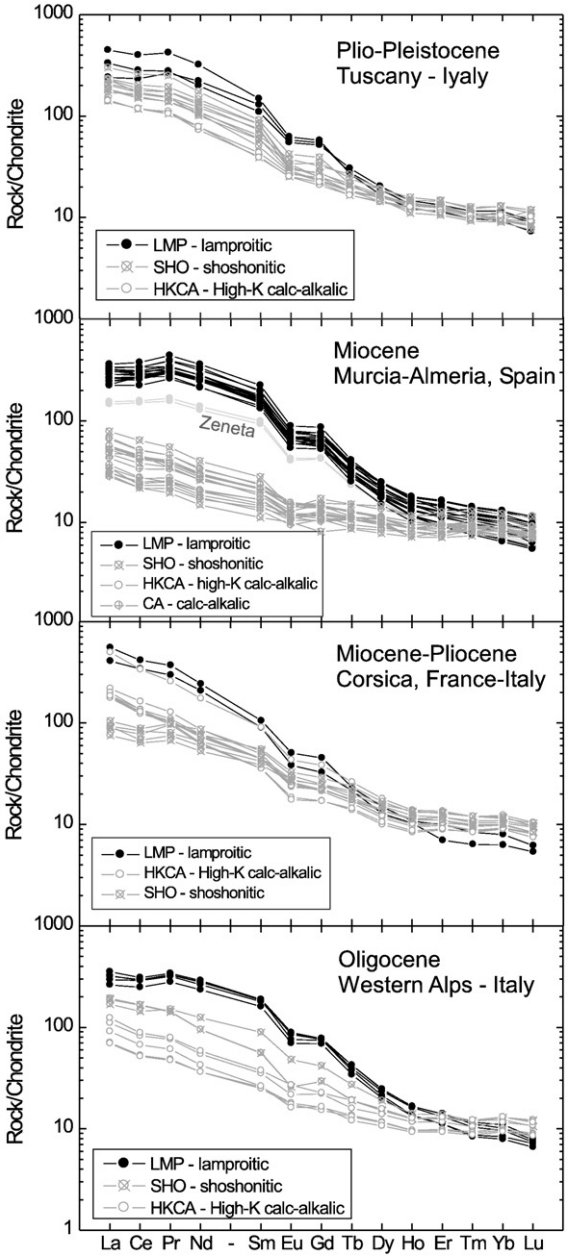

Fig. 3. Chondrite-normalised Rare Earth Elements patterns for samples from Western Mediterranean Orogenic areas. Normalising values are from Haskin et al. (1966). Note that Plio–Pleistocenic volcanic rocks from Tuscany have REE patterns significantly different, in terms of total abundances, modality, and fractionation, from those of Murcia-Almeria, Corsica, and Western Alps.

shown in the K_2O vs. SiO_2 diagram (Fig. 2). One trend, made up by rocks with similar MgO contents, connects lamproites with the field of high-K calc-alkaline rocks; a second trend, in which K_2O decreases slightly with increasing silica, connects high-K shoshonites with felsic high-K calc-alkaline rocks (Fig. 2). Rocks belonging to the second trend display typical two pyroxene assemblage with orthopyroxene often mantled by clinopyroxene (Ferrari et al., 1996). Two pyroxene high-K calc-alkaline rocks are rare and restricted to strongly differentiated types (i.e., Tolfa-Manziana; Ponza Island) (Pinarelli, 1991; Conte and Dolfi, 2002).

5. Trace element distributions

The rocks under consideration are variably enriched in incompatible trace elements, which positively correlate with K_2O at almost constant high MgO contents (Table 2). Lamproites generally have the highest Rare Earth Element contents (i.e., REE), but significant differences occur among the different provinces. Eu negative anomalies are common as well as a slight deviation from regular enrichment of La and Ce (Fig. 3). Chondrite-normalised Heavy Rare Earth Element (HREE) patterns cross cut those of shoshonitic, and high-K calc-alkaline rocks (Fig. 3). HREE of lamproites from Tuscany have $(Tb/Yb)_N$ values approaching those of associated shoshonitic, and high-K calc-alkaline rocks. REE abundances decrease regularly with decreasing K_2O from lamproite to calc-alkaline rocks in all Mediterranean provinces (Fig. 3; Table 2). Shoshonites from Corsica have distinctive REE patterns with respect to other shoshonites. They overlap the values of high-K calc-alkaline rocks for HREE, with clear inversion of enrichment of Light REE (LREE).

Primordial mantle normalised incompatible trace elements distribution (i.e., spider diagrams, Fig. 4), shows fractionation of High Field Strength Elements (HFSE), except Th, with respect to Large Ion Lithophile Elements (LILE), a typical characteristic of orogenic suites (e.g., Hoffman, 1996). This pattern is similar to that of Roman Province leucite-bearing rocks, Balkan lamproites, and arc rocks from the Aeolian and South Aegean volcanic arcs (e.g., Francalanci et al., 1993, 1999, 2004, 2007; Peccerillo, 2005; Perini et al., 2004; Prelević et al., 2004, 2005). The spider diagrams show troughs at Ba, Ta, Nb, and Ti, and peaks at Cs, Th, U, and Pb (Fig. 4). Beside these similarities, however, slight differences are observed among the most MgO-rich rocks of each Mediterranean magmatic province. Pb abundances are extremely variable with Murcia-Almeria being the most enriched and Corsica the least enriched ones. Corsica lamproite indeed shows different behaviour for Cs, U, and Pb with respect to rocks of other provinces and of associated shoshonites and calc-alkaline rocks, beside lack of Ti through; Western Alps rocks are characterised by a negative spike at Rb (Fig. 4). Th enrichments and U/Th values are also distinctively different in lamproites from the different provinces. U and Th enrichments are typically >1000× Primordial Mantle values (Sun and McDonough, 1989) only in shoshonites from Corsica and Tuscany (Fig. 4). P depletion in shoshonites and (high-K) calc-alkaline rocks is a peculiar characteristic of Tuscany, Corsica and Murcia-Almeria, but is almost missing in those from Western Alps (Fig. 4).

6. Radiogenic isotopes

Sr, Nd, and Pb isotopic compositions have been determined on selected samples. Lamproitic rocks display distinctive isotopic compositions with respect to associated shoshonitic, high-K calc-alkaline, and calc-alkaline rocks. In addition, lamproites from different Western Mediterranean provinces are far from having homogeneous isotopic compositions (Tables 3 and 4).

6.1. Western Alps

Oligocene lamproites from Western Alps have initial $^{87}Sr/^{86}Sr_i$ and initial $^{143}Nd/^{144}Nd_i$ values ranging from 0.71759 to 0.71645 and from 0.51201 to 0.51199, respectively. Initial lead isotopic values display a larger variability (i.e., $^{206}Pb/^{204}Pb_i = 18.66–18.50$; $^{207}Pb/^{204}Pb_i = 15.70–15.68$; $^{208}Pb/^{204}Pb_i = 39.04–38.67$; Table 4). $^{87}Sr/^{86}Sr_i$ values decrease rapidly passing from lamproites through shoshonites (0.71216–0.71069) to high-K calc-alkaline rocks (0.71152–0.70789), whereas

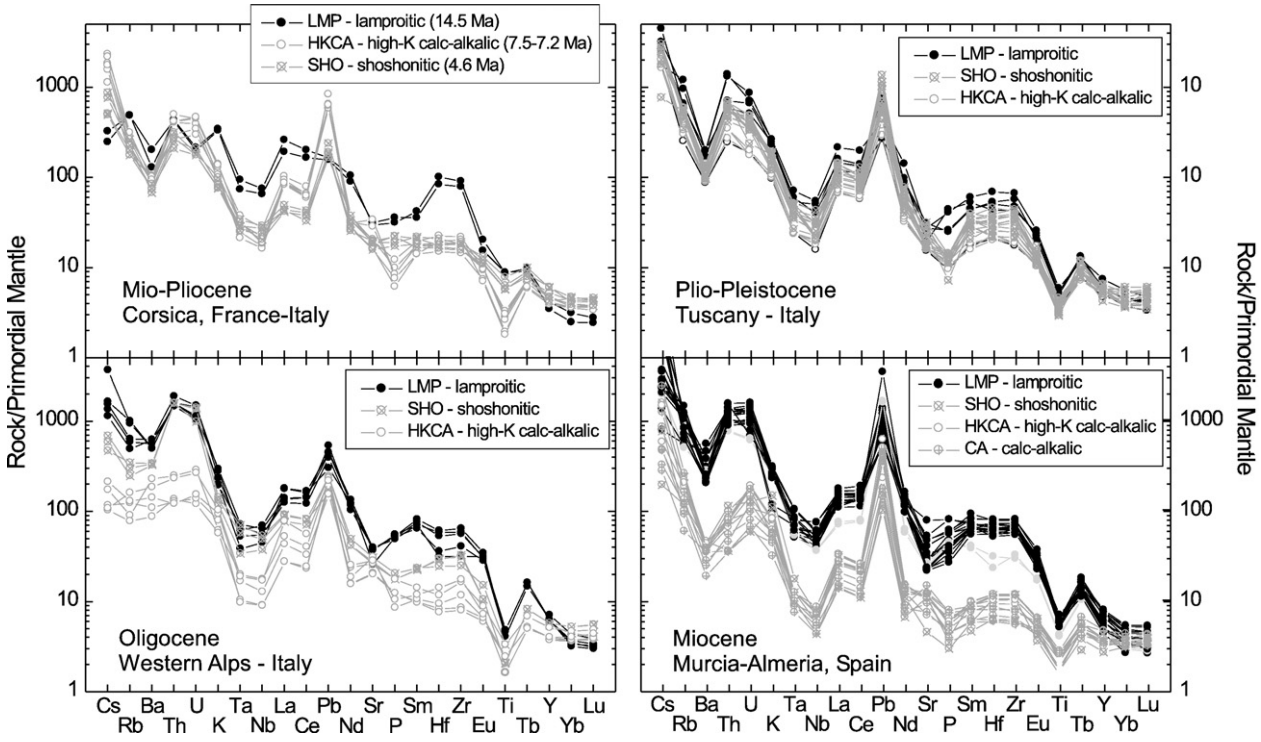

Fig. 4. Spider diagrams for the studied rocks with values normalised to Primordial Mantle (Sun and McDonough, 1989). Note that Miocenic volcanic rocks from Tuscany have no or small Pb positive spike with small Hf/Zr fractionation. On the other hand Murcia-Almeria and Tuscany rocks show the largest Pb positive spikes.

$^{143}Nd/^{144}Nd_i$ values increase through shoshonites (0.512097/8) to high-K calc-alkaline rocks (0.51230–0.51222; Fig. 5). Pb isotopes display a more complex picture. Shoshonitic rocks have $^{206}Pb/^{204}Pb_i$ (18.82–18.66) values higher than those of lamproites, with comparable $^{207}Pb/^{204}Pb_i$ (15.68–15.67) and $^{208}Pb/^{204}Pb_i$ (38.97–38.79) values (Fig. 6); high-K calc-alkaline rocks, however, have $^{206}Pb/^{204}Pb_i$ (18.65–18.60), $^{207}Pb/^{204}Pb_i$ (15.67–15.66), and $^{208}Pb/^{204}Pb_i$ (38.86–38.74) lower than shoshonites and similar to lamproites.

6.2. Corsica

Lamproites from Corsica have lower $^{87}Sr/^{86}Sr_i$ (0.71230–0.71226) and higher $^{143}Nd/^{144}Nd_i$ (0.51215/6) values than those of the Western Alps. Initial lead isotopic values are also higher than those of Western Alps lamproitic rocks (i.e., $^{206}Pb/^{204}Pb_i = 18.79$; $^{207}Pb/^{204}Pb_i = 15.69$; $^{208}Pb/^{204}Pb_i = 39.18$; Table 4). Analogously to Western Alps, $^{87}Sr/^{86}Sr_i$ values decrease rapidly passing from lamproites to associated rocks but shoshonites have lower values (0.70814–0.70808) than high-K calc-alkaline rocks (0.71021–0.70872), whereas $^{143}Nd/^{144}Nd_i$ values increase through shoshonites (0.51227–0.51225) to high-K calc-alkaline rocks (0.51235–0.51224; Fig. 5). The same holds true for initial leads isotopic values, which decreases passing through high-K calc-alkaline rock (i.e., $^{206}Pb/^{204}Pb_i = 18.73$; $^{207}Pb/^{204}Pb_i = 15.70$; $^{208}Pb/^{204}Pb_i = 39.08$), to shoshonite (i.e., $^{206}Pb/^{204}Pb_i = 18.66–18.65$; $^{207}Pb/^{204}Pb_i = 15.66–15.64$; $^{208}Pb/^{204}Pb_i = 38.97–38.96$). Shoshonites are younger than high-K calc-alkaline rocks, thus isotopic variation pattern is also correlated with time (Fig. 6).

6.3. Murcia-Almeria

Miocene lamproites from Murcia-Almeria have low and almost constant $^{143}Nd/^{144}Nd_i$ (0.51205–0.51201) values, but high and largely variable $^{87}Sr/^{86}Sr_i$ (0.72259–0.71642) values. These are among the most extreme isotopic values of the entire Western Mediterranean region (Table 3) and overlap the field of upper crustal continental rocks (Table 3). A narrow range of initial Pb isotopic values is observed (i.e., $^{206}Pb/^{204}Pb_i = 18.80–18.74$; $^{207}Pb/^{204}Pb_i = 15.71–15.69$; $^{208}Pb/^{204}Pb_i = 39.12–39.00$), which are among the highest isotopic values of the entire dataset (Table 4; Fig. 6). Decrease of $^{87}Sr/^{86}Sr_i$ and increase of $^{143}Nd/^{144}Nd_i$ values are observed passing from high-K calc-alkaline (0.71610–0.71367; 0.51218–0.51212), to calc-alkaline rocks (0.71285–0.70986; 0.51238–0.51222). Shoshonites display isotopic values similar to those of calc-alkaline rocks (0.71365–0.71024; 0.51243–0.51216; Table 3, Fig. 5). On the other hand, a characteristic trend is observed for initial lead isotopic variations. Passing from lamproite to associated rocks, initial lead isotopic values plot along an opposite trend with respect to that of rocks from other regions. $^{206}Pb/^{204}Pb_i$ increases with linear decreasing of $^{207}Pb/^{204}Pb_i$ and $^{208}Pb/^{204}Pb_i$ (Fig. 6).

6.4. Tuscany

Plio–Pleistocene lamproite (minette and lavas) from Tuscany have among the lowest $^{87}Sr/^{86}Sr_i$ (0.71672–0.71579) and the highest $^{143}Nd/^{144}Nd_i$ (0.51212–0.51209) values, respectively, among the Western Mediterranean lamproitic rocks (Fig. 5). With respect to other Western Mediterranean lamproitic rocks Tuscan lamproites show a larger Pb isotopic range reaching values at low $^{207}Pb/^{204}Pb_i$ and $^{208}Pb/^{204}Pb_i$ (Fig. 6) similar to those measured for shoshonitic rock from Tuscany and Corsica. With decreasing K_2O contents, at almost constant MgO abundance, $^{87}Sr/^{86}Sr_i$ values decrease linearly passing from shoshonites (0.71588–0.71325) to high-K calc-alkaline rocks (0.71347), whereas $^{143}Nd/^{144}Nd_i$ values do the opposite (Fig. 5).

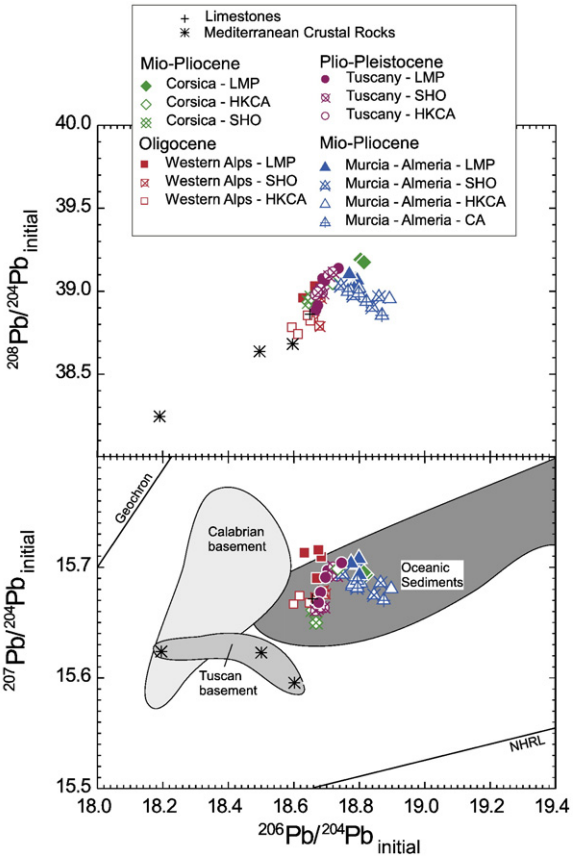

Fig. 6. $^{207}Pb/^{204}Pb$, and $^{208}Pb/^{204}Pb$ vs. $^{206}Pb/^{204}Pb$ for ultrapotassic to calc-alkaline mafic rocks of the Western Mediterranean compared with fields for Tuscan and Calabrian basements (Francalanci et al., 1993; Ayuso et al., 1994; Conticelli et al., 2002) and Oceanic sediments (White et al., 1985; White and Dupré, 1986; Ben Othman et al., 1989; McDermott and Hawkesworth, 1991; Plank and Langmuir, 1998). Note that Murcia-Almeria rocks plot on a totally different trend from the other groups. No overlapping with the Lead isotopic values of Dora Maira high-P metamorphic rocks, plotting outside of the picture: $^{206}Pb/^{204}Pb = 20.27–20.89$; $^{207}Pb/^{204}Pb = 15.76–15.80$; $^{208}Pb/^{204}Pb = 41.01–42.26$ (Tilton et al., 1989a,b), is observed.

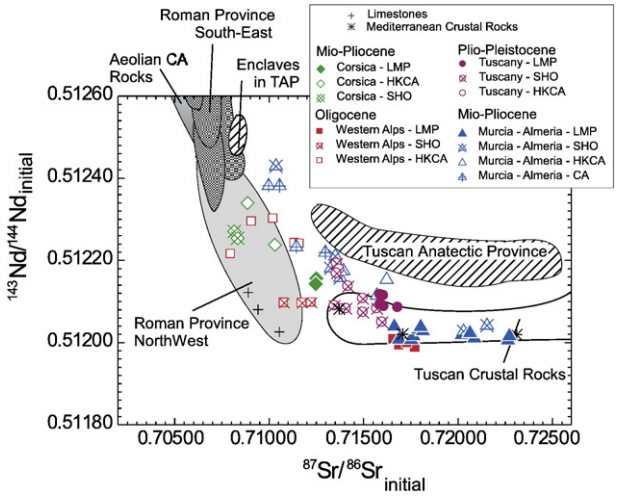

Fig. 5. Initial $^{143}Nd/^{144}Nd$ vs. initial $^{87}Sr/^{86}Sr$ for ultrapotassic to calc-alkaline mafic rocks of the Western Mediterranean compared with rocks from Roman Province, Aeolian Arc, and Tuscan Anatectic Province (Conticelli et al., 2002, 2007, 2008 and references therein; Francalanci et al., 2007; Tommasini et al., 2007). Note the distinctive differences between Corsica rocks and the rest, and that no overlapping among different provinces is observed.

7. Discussion

During the evolution of the Western Mediterranean region, magmatism along destructive plate margins produced rocks with different petrologic affinities, from calc-alkaline to ultrapotassic. In the four provinces under consideration, ultrapotassic rocks are rich in K_2O (7–14 wt.%), but poor in $Fe_2O_{3\ tot}$, CaO, Al_2O_3, and Na_2O relatively to typical mantle-derived primary magmas. On the other hand, MgO, Ni and Cr, are well within the values typical of mantle-derived primary magmas (Foley and Venturelli, 1989). Most of these high-MgO ultrapotassic rocks are characterised by $[(Na_2O+K_2O)/Al_2O_3]$ ratios <1 (0.70–0.94); only two samples have values >1 (1.08; SP 725, Murcia-Almeria; SIS 4, Corsica). Based on strict classification criteria most of them are lamprophyres (Le Maitre, 2002). According to Foley et al. (1987), however, they have a clear lamproitic affinity. In the areas under study, leucite-bearing ultrapotassic rocks are very rare in contrast to the nearby and younger ultrapotassic rocks of the Roman Magmatic Province, from which they are clearly distinguished. The most sticking feature of the four provinces studied is the time and spatial association of high-MgO lamproite-like rocks with shoshonitic, high-K calc-alkaline and calc-alkaline rocks. The overall ultrapotassic, shoshonitic and calc-alkaline rocks show many similarities in terms of distribution of trace elements and isotope geochemistry (Fig. 4), with typical fractionation of incompatible trace elements of orogenic magmas (Fig. 7). A further similarity between ultrapotassic and associated rocks is found in the strict correlation between K_2O and incompatible trace element contents (Fig. 8). Incompatible trace elements fractionation and isotopic enrichments argue for the presence of a clear crustal-derived signature in the overall Mediterranean lamproitic, shoshonitic, to calc-alkaline rock associations. Some differences, however, in the geochemical and isotopic signatures among the different provinces occur. When $^{87}Sr/^{86}Sr_i$ rather than an incompatible trace element is plotted against K_2O two distinct arrays are found (Fig. 8). The rocks from Western Alps, Murcia-Almeria, and Tuscany plot along an array at high initial $^{87}Sr/^{86}Sr$, which correlate positively with K_2O. On the other hand, the rocks from Corsica plot along a sub-parallel array at lower $^{87}Sr/^{86}Sr_i$ (Fig. 8).

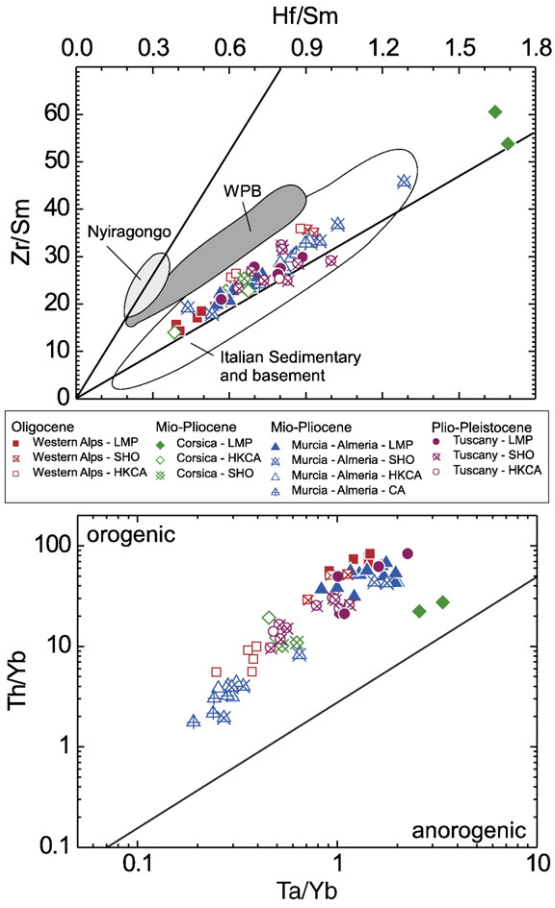

Fig. 7. Zr/Sm vs. Hf/Sm and Th/Yb vs. Ta/Yb for the studied rocks. Note that all of them fall well within the field of orogenic suites, overlapping the compositions of sedimentary and metasedimentary Italian and Spanish Continental Crustal rocks. Note that Corsica lamproites plot offset with respect to the general trend in the Th/Yb vs. Ta/Yb diagram approaching the orogenic/anorogenic divide with respect to other lamproitic rocks. On the other hand, on the Zr/Sm vs. Hf/Sm diagram Corsica lamproites still plot on the opposite end, with respect to other lamproitic rocks, of the general Mediterranean array, but also far away from within plate anorogenic magma.

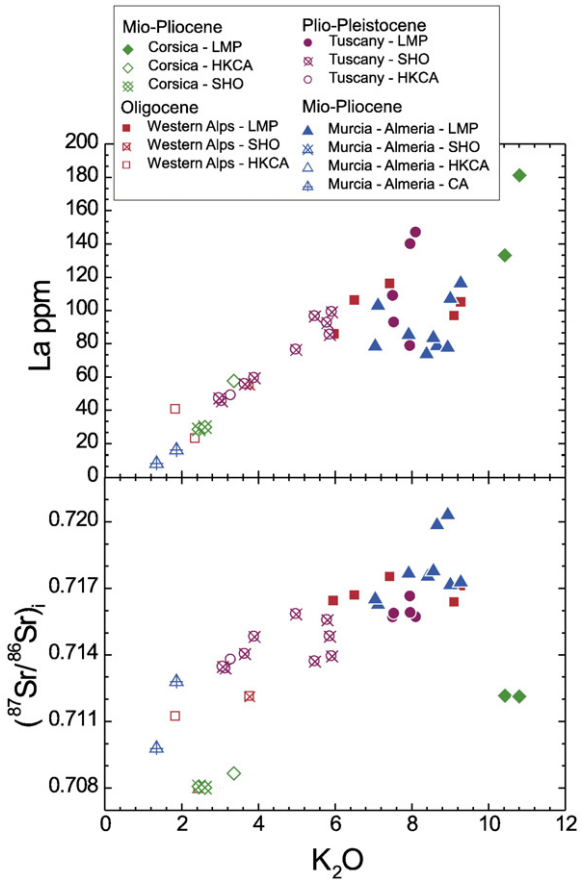

Fig. 8. La (ppm) and initial $^{87}Sr/^{86}Sr$ vs. K_2O wt.% for high-MgO ultrapotassic to calc-alkaline mafic rocks of the Western Mediterranean. Note that Corsica rocks plot on a distinct trend with respect to those from the other three provinces. In addition it is clear that there is a constant decreasing in the incompatible element contents and isotopic values with decreasing K_2O contents at similar degree of evolution. This speaks for a variation acquired by magmas directly in the mantle possible during partial melting of a heterogeneous mantle source.

7.1. The origin of the crustal signature

The mafic volcanic rocks of the Western Mediterranean show strong enrichments in radiogenic Sr and unradiogenic Nd isotopes with respect to mantle-derived volcanic rocks. In addition, lamproitic rocks, except Sisco, overlap continental crustal values (Fig. 5). The same holds true for lead isotopes with initial values well within the field of continental crustal rocks and oceanic sediments (Fig. 6); meanwhile initial isotopic values of Western Mediterranean lamproites plot, however, far from the values of crustal rocks of Dora Maira ($^{206}Pb/^{204}Pb$ = 20.27–20.89, $^{207}Pb/^{204}Pb$ = 15.76–15.80, and $^{208}Pb/^{204}Pb$ = 41.01–42.26; Tilton et al., 1989a,b), which have been

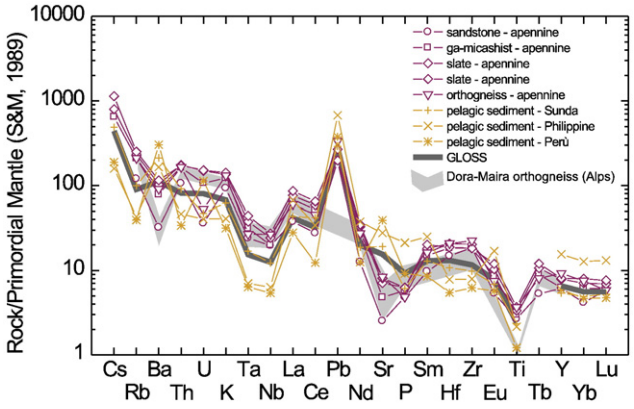

Fig. 9. Spider diagrams for the sedimentary and metasedimentary Continental Crustal rocks from several different Earth's localities normalised to Primordial Mantle to facilitate comparison with mafic high-MgO rocks (Sun and McDonough, 1989). Note that Western Mediterranean Continental Crustal rocks have similar patterns negative through at Ba, Ta, Nb, Sr, and Ti, meanwhile those from Sunda, Philippines and Peru have positive peaks at Sr and Ba. Then the similarity between patterns of ultrapotassic rocks from the Western Mediterranean and Dora Maira rocks does not uniquely speak for a strict relationship, because similar patterns are shown also by Apennine Continental Crustal rocks. Data from White et al. (1985); White and Dupré (1986); Ben Othman et al. (1989); McDermott and Hawkesworth (1991); Plank and Langmuir (1998); Peccerillo (1999), and this work.

taken as the possible crustal end-member in the genesis of lamproitic magmas (Peccerillo, 1999). Incompatible trace elements are also extremely fractionated with differential enrichments of large ion lithophile, Th, Hf, and Zr with respect to Sr and others high field strength elements (i.e., Ta, Nb, P, and Ti). These characteristics recall closely the distribution of trace elements in crustal rocks (Rudnick and Fountain, 1995). Particularly the strong positive spike at Pb is clearly distinctive of a recent addition of a crustal component (Fig. 9; Taylor and McLennan, 1985, 1988).

In spite of the high MgO contents of the ultrapotassic and associated rocks, some authors have taken all these characteristics as the evidence for a strong interaction (i.e., crustal assimilation) between magmas and crustal rocks during ascent to surface (e.g., Ferrara et al., 1986; Gasperini et al., 2002). To tackle this point, Conticelli (1998) has brought several arguments against crustal contamination in the genesis of the crustal-derived geochemical and isotopic characteristics of most of the Mg-rich Italian ultrapotassic rocks: 1) the high mg#, Ni and Cr contents of the most primitive samples; 2) the sub-aphyric textures, which exclude the possibility of acquisition of mafic character by accumulation of mafic phases; 3) the highly-forsteritic olivine on the liquidus; 4) the presence of mantle xenoliths in some lavas testifying the rapid ascent through the crust; 5) the occurrence of the strongest enrichments in terms of isotopes and trace elements in the lamproite-like products, which also generally display the highest MgO contents. Moreover, the trace elements contents of these rocks are, in many cases, higher than those of crustal rocks and sediments (e.g., Taylor and McLennan, 1985, 1988; Rudnick and Fountain, 1995; Plank and Langmuir, 1998) rendering their Sr, Nd, and Pb isotopic systems relatively immune to shallow level crustal contamination.

The result of long-term Sr isotopic ingrowths in a sub-continental lithospheric mantle has been argued to explain the strong enrichment of radiogenic Sr in lamproites from within plate setting (Davies et al., 2006). High field strength elements fractionation, however, is not affected by such a process. To explain this further geochemical characteristic found in many lamproites, Davies et al. (2006) claimed for the occurrence of residual rutile ± amphibole (Ionov and Hofmann, 1995) during partial melting; the possibility that either oceanic crust or sediments have been recycled into within plate lamproitic magma mantle sources has not been excluded (Murphy et al., 2002; Davies et al., 2006). Time ingrowth of Sr-isotopes may holds true for within plate continental lamproites, such as those of Aldan shield, but problems arise when interpreting Western Mediterranean lamproitic rocks, which are associated with high-MgO subduction-related magmatic rocks (i.e., minette, shoshonite, high-K basaltic andesite, basaltic andesite) at a continental destructive plate margin. In addition, covariation of isotopic crustal signature with K_2O contents is shown by the Western Mediterranean mafic lamproitic to calc-alkaline rocks (Tables 2 and 3). The same covariation is observed for incompatible trace element contents, with lamproites having the highest levels (Fig. 8). These geochemical and isotopic characteristics speak against a uniform isotopic reservoir within the upper mantle source of magmas, as it should be if long-time decay occurred in an isolated mantle source domain. In addition, Western Mediterranean ultrapotassic to calc-alkaline rocks are characterised by distinctive low U/Th ratios similarly to other high-MgO ultrapotassic to calc-alkaline rocks at plate margins (e.g., van Bergen et al., 1992; Francalanci et al., 1993, 2000, 2007; Carmichael et al., 1996; Altherr et al., 2004; Cvetković et al., 2004a; Avanzinelli et al., 2008, and references therein). On the other hand, within plate lamproites have opposite U/Th values (e.g., Mitchell and Bergman, 1991; Murphy et al., 2002; Davies et al., 2006; Mirnejad and Bell, 2006). Eventually, to achieve the strong enrichment in radiogenic Sr and unradiogenic Nd isotopes of the overall Western Mediterranean lamproites rocks their mantle sources should have been isolated for a period longer than 1.5 Ga (Turner et al., 1999).

Such a long time would have allowed a general Sr and Nd isotopic homogenisation of the magma source/s, leading to a common isotopic signature for the overall high-MgO magmas produced. This is obviously not consistent with the high isotopic variability observed in the Western Mediterranean provinces (Table 3; Fig. 5), which requires either a non-unique ancient magma source or the absence of isotopic homogenisation within their mantle sources, and thus relatively recent metasomatism. We believe the latter most feasible; the high Th/U, and Pb/U ratios of Western Mediterranean high-Mg rocks would give, in fact, lead isotopic values (recalculated at the time of the possible Proterozoic enriching event) unrealistic for any possible Earth's component. The very high Pb of these high-MgO magmas indeed tends to buffer the time ingrowth effect on the isotopic values at least on the $^{206}Pb/^{204}Pb$ isotopic ratio.

In excluding crustal contamination and long-term isolation of the sub-continental lithospheric mantle we must argue that crustal signature is a primary characteristic of the source of magmas acquired through sediment recycling into the upper mantle. Sedimentary and metamorphic rocks from the Alpine and Apennine have similar incompatible trace element patterns (Table 2; Fig. 9) closely resembling the Western Mediterranean ultrapotassic and associated rocks patterns (Fig. 4). Moreover also the isotopic compositions of the studied rocks are similar to the values of modern oceanic pelagic sediments (Fig. 6; White et al., 1985; Ben Othman et al., 1989; Hamelin et al., 1990; Plank and Langmuir, 1998). Decoupling of Th from other HFS elements is a typical feature of recycled sediments into the upper mantle at destructive plate margins through subduction (Elliott et al., 1997). Th positive anomalies are shown by most of the studied lamproites and associated rocks with normalised Th/U >1 arguing for sediment recycling through melts rather than fluids.

Previous studies have already interpreted lamproitic magmas as the products of partial melting of metasomatised sub-continental refractory lithospheric mantle (Foley et al., 1987; Foley and Venturelli, 1989; Conticelli, 1998; Prelević and Foley, 2007). Recycled sediments, in forms of fluids and/or melts re-fertilise the refractory lithospheric mantle establishing a new mineralogy, possibly accommodated in a metasomatised vein network (Foley, 1992). However, some issues remain debated such as: i) the possibility of large amounts of sediments recycling, which is needed to provide the strong compositional and isotopic signature observed in lamproites; ii) the typology

of the metasomatising agents in the different provinces; iii) the mechanism for producing, within the same magmatic province, ultrapotassic magmas associate to sub-alkaline calc-alkaline magmas.

Sediments recycling within the mantle have long been questioned due to their lower densities than mantle rocks. Density changes with pressure in sedimentary rocks have been recently experimentally determined (Massonne et al., 2007). These experiments indicate that pelagic sediments during subduction acquire densities higher than mantle wedge peridotites, prior to reach P–T conditions of partial melting. However, conditions for entering large amounts of sediments into subduction might have been achieved when oceanic crust exhausted and then continental collision occurred. Once subducted the oceanic crust and the overlaying sediment successions undergo metamorphism, dehydration and possibly melting (e.g. Johnson and Plank, 1999; Schmidt et al., 2004; Kessel et al., 2005), then producing the metasomatic agents. When considering slab-derived components the distinction between fluids and melts becomes questionable, because most of the processes involved might occur at pressures above the second critical end point where only one phase can be present. According to Hermann et al. (2006), however, even at these high- or ultra-high pressure conditions the supercritical liquids can be described in terms of their composition and physical properties, and a distinction between fluid-like and melt-like liquids can be made. In the case of metapelites the second critical end point at about 3.5 GPa and 650 °C (Hermann et al., 2006). Above this critical end point a "supercritical field" does exist, where the "liquid" phase could have a composition comparable to aqueous fluids (i.e., at low T, >70 wt.% H_2O), hydrous melt (i.e. at high T, <30 wt.% H_2O) or could be in a transition zone where the solubility of trace elements rapidly increases with T (Hermann et al., 2006). Keeping that in mind, in the following discussion we will refer to either metasomatic fluids or melts, assuming that different metasomatic agents, whose composition depend on their partition coefficients between fluid/melt and residual solid, might be liberated at different depth and temperature.

A further aspect to be considered is that fluids and melts are likely to re-fertilise the mantle at different scales, according to their physical properties. Melts prefer to rise along an intricate pathway of fractures, then reacting with surrounding peridotitic mantle to produce fairly large veins with peridotite-modified paragenesis (Irving, 1980; Suen and Frey, 1987; Menzies et al., 1991; Foley, 1992; Shaw et al., 2005). Fluids on the other hand, may pervasively flow within the entire upper mantle through smaller fractures than melts, producing a largely cryptic metasomatised mantle after reaction with the peridotite. The composition of such metasomatised lithospheric mantle source, which will melt in different proportions to generate the erupted magmas, depends on a large numbers of factors; the most important are: i) the original composition of the lithospheric mantle; ii) the presence of fluids phases, their origin (i.e. oceanic crust or sediments) and composition; iii) the amount and composition of the metasomatic sediment-derived melts, which depends on the mineral assemblage and degree of melting of the original sediments assemblage.

An important consequence of such a complex scenario is that some characteristics of the studied magmas can be misinterpreted. Eu negative anomaly persistently occurs in the overall high-MgO samples (Fig. 3). This feature is generally ascribed to plagioclase fractionation, but plagioclase does not crystallise in lamproitic magmas. The lowest Eu^*/Eu values (0.6–0.7) are shown by lamproites, and tend to increase slightly passing from shoshonite to calc-alkaline rocks, approaching the unity (Fig. 10). Eu^*/Eu >1 is shown by calc-alkaline rocks from Murcia-Almeria (Fig. 10). Carbonate-free sedimentary rocks also show low Eu^*/Eu values (0.5–0.8), which increase with increasing carbonate component. Limestone from Italian region has Eu^*/Eu >1. Therefore recycling of sediments within the mantle source will provide the europium anomalies observed in the studied samples. The lowest values shown by lamproites agree with a higher amount of recycled sediments with respect to shoshonite, and calc-alkaline rocks,

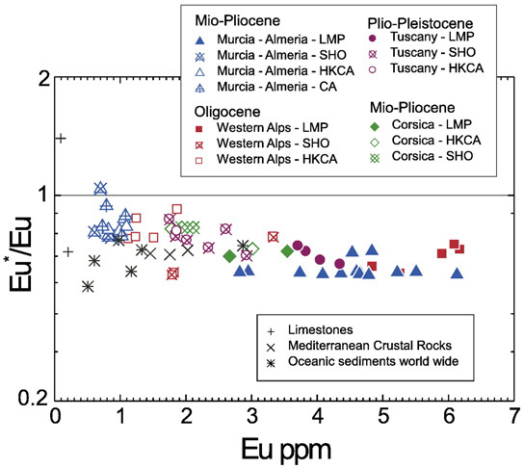

Fig. 10. Semi-logarithmic Eu^*/Eu values vs. Eu (ppm) diagram for lamproitic to calc-alkaline rocks of the Western Mediterranean region, and crustal sedimentary rocks of the Italian and Spanish regions. Note that lamproitic rocks show the lowest Eu^*/Eu values, overlapping the values of carbonate-free sedimentary rocks, but the highest Eu absolute contents among magmatic rocks. Sedimentary carbonate rocks show Eu^*/Eu values straddling the unity value. Following decreasing K_2O contents (passing from lamproitic to calc-alkalic rocks) Eu^*/Eu values increase accordingly.

suggesting that lamproitic magmas are from the most metasomatised portion of the mantle source located in the veins. Also consistent with this interpretation is the fractionation of the REE. Lamproitic rocks display highly fractionated HREE (Fig. 3). High MREE/HREE ratios are largely interpreted as indices of residual garnet during melting. It has been shown that U/Th disequilibria in potassic and ultrapotassic rocks (Avanzinelli et al., 2008) do not reflect the occurrence of residual garnet within the mantle source, but are due to the melting process of the sediments (Johnson and Plank, 1999). This confirms that the composition of the metasomatised portion of the mantle is strongly dominated by that of the sediment melts. Again, the lower extent of HREE fractionation in shoshonitic and HKCA rocks confirms that the sediment-related component is diluted in these magmas.

Given the large numbers on unknown parameter and the different provinces involved in this study any attempt of quantitative modelling is impossible. In the following paragraph we will firstly discuss the differences among the Western Mediterranean provinces focusing mostly on the lamproitic terms in order to investigate the nature of the possible contaminants. Subsequently we will investigate the processes responsible for the transition from lamproitic to shoshonitic and HKCA magmas in the various provinces, along with their time relationships.

7.2. Comparison between the different provinces

Considering Sr and Nd isotopes (Fig. 5), the ultrapotassic to calc-alkaline rocks from the different provinces of Western Mediterranean are distributed along a mixing line between a mantle and a pelitic sediment end-member (hatched field of Fig. 5). The concave hyperbolic shape of the distribution requires a sedimentary end-member with extremely low Sr/Nd ratio. Lamproitic samples are consistently the most enriched in radiogenic Sr among the rocks of each province. $^{87}Sr/^{86}Sr$ in lamproites is commonly decreasing from Murcia to Corsica, through Western Alps and Tuscany. At first glance this might suggest a rather simple scenario where the composition of the analysed rocks is simply dictated by the amount of recycled sediments. A closer look, however, highlights important differences between the provinces. Indeed, the Sr and Nd isotope variations are not coupled with Pb isotopes or trace element contents. Among lamproites Corsica samples display the most radiogenic Pb, followed by Murcia-Almeria, Tuscany and Western Alps. The overall pattern is

further complicated when shoshonitic to calc-alkaline rocks are considered, with the Murcia-Almeria rocks showing a clear trend towards higher $^{206}Pb/^{204}Pb$ but lower $^{207}Pb/^{204}Pb$ and $^{208}Pb/^{204}Pb$. In addition Tuscan lamproites show large variation in Pb isotopes despite almost constant $^{87}Sr/^{86}Sr$, but the opposite is observed in Murcia-Almeria lamproites. The different provinces of Western Mediterranean ultrapotassic to calc-alkaline rock are well distinguished in a diagram where initial $^{87}Sr/^{86}Sr$ vs. Ce/Sr values are plotted (Fig. 11). Each magmatic province draws different trends from a common depleted end-member (low $^{87}Sr/^{86}Sr$ and Ce/Sr) to three distinguished enriched ones at high Ce/Sr and variable Sr isotopic ratio, representative of the recycled sediment melts. Such features are compatible with melts from various siliciclastic sedimentary rocks (Ce/Sr = 0.69–0.90, $^{87}Sr/^{86}Sr$ = 0.71767–0.73627, $^{143}Nd/^{144}Nd$ = 0.51189–0.51206; Table 3), also reported in Fig. 11; no other Earth's reservoir has Ce/Sr as high as those found in Western Mediterranean ultrapotassic rocks (Figs. 11 and 12) and in particular carbonate-rich sediments have very low Ce/Sr (Fig. 11).

From these data we suggest that different terrigenous sedimentary rocks have been involved in the crustal recycling process producing different metasomatic agents. These affected the mantle sources of ultrapotassic rocks providing the entire compositional spectrum observed in the Western Mediterranean. Some further considerations are required, however, to explain the low $^{87}Sr/^{86}Sr$ of Corsica rocks. The most feasible explanation implies a lower amount of sediments recycled within their mantle source with respect to the other provinces. However, this does not explain the higher radiogenic Pb and/or the comparable Ce/Sr ratios.

In the previous paragraph we interpreted the Eu anomalies measured in most of the studied rocks as inherited from clay-rich sediments, pointing out that carbonate-rich sediments has higher Eu^*/Eu ratios. Among lamproites, the Sisco one has the lowest Eu contents and the highest Eu^*/Eu values, respectively (Fig. 10). This indicates a higher amount of carbonate component in the recycled sediments, which is also consistent with the less radiogenic Sr and high radiogenic Pb of Corsica samples. On the other hand, the high Ce/Sr values of Corsica ultrapotassic rocks, which is similar to that of the other provinces (Fig. 11), argues against this hypothesis. As a possible explanation to the high Ce/Sr we argue for the presence of residual wollastonite during the carbonate-rich sediment melting. Due to its relatively high D_{Sr}/D_{Ce} (Law et al., 2000), residual wollastonite would buffer the Ce/Sr of the metasomatic melts at higher values relative to the original carbonate. However, the presence of a carbonate-rich component in the recycled sediment should have produced also an increase in other tracers; Th/U of carbonates is considerably lower than in pelitic sediments and is not affected by residual wollastonite, but the Th/U of Corsica samples is not different from that of the other provinces.

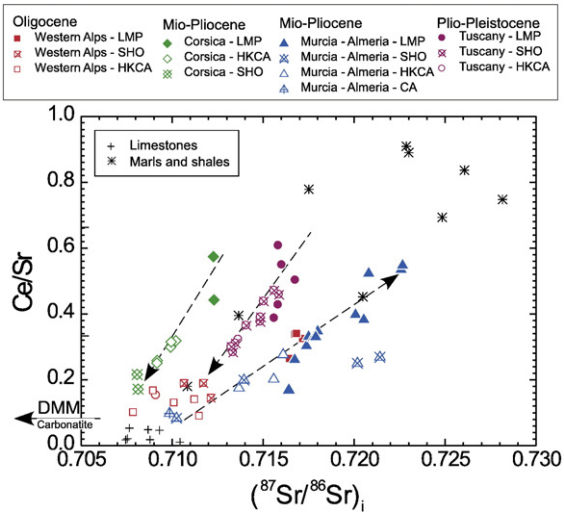

Fig. 11. Ce/Sr vs. initial $^{87}Sr/^{86}Sr$ for ultrapotassic to calc-alkaline mafic rocks of the Western Mediterranean. Note that ultrapotassic to calc-alkaline associations from different magmatic provinces plot along different trends speaking for different metasomatic events affecting possibly slightly different lithospheric upper mantle reservoirs.

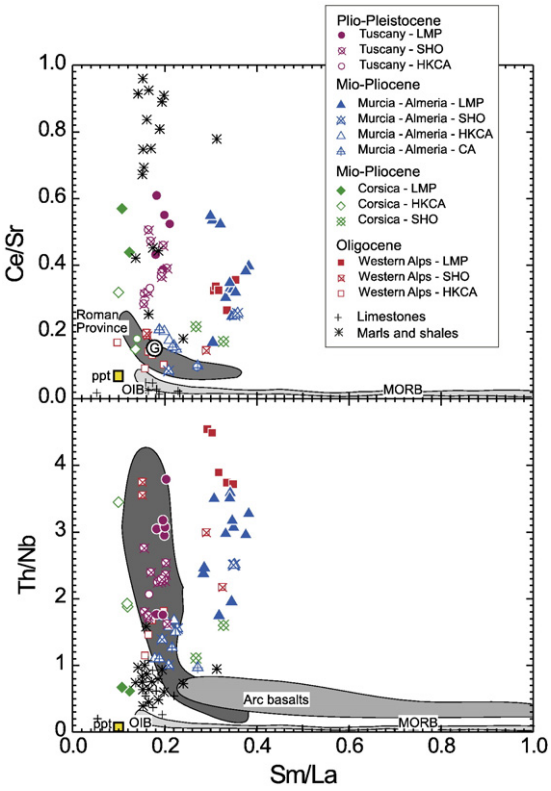

Fig. 12. Th/Nb, and Ce/Sr vs. Sm/La diagrams. Note that rocks from different provinces plot along different trends (source of data: Conticelli et al., 1991, 1997, 2002, 2007, 2008; Elliott et al., 1997; Perini et al., 2004; Plank, 2005, Boari and Conticelli, 2007).

An alternative hypothesis is the involvement of an asthenospheric withinplate-like component (Prelević et al., 2008). The effect of the addition of a siliciclastic sediment melt on a more enriched peridotite would have less leverage on the final composition of the vein with respect to the same addition on a residual mantle. The resulting metasomatic vein network would probably have a less pronounced orogenic signature (Fig. 7), lower Sr and higher Nd isotope ratios. As for Pb isotopes the slightly more radiogenic composition of these rocks could be due either to an intrinsic characteristic of the recycled sedimentary component or assuming a Pb composition of the withinplate component similar to the RPV rocks (Radiogenic Pb Volcanics) of rocks from nearby Sardinia (Lustrino and Wilson, 2007).

7.3. Genetic relationships between ultrapotassic (lamproitic), shoshonitic and calc-alkaline magmas

In the previous paragraph we focused on the differences between the ultrapotassic terms of each province in order to investigate the recycled sedimentary component. In the following discussion we will examine the transition from lamproites to less enriched compositions (shoshonites and calc-alkaline) in both chronologic and geochemical trend, in order to shed some light on the possible processes and components affecting this transition.

According to Foley (1992) the wide compositional spectrum observed may be due to the different proportions of vein and wall

rock components. As already outlined the mineralogy of the vein network has been stabilised following the interaction of the peridotite with K-rich granitic melts from subducted sediments, whilst the surrounding peridotite might be more pervasively affected by slab-related fluid addition from the dehydration of either the subducting oceanic crust or the sediment. The newly formed paragenesis within the veins has a lower solidus than surrounding depleted lithospheric mantle (Foley, 1992). Increasing the temperature in a post-collisional setting, possibly due to upraise of the underlying astenosphere (Prelević et al., 2008), first leads to partially melt the vein and then the surrounding peridotite if the temperature is sufficiently raised. Alternatively, magmas from pure vein partial melting can mix in different proportions with calc-alkaline magmas produced by partial melting of surrounding peridotitic mineralogy to produce the wide spectrum observed between calc-alkaline to shoshonitic rocks. Because the choice between these two mechanisms is difficult to establish, then we will refer only to an increasing interaction between vein/surrounding mantle for explaining the possible dilution of the alkaline character of high-Mg magmas with time within a defined magmatic province.

In Tuscany the transition from lamproitic to high-K calc-alkaline rocks, through shoshonite, is a striking time-related feature. Lamproites are the oldest rocks and high-K calc-alkaline are among the youngest (i.e., Radicofani neck bottom, authors' unpublished data) with a clear decreasing of K_2O with time. This characteristic is strongly suggestive of increasing contribution of a lithospheric mantle component to the hybrid vein-derived magmas with time. Minette and lamproitic magmas of the Tuscan Province reflect lower degree of partial melting, which involves mainly the vein components. Shoshonitic and high-K calc-alkaline magmas reflect slightly higher degrees of melting where the surrounding peridotitic wall rock interacted with the vein melts. This is reflected in a downward trend with time in Fig. 11. In terms of Pb isotope composition (Fig. 6), a clear trend towards a mantle-derived end-member at low $^{207}Pb/^{204}Pb$ and $^{208}Pb/^{204}Pb$ (i.e., DMM surrounding peridotite) is observed, but some overlap exists between the composition of the widely variable lamproites and the related less-enriched rocks. Such an overlap is, however, less surprising when the Pb contents of these rocks are considered. Although a general decrease of incompatible trace elements is observed from lamproites to shoshonites, in Tuscany the lead content is comparable if not inverted, indicating that the lead enrichment, and thus its isotopic signature, is not diluted as that of other elements.

In Murcia-Almeria volcanic rocks follow a similar array but with opposite time relationships. Calc-alkaline rocks are the oldest ones, along with high-K calc-alkaline, shoshonitic are intermediate in ages, whereas ultrapotassic lamprophyres and lamproites are the youngest ones (Benito et al., 1999; Turner et al., 1999; Duggen et al., 2005). On the basis of radiometric ages and spatial distribution, a westward migration of magmatism with time is inferred in Southern Spain. Lamproitic rocks are the most recent ones among the subduction-related rocks (Turner et al., 1999; Duggen et al., 2005). With lamproitic magmas having a lower melting point than the shoshonitic and calc-alkaline ones (Foley, 1994), vein–wall rocks interaction within the mantle is then not a feasible process for the transition from calc-alkaline to ultrapotassic magmas. Turner et al. (1999) argue for a genesis from strongly different mantle and crustal reservoirs during convective removal of lithosphere. Our data indicate, however, that there is a geochemical and isotopic link between calc-alkaline and ultrapotassic rocks through shoshonites, at least on the basis of the crustal signature, arguing for a common metasomatic agent. In the diagram of Fig. 11, in the Spanish rocks Ce/Sr starts to increase rapidly with time, suggesting a late arrival of recycled sediments within the lithospheric mantle wedge.

The most prominent geochemical characteristic of the transition from calc-alkaline to lamproitic rocks in Spain is the decrease of $^{207}Pb/^{204}Pb$ and $^{208}Pb/^{204}Pb$, despite an increase of $^{206}Pb/^{204}Pb$ (Fig. 6). The origin of the mantle end-member is not easy to determine. Trace element contents of shoshonites, high-K calc-alkaline and calc-alkaline rocks are much less enriched than lamproitic ones except for Cs, Rb, Pb, which are almost comparable. Beside, Th/U ratio decreases from lamproites to K_2O less-enriched rocks (Fig. 12). All the abovementioned features point to a fluid-related component pervasively affecting the mantle source. The mantle-like Pb isotope ratio seems to suggest a provenance from altered oceanic crust rather than recycled sediments. In summary, the geochemical link observed between low-K and high-K rocks in Southern Spain is possibly related to a mantle source previously metasomatised by fluids derived from the oceanic crust and later re-fertilised by oceanic pelagic sedimentary component.

Strict relationships between lamproitic rocks of Sisco (14.2 Ma; Civetta et al., 1978) and high-K calc-alkaline rocks of Capraia (7.5–6.9 Ma; Aldighieri et al., 2004) have been found on a mineralogical ground (Chelazzi et al., 2006). Geochemical and isotopic characteristics are consistent with such close relationship; Peccerillo et al. (1987) erroneously included Sisco and Capraia rocks in the Tuscan Province in spite of their strongly different ages. Shoshonites, which have some geochemical differences with preceding rocks, are poured out some three million years later then the youngest HKCA episode at Capraia Island (4.6 Ma; Aldighieri et al., 2004). The composition of Sisco lamproite was previously interpreted either as due to involvement of carbonates in the sedimentary component or to involvement of a withinplate-like component similar to the RVP of Sardinia. Corsica rocks represent a separate magmatic province and draw a singular trend in the Ce/Sr vs. initial $^{87}Sr/^{86}Sr$ diagram suggesting a single sedimentary end-member (Fig. 11).

Pb isotope ratios decrease from lamproites to high calk-alkaline rocks. Assuming again that the latter are affected more deeply by the composition of the mantle surrounding the metasomatic veins, Pb isotope suggests either that the claimed withinplate-like mantle affects only the lamproitic terms, or that the lead isotopic signature of Corsica rocks is not affected by this component. In this regard, the lower Th/Nb (Fig. 13) of lamproite with respect to high-K calc-alkaline rocks might support the first hypothesis. The association of lamproitic to high-K calc-alkaline rocks contrasts a process based on a pure two end-member mixing. The array observed is better explained by vein–wall rocks interaction similar to Tuscany province. Metasomatised veins were isotopically and geochemically different from those of

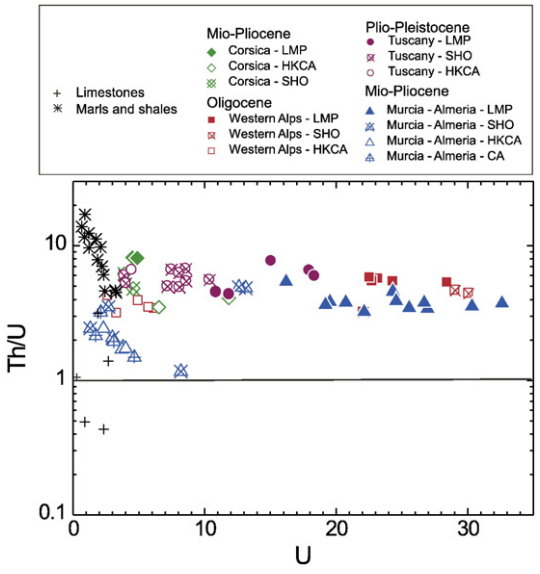

Fig. 13. U/Th vs. U in Western Mediterranean high-MgO rocks. Note that calc-alkalic and high-K calc-alkaline rocks from Murcia-Almeria plot along a trend of decreasing Th/U with increasing U.

Tuscany in spite of their vicinity. We might argue that most of the sedimentary recycled components of Tuscany were acquired after Corsica magmatism developed. Corsica shoshonites, on the other hand, are related to Corsica ultrapotassic and calc-alkaline rocks, because they have a common mantle source, but an influence of a deep asthenospheric flux occurred. This would also explain the time gap of about three million years between High-K calc-alkaline rocks and shoshonitic ones.

The Western Alps is the oldest event of ultrapotassic to calc-alkaline magmatism in the Western Mediterranean region. It has many geochemical and isotopic similarities with the younger ones, but also significant differences (Table 2; Figs. 3 and 4). Trace elements vs. initial isotopic values of the Western Alps samples overlap trends of the Murcia-Almeria province, but they fall on different array with respect to Tuscany and Corsica (Figs. 10, 13 and 14). The lack of detailed geochronologic studies of this area (Callegari et al., 2004, and references therein) precludes the possibility of establishing a chronological sequence between the different events. As already observed in the other Western Mediterranean provinces, regular decreasing of radiogenic Sr and incompatible trace elements contents is observed with K_2O decreasing. Then in our view the variation of K_2O is somewhat related to dilution of the alkaline character of the magma in favour of the calc-alkaline one, but we cannot confirm the possibility of a vein–surrounding peridotite interaction process to produce the compositional spectrum observed.

In summary similar magmatic associations are observed within the Western Mediterranean basin. These are linked all together in the frame of a general subduction-related and collisional magmatism but, sediments recycling and metasomatism follow different pathways. The resulting composition of the erupted magmas depends mainly on the composition and isotopic signatures of the recycled sedimentary components in the different regions; a secondary but significant role is played by the overall composition of the peridotitic mantle prior to vein formation. This peridotitic mantle cannot be considered homogenous and might display different geochemical and isotopic signatures and/or be affected by pervasive addition of fluids from the altered oceanic crust.

7.4. Partial melting and mantle xenoliths and genesis of UK mafic rocks

Within the investigated volcanic localities mantle ultramafic xenoliths are found in the Murcia-Almeria at Tallante (Capedri et al., 1989; Beccaluva et al., 2004; Shimizu et al., 2004), and in Tuscany (Conticelli and Peccerillo, 1990).

At Tallante high-P ultramafic nodules are hosted by Na-alkaline anorogenic volcanism post-dating the ultrapotassic to calc-alkaline Murcia-Almeria events. Most of these xenoliths show anhydrous peridotite parageneses, with variable trace element enrichment and Sr–Nd isotopic composition varying from the Depleted Mantle (DMM) to Enriched Mantle (EMI) end-members ($^{87}Sr/^{86}Sr$ = 0.70213–0.70476; $^{143}Nd/^{144}Nd$ = 0.51339–0.51250; Beccaluva et al., 2004), testifying the occurrence of cryptic metasomatic reactions possibly induced by silica under-saturated alkaline melts. The occurrence of these metasomatic reactions is also testified by the widespread presence of composite xenoliths in which peridotite is crosscut by veins and lenses. The latter are constituted by femic parageneses – including clinopyroxene (cpx), amphibole (amph), phlogopite (phl) and plagioclase (plg) – with bulk compositions approaching that of the host alkaline basalts, and with Sr–Nd isotopic composition within 0.70410–0.70546 and 0.51261–0.51258 ranges, respectively (authors' unpublished data).

Within the same xenoliths suite, however, other samples display a totally distinct style of metasomatism that induces orthopyroxene (opx), plg, phl and amph crystallisation, forming mantle domains characterised by "hydrous" opx-rich peridotites, locally crosscut by felsic veinlets containing plg and opx + quartz (qtz) + phl + amph (i.e., anorthosites, diorites gabbronorites). These mantle domains possibly share compositional analogies with the mantle source of the Murcia-Almeria ultrapotassic magmas. In this case, the neo-formation of opx + qtz (Shimizu et al., 2004) in the metasomatic parageneses indicates that the causative agents were silica-oversaturated melts rich in alkalis, in turn related to recycle within the mantle (and melting) of continental crustal lithologies via subduction (Beccaluva et al., 2004). Analogous qtz-bearing felsic veinlets induced by silica-oversaturated metasomatic agents in mantle xenoliths are extremely rare, but are documented in another supra-subduction xenoliths suite from Kamchatka arc (Kepezhinskas et al., 1995; Coltorti and Bonadiman, 2006). Further evidence of opx-generating metasomatic agents are observed in i) high-P ultramafic xenoliths from Serbia and the Pannonian area (Cvetković et al., 2004b; Kovács et al., 2007), and ii) in the Finero peridotite massif (Zanetti et al., 1999). In the latter case orthopyroxene crystallised beside phlogopite during metasomatism. Both cases are also thought to be generated by subduction-related agents in a mantle wedge setting. The above considerations are confirmed by the Sr and Nd isotopic signature of the opx-rich hydrous xenoliths and related felsic veinlets, showing $^{87}Sr/^{86}Sr$ up to 0.70856 and $^{143}Nd/^{144}Nd$ down to 0.51211, which indicate a clear "continental" crust fingerprint, implying a "continental" affinity of the subducted lithologies (Beccaluva et al., 2004). These values are, however, much lower than values shown by the Murcia-Almeria lamproites, but within the range of Corsica ones.

In central Italy, high-P ultramafic micronodules are directly hosted by lamproitic rocks at Torre Alfina, consisting of phl-bearing peridotites and sometimes glimmerites (rocks mainly constituted by phlogopite). Further occurrences of mantle xenoliths are recorded in the neighbouring Intra-Apennine Volcanic belt, where peridotite fragments including phlogopite are often recorded (Woolley and Church, 2005). Therefore, unlike mantle xenoliths from anorogenic intraplate magmas, the widespread presence of phlogopite and amphibole with peculiar geochemical signature (Coltorti and Bonadiman, 2006; Coltorti et al., 2006, 2007a,b; Bianchini et al., 2008) in the xenoliths exhumed in the investigated localities suggests that lamproite mantle sources were deeply modified by subduction-related fluids/melts. Coherently, a comparable enrichment of compositionally similar phlogopite in mantle materials has only been observed in mantle xenoliths affected by orogenic metasomatism (Brandon et al., 1999; Grégoire et al., 2001; Franz et al., 2002), and in the Finero peridotite massif of the Western Alps, classically interpreted as a mantle domain pervasively re-fertilised by subduction-

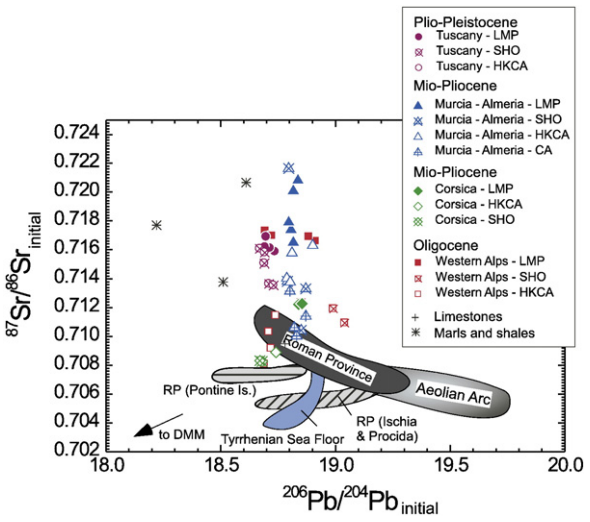

Fig. 14. Initial $^{143}Nd/^{144}Nd$ and initial $^{87}Sr/^{86}Sr$ vs. $^{206}Pb/^{204}Pb$ for ultrapotassic to calc-alkaline mafic rocks of the Western Mediterranean compared with rocks from Roman Province, Aeolian Arc, and Tuscan Anatectic Province (data for comparison are from Conticelli et al., 2002, 2007, 2008, and references therein).

related metasomatic agents (Zanetti et al., 1999; Coltorti et al., 2007b and references therein). Accordingly, the isotopic composition of phlogopite mantle xenocrysts exhumed by the intra-Apennine volcanic rocks display high Sr and low Nd isotopic ratios (0.7114–0.7154 and 0.51206, respectively) (Castorina et al., 2000), similar to those recorded in the Finero peridotite massif (Rivalenti and Mazzuchelli, 2000), further supporting the involvement of continental crust components in the subduction processes.

7.5. Geodynamic framework

Peccerillo (1999) first recognised the possibility that Tuscan, Corsica and Western Alps lamproites were connected to a similar geodynamic setting on the basis of their geochemical similarities. Recently Peccerillo and Martinotti (2006) and Prelević and Foley (2007) extended the geodynamic link to the Murcia-Almeria ones. Peccerillo and Martinotti (2006) also suggested that lamproites have strongly different metasomatism with respect to recent calc-alkaline magmatism and the leucite-bearing ultrapotassic to shoshonitic magmatism of the Mediterranean. Beside first order petrologic and geochemical similarities, lamproites, shoshonites and calc-alkaline rocks from the Western Mediterranean display slight but significant geochemical and isotopic differences that cannot be reconciled with a unique metasomatic agent produced in a similar geodynamic setting.

A large amount of paleogeographic reconstructions have been proposed to account for the tectonic evolution of the Alpine and Mediterranean region during Cretaceous to Neogene. All the models are in agreement to assume the convergence between Africa and Eurasia plates as the main cause for the formation of the Alpine–Mediterranean orogens, which was responsible of the subduction of the different oceanic realms followed by the main episodes of continental collision. These models also agree on the fact that the Alpine chain is mostly formed by Europe-vergent structures, formed as a consequence of south-eastward subduction and underthrusting of oceanic and European continental lithosphere. In addition, significant differences are observed among mafic volcanic rocks from the different examined areas, which might not be reconciled with a unique ancient metasomatic agent. Conversely, two contrasting models have been proposed to describe the earlier stage of tectonic evolution of the western Mediterranean. In the first class of models an earlier south-eastward subduction of the European lithosphere beneath the African plate has been proposed (Doglioni et al., 1997, 1999). This south-eastward subduction should represent the south-western prolongation of the European subduction recognised in the Western Alps by deep seismic data and geological reconstructions. In such models subduction flipped from southeast to northwestward polarity during the Late Eocene–Oligocene, in correspondence with the first episodes of calk-alkaline volcanism in Provence and Sardinia, and with the starting of extensional processes in the Ligure-Provençal back-arc basin. On this base an eastward dipping, continuous, subduction plane has been proposed for the entire region located between Gibraltar, Corsica–North Apennines and Western Alps.

In the second class of models there is no flip in subduction and the northward subduction of the African–Apulia lithosphere beneath the Eurasia plate was active since Cretaceous–Oligocene times (Principi and Treves, 1984; Faccenna et al., 2004). The Europe-vergent units of Corsica are interpreted as part of a double verging orogenic wedge, whose main body is represented by the Adriatic-vergent Apenninic units. In these models the subduction system related to the Western Alps, where the subduction plate subducted below the Adriatic–African one, should be distinct from that related to Apennines and Corsica, where the Apulian lithosphere subducts underneath the European plate. The transition between the two subduction systems, showing opposite polarity, should be located at the boundary between Alps and northern Apennines, where a complex deformation belt is well described in the geological literature.

On the other hand, for the Murcia-Almeria lamproite–shoshonite–calc-alkaline rocks associations Turner et al. (1999) have claimed a partial melting of the Mechanical Boundary Layer beneath the Alboran–Betic domain as a consequence of convective removal of its lithospheric roots. The erosion of the Thermal Boundary layer would have consequently brought to the elevation of about 5000 m of this domain and subsequently the collapse of the axial zone. As opposite Duggen et al. (2005) suggested an east-dipping subduction beneath the Gibraltar Arc, which may be reconciled with the roll back of the west-dipping subduction plane.

The presence of such peculiar orogenic volcanism in the Western Mediterranean is strongly suggestive for a common link among the different provinces of lamproitic to calc-alkaline magmatism. Then we found difficulties to believe that different geodynamic engines acted differently in such a restricted area to provide similar rock associations. Peccerillo and Martinotti (2006) already pointed out the strict petrologic and geodynamic relationships among these four Western Mediterranean magmatic provinces, suggesting the possibility that ultrapotassic to calc-alkaline magmatism were produced by partial melting of an upper mantle metasomatised by a very old, Cretaceous to Eocenic, south-eastward dipping subduction event. This hypothesis, however, does not explain: i) the delay of the magma production, in some cases as large as 40 Ma, ii) the lack of volcanism related to the south-eastward subduction beneath Betic area (Doglioni et al., 1999), iii) the existing close geochemical relationships between Tuscan and Roman magmas (Conticelli and Peccerillo, 1992; Conticelli et al., 2002; Avanzinelli et al., 2008), which suggests a close relationships between the two ultrapotassic provinces; iv) lack of remnants of any eastward subducted plate beneath the Tuscan province (Mele, 1998).

In our opinion the geochemical characteristics, age and geographic migration of magmatism in the Western Mediterranean region might be explained by the continuous retreat of the African–Ionian–Adriatic subducting lithosphere from the Iberia margin to the Adriatic Sea and to the Calabrian and Gibraltar arcs (Faccenna et al., 2001; Rosembaum et al., 2002). In Central-Southern Italy ultrapotassic magmatism is widespread along the western edge of the peninsula from Tuscany to Vesuvius. It developed diachronous from north-west to south-east, and it was synchronous to the retreat of the subduction. Changing of petrologic and geochemical characteristics from Leucite-Free Tuscan to Leucite-Bearing Roman magma occurs during the lower Pleistocene, when Adria plate starts to break and when carbonate sediments arrive at mantle level via subduction mixed to the siliciclastic ones. Then the passage from Tuscan to Roman magmas might be easily explained just with the changing of the composition of the sedimentary material brought into the upper mantle by the Adria subduction (Conticelli et al., 2002; Avanzinelli et al., 2008). In the last 200 ky in Italy magmatism migrated to southeast as a result of increasing influence of the Ionian subduction beneath the Calabrian Arc.

8. Summary and conclusion

In the Western Mediterranean region high-Mg ultrapotassic rocks with a lamproitic affinity are found intimately associated, in space and time, with shoshonitic and calc-alkaline rocks. This association is found in four different areas at different times in the last 30 My. They have a clear orogenic signature, and trace element distribution clearly indicates that they have been generated in a modified lithospheric mantle.

A clear geochemical and isotopic crustal signature is commonly found in all high-Mg rocks of the four different magmatic provinces. This signature has not been acquired during magma ascent but represents a primary characteristic of the magmas. An upper crustal sedimentary component derived from partial melting of siliciclastic sediments combined to variable proportions of sedimentary carbonate component is found to be responsible for the mantle

metasomatism. In south-eastern Spain crustal recycling, following continental collision, has been preceded by metasomatism produced by fluid derived by dehydratation of an oceanic subducted slab.

Different degrees of partial melting of the metasomatised portion of the mantle are responsible for the genesis of ultrapotassic rocks. Dilution of incompatible trace elements coupled to regular variation of Sr, Nd and Pb isotopes with decreasing K_2O at relatively constant Mg is suggested to be related to the increasing interaction between melts derived from veins and melts derived by partial melting of the surrounding mantle (Tuscany and Corsica).

Significant geochemical and isotopic differences among the four different magmatic provinces argue for different compositions of the metasomatic agents invading the lithospheric upper mantle sources of the magmas in each Western Mediterranean province. This suggests a not unique metasomatic agent. Different metasomatic agents were generated at different times by recycling of different sedimentary materials. This spatial and temporal migration correlates well with the migration of the trench following the retreat of the subduction plane from the Iberian margin to present day configuration.

Acknowledgements

We wish to thank Riccardo Vannucci for allowing access to LA-ICPMS facilities, and Maurizio Ulivi for technical support. Focusing and stirring discussions with Steve Foley, Guido Giordano, Angelo Peccerillo, Giampiero Poli, Claudio Faccenna, Leone Melluso, and Luigi Beccaluva are greatly appreciated. Thoughtful reviews by C. Wagner and anonymous greatly improved the original manuscript. Editorial handling by M. Coltorti is greatly appreciated. Financial support was provided by the Università degli Studi di Firenze (DST — ex 60% funds) issued to Sandro Conticelli, by the Italian Ministry of Education and Research (MIUR) through PRIN_2004 (# 2004040502_001) and FIRB_2001 (# RBAU01FX8M_003) grants. D.P. was financed by the Deutsche Forshungsgemeinschaft.

References

Agostini, S., Doglioni, C., Innocenti, F., Manetti, P., Savaşçin, M.Y., Tonarini, S., 2005. Tertiary high-Mg volcanic rocks from Western Anatolia and their geodynamic significance for the evolution of the Aegean area. In: Fytikas, M., Vougioukalakis, G.E. (Eds.), The South Aegean Active Volcanic Arc, Present Knowledge and Future Perspectives, Developments in Volcanology, vol. 7. Elsevier, Amsterdam, pp. 345–362.

Anderson, H.J., Jackson, P.K., 1987. The deep seismicity of the Tyrrhenian Sea. Geophysical Journal of the Royal Astronomical Society 91, 613–637.

Aldighieri, B., Groppelli, G., Norini, F., Testa, B., 2004. Capraia Island: morphology and geology of a complex volcanic activity during the Miocene and Pliocene. In: Morini, D., Bruni, P. (Eds.), The Regione Toscana project of Geological Mapping, Case Histories and Data Acquisition. Toscana per L'Ambiente. Regione Toscana, Firenze, pp. 51–59.

Altherr, R., Meyer, H.-P., Holl, A., Volker, F., Alibert, C., McCulloch, M.T., Majer, V., 2004. Geochemical and Sr–Nd–Pb isotopic characteristics of late Cenozoic leucite lamproites from the East European Alpine belt (Macedonia and Yugoslavia). Contributions to Mineralogy and Petrology 147, 58–73.

Avanzinelli, R., Boari, E., Conticelli, S., Francalanci, L., Guarnieri, L., Perini, G., Petrone, C.M., Tommasini, S., Ulivi, M., 2005. High precision Sr, Nd, and Pb isotopic analyses and reproducibility using new generation thermal ionisation mass spectrometer: aims and perspective for isotope geology applications. Periodico di Mineralogia 75, 187–207.

Avanzinelli, R., Elliot, T., Tommasini, S., Conticelli, S., 2008. Constraints on the genesis of the potassium-rich Italian volcanics from U/Th disequilibrium. Journal of Petrology 49, 195–223.

Ayuso, R.A., Messina, A., De Vivo, B., Russo, S., Woodruff, L.G., Sutter, J.F., Belkin, H.E., 1994. Geochemistry and argon thermochronology of the Variscan Sila Batholith, southern Italy: source rocks and magma evolution. Contributions to Mineralogy and Petrology 117, 87–109.

Barberi, F., Ferrara, G., Franchi, F., Serri, G., Tonarini, S., Treuil, M., 1986. Geochemistry and geochronology of the Capraia Island volcanic Complex (North Tyrrhenian Sea, Italy). Terra Cognita abstract 6, 185.

Barton, M., 1979. A comparative study of some minerals occurring in the potassium-rich alkaline rocks of the Leucite Hills, Wyoming, the Vice Volcano, Western Italy, and the Toro–Ankole region, Uganda. Neues Jahrbuch Mineralogische Abathlungen 137, 113–134.

Beccaluva, L., Bianchini, G., Bonadiman, C., Siena, F., Vaccaro, C., 2004. Coexisting anorogenic and subduction related metasomatism in mantle xenoliths from the Betic Cordillera (Southern Spain). Lithos 75, 67–87.

Bell, K., Castorina, F., Lavecchia, G., Rosatelli, G., Stoppa, F., 2004. Is there a mantle plume below Italy? EOS, Transactions of the American Geophysical Union 85, 541–547.

Benito, R., López-Ruiz, J., Cebriá, J.M., Hertogen, J., Doblas, M., Oyarzun, R., Demaiffe, D., 1999. Sr and O isotope constraints on source and crustal contamination in the high-K calc-alkaline and shoshonitic Neogene volcanic rocks of SE Spain. Lithos 46, 773–802.

Ben Othman, D., White, W.M., Patchett, J.P., 1989. The geochemistry of marine sediments, island arc magma genesis, and crust–mantle recycling. Earth and Planetary Science Letters 94, 1–21.

Bianchini, G., Beccaluva, L., Siena, F., 2008. Post-collisional and intraplate Cenozoic volcanism in the rifted Apennines/Adriatic domain. Lithos. doi:10.1016/j.lithos.2007.07.011.

Boari, E., Conticelli, S., 2007. Mineralogy and petrology of associated Mg-rich ultrapotassic, shoshonitic, and calc-alkaline rocks: the Middle Latin Valley monogenetic volcanoes, Roman Magmatic Province, Southern Italy. Canadian Mineralogist 45, 1727–1754.

Brandon, D.A., Becker, H., Carlson, R.W., Shirey, S.B., 1999. Isotopic constraints on time scales and mechanisms of slab material transport in the mantle wedge: evidence from the Simcoe mantle xenoliths, Washington, USA. Chemical Geology 160, 387–407.

Callegari, E., Cigolini, C., Medeot, O., D'Antonio, M., 2004. Petrogenesis of calc-alkaline and shoshonitic post-collisional Oligocene volcanics of the Cover Series of the Sesia Zone, Western Italian Alps. Geodinamica Acta 17, 1–29.

Capedri, S., Venturelli, G., Salvioli-Mariani, E., Crawford, A.J., Barbieri, M., 1989. Upper-mantle xenoliths and megacrysts in alkali basalt from Tallante, south-eastern Spain. European Journal of Mineralogy 1, 685–699.

Carmichael, I.S.E., Lange, R.A., Luhr, J.F., 1996. Quaternary minettes and associated volcanic rocks of Mascota, western Mexico: a consequence of plate extension above a subduction modified mantle wedge. Contributions to Mineralogy and Petrology 124, 302–333.

Carmignani, L., Carosi, A., Di Pisa, A., Gattiglio, M., Musumeci, G., Oggiano, G., Pertusati, P.C., 1994. The Hercynian chain in Sardinia (Italy). Geodinamica Acta 7, 31–47.

Castorina, F., Stoppa, F., Cundari, A., Barbieri, M., 2000. An enriched mantle source for Italy's melilitite–carbonatite association as inferred by its Nd–Sr isotope signature. Mineralogical Magazine 64, 625–639.

Cellai, D., Conticelli, S., Menchetti, S., 1994. Crystal-chemistry of clinopyroxenes in Italian lamproites and kamafugites: implications on their genesis. Contributions to Mineralogy and Petrology 116, 301–315.

Chelazzi, L., Bindi, L., Olmi, F., Peccerillo, A., Menchetti, S., Conticelli, S., 2006. A lamproitic component in the high-K calc-alkaline volcanic rocks of the Capraia Island, Tuscan Magmatic Province: evidence from clinopyroxene crystal chemical data. Periodico di Mineralogia 75, 75–94.

Chopin, C., 1984. Coesite and pure pyrope in high grade blueschists of the Western Alps, a first record and some consequences. Contributions to Mineralogy and Petrology 86, 107–118.

Cifelli, F., Mattei, M., Rossetti, F., 2007. Tectonic evolution of arcuate mountain belts on top of a retreating subduction slab: the example of the Calabrian Arc. Journal of Geophysical Research 112, B09101. doi:10.1029/2006JB004848.

Cifelli, F., Mattei, M., Porreca, M., 2008. New paleomagnetic data from Oligocene–upper Miocene sediments in the Rif chain (northern Morocco): insights on the Neogene tectonic evolution of the Gibraltar arc. Journal of Geophysical Research 113, B02104. doi:10.1029/2007JB005271.

Cipollari, P., Cosentino, D., 1995. Miocene unconformities in the central Apennines: geodynamic significance and sedimentary basin evolution. Tectonophysics 252, 375–389.

Civetta, L., Orsi, G., Scandone, P., Pece, R., 1978. Eastward migration of the Tuscan Anatectic magmatism due to anticlockwise rotation of the Apennines. Nature 276, 604–606.

Collombet, M., Thomas, J.C., Chauvin, A., Tricart, P., Bouillin, J.P., Gratier, J.P., 2002. Counterclockwise rotation of the western Alps since the Oligocene: new insights from paleomagnetic data. Tectonics 21, 1–10.

Coltorti, M., Bonadiman, C., Faccini, B., Siena, F., 2006. Metasomatism in intraplate and suprasubduction lithospheric mantle. Geochimica et Cosmochimica Acta 70 (Supplement 1), A1–09.

Coltorti, M., Arai, S., Bonadiman, C., Faccini, B., Ishimaru, S., 2007a. Nature of the metasomatising agents in suprasubduction and intraplate settings as deduced by glass and amphibole geochemistry. Geochimica et Cosmochimica Acta 71, A–184.

Coltorti, M., Bonadiman, C., Faccini, B., Ntaflos, T., Siena, F., 2007b. Slab melt and intraplate metasomatism in Kapfenstein mantle xenoliths (Styrian Basin, Austria). Lithos 94, 66–89.

Comas, M.C., Platt, J.P., Soto, J.I., Watts, A.B., 1999. The origin and tectonic history of the Alborán Basin: insights from ODP Leg 161 results. In: Zahn, R., Comas, M.C., Klaus, A. (Eds.), Proceedings of the Ocean Drilling Program, Scientific Results 161, College Station, TX (Ocean Drilling Program), pp. 555–580.

Conceição, R.V., Green, D.H., 2004. Derivation of potassic (shoshonitic) magmas by decompressing melting of phlogopite+pargasite lherzolite. Lithos 72, 209–229.

Conte, A.M., Dolfi, D., 2002. Petrological and geochemical characteristics of Plio–Pleistocene Volcanics from Ponza Island (Tyrrhenian Sea, Italy). Mineralogy and Petrology 74, 75–94.

Conticelli, S., 1998. Effects of crustal contamination on ultrapotassic magmas with lamproitic affinity: mineralogical, geochemical and isotope data from the Torre Alfina lavas and xenoliths, Central Italy. Chemical Geology 149, 51–81.

Conticelli, S., Peccerillo, A., 1990. Petrological significance of high-pressure ultramafic xenoliths from ultrapotassic rocks of Central Italy. Lithos 24, 305–322.

Conticelli, S., Peccerillo, A., 1992. Petrology and geochemistry of potassic and ultrapotassic volcanism in central Italy: petrogenesis and inferences on the evolution of the mantle sources. Lithos 28, 221–240.

Conticelli, S., Francalanci, L., Santo, A.P., 1991. Petrology of the final stage Latera lavas: mineralogical, geochemical and Sr-isotopic data and their bearing on the genesis of

some potassic magmas in Central Italy. Journal of Volcanology and Geothermal Researches 46, 187–212.
Conticelli, S., Manetti, P., Menichetti, S., 1992. Petrology, chemistry, mineralogy and Sr-isotopic features of Pliocenic orendites from South Tuscany: implications on their genesis and evolutions. European Journal of Mineralogy 4, 1359–1375.
Conticelli, S., Francalanci, L., Manetti, P., Cioni, R., Sbrana, A., 1997. Petrology and geochemistry of the ultrapotassic rocks from the Sabatini Volcanic District, Central Italy: the role of evolutionary processes in the genesis of variably enriched alkaline magmas. Journal of Volcanology and Geothermal Researches 75, 107–136.
Conticelli, S., Bortolotti, V., Principi, G., Laurenzi, M.A., Vaggelli, G., D'Antonio, M., 2001. Petrology, mineralogy and geochemistry of a mafic dyke from Monte Castello, Elba Island, Italy. Ofioliti 26, 249–262.
Conticelli, S., D'Antonio, M., Pinarelli, L., Civetta, L., 2002. Source contamination and mantle heterogeneity in the genesis of Italian potassic and ultrapotassic volcanic rocks: Sr–Nd–Pb isotope data from Roman Province and Southern Tuscany. Mineralogy and Petrology 74, 189–222.
Conticelli, S., Melluso, L., Perini, G., Avanzinelli, R., Boari, E., 2004. Petrologic, geochemical, and isotopic characteristics of potassic and ultrapotassic magmatism in Central-Southern Italy: inferences on its genesis and on the nature of mantle sources. Periodico di Mineralogia 73, 153–164.
Conticelli, S., Carlson, R.W., Widow, E., Serri, G., 2007. Chemical and isotopic composition (Os, Pb, Nd, and Sr) of Neogene to Quaternary calc-alkaline, shoshonitic, and ultrapotassic mafic rocks from the Italian peninsula: Inferences on the nature of their mantle sources. In: Beccaluva, L., Bianchini, G., Wilson, M. (Eds.), Cenozoic Volcanism in the Mediterranean Area, Geological Society of America, Special Papers, 418, pp. 171–202.
Conticelli, S., Marchionni, S., Rosa, D., Giordano, G., Boari, E., Avanzinelli, R., in press. Shoshonite and sub-alkaline magmas from an Ultrapotassic Volcano: Sr–Nd–Pb isotope data on the Roccamonfina volcanic rocks, Roman Magmatic Province, Southern Italy. Contributions to Mineralogy and Petrology. doi:10.1007/s00410008-0319-8.
Contini, S., Venturelli, G., Toscani, L., Capedri, S., Barbieri, M., 1993. Cr–Zr–armalcolite-bearing lamproites of Cancarix, SE Spain. Mineralogical Magazine 57, 203–216.
Cvetković, V., Downes, H., Prelević, D., Jovanović, M., Lazarov, M., 2004b. Characteristics of the lithospheric mantle beneath East Serbia inferred from ultramafic xenoliths in Palaeogene basanites. Contributions to Mineralogy and Petrology 148, 335–357.
Cvetković, V., Prelević, D., Downes, H., Jovanović, M., Vaselli, O., Pécskay, Z., 2004a. Origin and geodynamic significance of Tertiary postcollisional basaltic magmatism in Serbia (Central Balkan Peninsula). Lithos 73, 161–186.
Dal Piaz, G.V., Venturelli, G., Scolari, A., 1979. Calc-alkaline to ultrapotassic postcollisional volcanic activity in the internal Northwestern Alps. Memorie Società Geologica Università di Padova 32, 4–16.
Davies, G.R., Stolz, A.J., Mahotkin, I.L., Nowell, G.M., Pearson, D.G., 2006. Trace element and Sr–Pb–Nd–Hf isotope evidence for ancient, fluid-dominated enrichment of the source of Aldan Shield lamproites. Journal of Petrology 47, 1119–1146.
Dercourt, J., Zonenshein, L.P., Ricou, L.E., Khazmin, V.G., Le Pichon, X., Knipper, A.L., Grandjacquet, C., Sbortshikov, I.M., Geyssant, J., Lepvrier, C., Pechersky, D.H., Bowlin, J., Sibouet, J.C., Savostin, L.A., Sorokhtin, O., Westphal, M., Bazhenov, M.L., Lauer, J.P., Biju-Duval, B., 1986. Geological evolution of the Tethys belt from the Atlantic to the Pamir since the Lias. Tectonophysics 123, 241–315.
Deniel, C., Pin, C., 2001. Single-stage method for the simultaneous isolation of lead and strontium from silicate samples for isotopic measurements. Analytical Chimica Acta 426, 95–103.
Dewey, J.F., Helman, M.L., Turco, E., Hutton, D.H.W., Knott, S.D., 1989. Kinematics of the Western Mediterranean. In: Coward, M.P., Dietrich, D., Park, R.G. (Eds.), Alpine Tectonics, Geological Society of London, 45. Special Publication, pp. 265–283.
Doglioni, C., Gueguen, E., Sabat, F., Fernandez, M., 1997. The western Mediterranean extensional basins and the Alpine orogen. Terra Nova 9, 109–112.
Doglioni, C., Harabaglia, P., Merlini, S., Mongelli, F., Peccerillo, A., 1999. Orogens and slabs vs. their direction of subductions. Earth Science Reviews 45, 167–208.
Duggen, S., Hörnle, K., van den Bogaard, P., Harris, C., 2004. Magmatic evolution of the Alboran region: the role of subduction in forming the Western Mediterranean and causing the Messinian salinity crisis. Earth and Planetary Science Letters 218, 91–108.
Duggen, S., Hörnle, K., van den Bogaard, P., Garbe-Schönberg, D., 2005. Post-collisional transition from subduction- to intraplate-type magmatism in the westernmost Mediterranean: evidence for continental-edge delamination of subcontinental lithosphere. Journal of Petrology 46, 1155–1201. doi:10.1093/petrology/egi013.
Elliott, T., Plank, T., Zindler, A., White, W., Bourdon, B., 1997. Element transport from slab to volcanic front at the Mariana arc. Journal of Geophysical Research 102, 14991–15019.
Faccenna, C., Funiciello, F., Giardini, D., Lucente, P., 2001. Episodic back-arc extension during restricted mantle convection in the Central Mediterranean. Earth and Planetary Science Letters 187, 105–116.
Faccenna, C., Piromallo, C., Crespo-Blanc, A., Jolivet, L., Rossetti, F., 2004. Lateral slab deformation and the origin of the western Mediterranean arcs. Tectonics 23, TC1012. doi:10.1029/2002TC001488.
Ferrara, G., Tonarini, S., 1985. Radiometric geochronology in Tuscany: results and problem. Rendiconti Società Italiana Mineralogia e Petrologia 40, 110–124.
Ferrara, G., Preite-Martinez, M., Taylor Jr., H.P., Tonarini, S., Turi, B., 1986. Evidence of crustal assimilation, mixing of magmas and a ^{87}Sr-rich upper mantle. Contributions to Mineralogy and Petrology 92, 269–280.
Ferrari, L., Conticelli, S., Burlamacchi, L., Manetti, P., 1996. Volcanological evolution of the Monte Amiata Volcanic Center, Southern Tuscany, Central Italy: new geological and petrochemical data. Acta Vulcanologica 8, 41–56.
Foley, S.F., 1990. A review and assessment of experiments on kimberlites, lamproites and lamprophyres as a guide to their origin. Proceedings Indian Academy of Sciences, Earth Science Reviews 99, 77–80.
Foley, S.F., 1992. Vein-plus-wall-rock melting mechanisms in the lithosphere and the origin of potassic alkaline magmas. Lithos 28, 435–453.
Foley, S.F., 1994. Geochemische und experimentelle Untersuchungen zur genese der kalireichen Magmatite. Neues Jahrbuch fur Mineraleralogie Abathlung 167, 1–55.
Foley, S.F., Venturelli, G., 1989. High-K_2O rocks with high MgO, high SiO_2, affinities. In: Crawford, A.J. (Ed.), Boninites. Unwin Hyman, London, pp. 72–88.
Foley, S.F., Venturelli, G., Green, D.H., Toscani, L., 1987. The ultrapotassic rocks: characteristics classification and constraints for petrogenetic models. Earth Science Reviews 24, 81–134.
Francalanci, L., Taylor, S.R., McCulloch, M.T., Woodhead, J., 1993. Geochemical and isotopic variations in calc-alkaline rocks of the Aeolian Arc (Southern Tyrrhenian Sea, Italy): constraints on the magma genesis. Contributions to Mineralogy and Petrology 113, 300–313.
Francalanci, L., Tommasini, S., Conticelli, S., Davies, G.H., 1999. Sr isotope evidence for short magma residence time for the 20th century activity at Stromboli volcano, Italy. Earth and Planetary Science Letters 167, 61–69.
Francalanci, L., Innocenti, F., Manetti, P., Savasçin, M.Y., 2000. Neogene alkaline volcanism of the Afyon–Isparta area, Turkey: petrogenesis and geodynamic implications. Mineralogy and Petrology 70, 285–312.
Francalanci, L., Tommasini, S., Conticelli, S., 2004. The volcanic activity of Stromboli in the 1906–1998 A.D. period: mineralogical, geochemical and isotope data relevant to the understanding of Strombolian activity. Journal of Volcanology and Geothermal Researches 131, 179–211.
Francalanci, L., Vougioukalakis, G.E., Perini, G., Manetti, P., 2005. A west–east traverse along the magmatism of the South Aegean volcanic arc in the light of volcanological, chemical and isotope data. In: Fytikas, M., Vougioukalakis, G.E. (Eds.), The South Aegean Active Volcanic Arc, Present Knowledge and Future Perspectives, Developments in Volcanology, 7. Elsevier, Amsterdam, pp. 65–111.
Francalanci, L., Avanzinelli, R., Tommasini, S., Heumann, A., 2007. A west–east geochemical and isotopic traverse along the volcanism of the Aeolian Island arc, Southern Tyrrhenian Sea, Italy. In: Beccaluva, L., Bianchini, G., Wilson, M. (Eds.), Cenozoic Volcanism in the Mediterranean Area, Geological Society of America, Special Papers, 418, pp. 235–263.
Franz, L., Becker, K.-P., Kramer, W., Herzig, P., 2002. Metasomatic mantle xenoliths from the Bismark Microplate (Papua New Guinea) — thermal evolution, geochemistry and extent of slab-induced metasomatism. Journal of Petrology 43, 315–343.
Gasperini, D., Blichert-Toft, J., Bosch, D., Del Moro, A., Macera, P., Albarede, F., 2002. Upwelling of deep mantle material through a plate window: evidence from the geochemistry of Italian basaltic volcanics. Journal of Geophysical Research 107. doi:10.1029/2001JB000418.
Giardini, D., Velonà, M., 1991. Deep seismicity of the Tyrrhenian Sea. Terra Nova 3, 57–64.
Grégoire, M., McInnes, B.I.A., O'Reilley, S.Y., 2001. Hydrous metasomatism of oceanic subarc mantle, Lihir, Papua New Guinea — Part 2. Trace element characteristics of slab-derived fluids. Lithos 59, 91–108.
Guarnieri, L., 2007. Il magmatismo Mio–Pliocenico della cordigliera Betica (Spagna Meridionale): Caratterizzazione geochimica ed isotopica delle sorgenti sub-crostali e confronti con il magmatismo Alpino ed Appenninico. Ph.D. Thesis, Firenze, 135 pp.
Hamelin, B., Grousset, F., Sholkowitz, E.R., 1990. Pb isotopes in superficial pelagic sediments from the North Atlantic. Geochimica et Cosmochimica Acta 54, 37–47.
Haskin, L.A., Frey, F.A., Schmitt, R.A., Smith, R.H., 1966. Meteoric, solar and terrestrial rare Earth distributions. Physic and Chemistry of the Earth 7, 162-132.
Hawkesworth, C.J., Vollmer, R., 1979. Crustal contamination versus enriched mantle: $^{143}Nd/^{144}Nd$ and $^{87}Sr/^{86}Sr$ evidence from the Italian volcanics. Contributions to Mineralogy and Petrology 69, 151–165.
Hermann, J., Spandler, C., Hack, A., Korsakov, A.V., 2006. Aqueous fluids and hydrous melts in high-pressure and ultra-high pressure rocks: implications for element transfer in subduction zones. Lithos 92, 399–417.
Hoffman, A.W., 1996. Mantle geochemistry: the message from oceanic volcanism. Nature 385, 219–229.
Horvath, F., Berckheimer, H., 1982. Mediterranean backarc-basins. In: Berckheimer, H., Hsü, K. (Eds.), Alpine-Mediterranean-Geodynamics. AGU Geodynamics Series, pp. 141–163.
Innocenti, F., Serri, G., Ferrara, P., Manetti, P., Tonarini, S., 1992. Genesis and classification of the rocks of the Tuscan Magmatic Province: thirty years after Marinelli's model. Acta Vulcanologica 2, 247–265.
Innocenti, F., Agostini, S., Di Vincenzo, G., Doglioni, C., Manetti, P., Savaşçin, M.Y., Tonarini, S., 2005. Neogene and Quaternary volcanism in Western Anatolia: magma sources and geodynamic evolution. Marine Geology 221, 397–421.
Ionov, D.A., Hofmann, A.W., 1995. Nb–Ta-rich mantle amphiboles and micas: implications for subduction-related metasomatic trace element fractionations. Earth and Planetary Science Letters 131, 341–356.
Irving, A.J., 1980. Petrology and geochemistry of composite ultramafic xenoliths in alkaline basalts and implications for magmatic processes within the mantle. American Journal of Sciences 280, 389–426.
Johnson, M.C., Plank, T., 1999. Dehydration and melting experiments constrain the fate of subducted sediments. Geochemistry Geophysics and Geosystem G^3 7, 1999GC000014.
Kepezhinskas, P.K., Defant, M.J., Drummond, M.S., 1995. Na metasomatism in the island arc mantle by slab melt–peridotite interaction: evidence from mantle xenoliths in the North Kamchatka arc. Journal of Petrology 36, 1505–1527.
Kessel, R., Schmidt, M.W., Ulmer, P., Pettke, T., 2005. Trace element signature of subduction-zone fluids, melts and supercritical liquids at 120–180 km depth. Nature 437, 724–727. doi:10.1038/nature03971.
Kovács, I., Csontos, L., Szabó, C., Bali, E., Falus, G., Benedek, K., Zajacz, Z., 2007. Paleogene–Early Miocene igneous rocks and geodynamics of the Alpine–Carpathian–Pannonian–Dinaric region: an integrated approach. In: Beccaluva, L., Bianchini, G., Wilson, M. (Eds.), Volcanism in the Mediterranean Area, Geological Society of America Special Papers, 418, pp. 93–112.

Law, K.M., Blundy, J.D., Wood, B.J., Ragnarsdottir, K.V., 2000. Trace element partitioning between wollastonite and silicate–carbonate melt. Mineralogical Magazine 64, 651–661.
Le Maitre, R.W. (Ed.), 2002. Igneous Rocks: A Classification and Glossary of Terms. Cambridge University Press. 236 pp.
Lippitsch, R., Kissling, E., Ansorge, J., 2003. Upper mantle structure beneath the Alpine orogen from high-resolution teleseismic tomography. Journal of Geophysical Research 108 (B8). doi:10.1029/2002JB002016 2376.
Lonergan, L., White, N., 1997. Origin of the Betic–Rif mountain belt. Tectonics 16, 504–522.
Lustrino, M., Wilson, M., 2007. The circum-Mediterranean anorogenic Cenozoic Igneous Provinces. Earth Science Review 81, 1–55.
Martelli, M., Nuccio, P.M., Stuart, F.M., Burgess, R., Ellam, R.M., Italiano, F., 2004. Helium–strontium isotope constraints on mantle evolution beneath the Roman Comagmatic Province, Italy. Earth and Planetary Science Letters 224, 295–308 3–4.
Mascle, G.H., Tricart, P., Torelli, L., Bouillin, J.P., Rolfo, F., Lapierre, H., Monié, P., Depardon, S., Mascle, J., Peis, D., 2001. Evolution of the Sardinia Channel (Western Mediterranean): new constraints from a diving survey on Cornacya seamount off SE Sardinia. Marine Geology 179, 179–202.
Massonne, H.-J., Willner, A.P., Gerya, T., 2007. Densities of metapelitic rocks at high to ultrahigh pressure conditions: what are the geodynamic consequences. Earth and Planetary Science Letters 256, 12–27.
Mattei, M., Cipollari, P., Cosentino, D., Argentieri, A., Rossetti, F., Speranza, F., Di Bella, L., 2002. The Miocene tectono-sedimentary evolution of the Southern Tyrrhenian Sea: stratigraphy, structural and paleomagnetic data from the on-shore Amantea basin (Calabrian arc, Italy). Basin Research 14, 147–168.
Mattei, M., Petrocelli, V., Lacava, D., Schiattarella, M., 2004. Geodynamic implications of Pleistocene ultra-rapid vertical-axis rotations in the Southern Apennine (Italy). Geology 32 (9), 789–792. doi:10.1130/G20552.1.
Mattei, M., Cifelli, F., Martín Rojas, I., Crespo Blanc, A., Comas, M., Faccenna, C., Porreca, M., 2006. Neogene tectonic evolution of the Gibraltar Arc: new paleomagnetic constrains from the Betic chain. Earth and Planetary Science Letters. doi:10.1016/j.epsl.2006.08.012.
Mattei, M., Cifelli, F., D'Agostino, N., 2007. The evolution of the Calabrian Arc: evidence from paleomagnetic and GPS observations. Earth and Planetary Science Letters 263, 259–274.
McDermott, F., Hawkesworth, C.J., 1991. Th, Pb, and Sr isotope variations in young arc volcanics and oceanic sediments. Earth and Planetary Science Letters 104, 1–15.
Mele, G., 1998. High-frequency wave propagation from mantle earthquakes in the Tyrrhenian Sea: new constraints for the geometry of the south Tyrrhenian subduction zone. Geophysical Research Letters 25, 28–77.
Menzies, M.A., Dupuy, C., Nicolas, A., 1991. Orogenic lherzolites and mantle processes. Journal of Petrology 306.
Mitchell, R.H., Bergman, S.C., 1991. Petrology of Lamproites. Plenum Press, New York. 450 pp.
Mirnejad, H., Bell, K., 2006. Origin and source evolution of the Leucite Hills lamproites: evidence from Sr–Nd–Pb–O isotopic compositions. Journal of Petrology 47, 2463–2489. doi:10.1093/petrology/egl051.
Murphy, D.T., Collerson, K.D., Kamber, B.S., 2002. Lamproites from Gaussberg, Antarctica: possible transition Zone melts of Archean Subducted Sediments. Journal of Petrology 43, 981–1001.
Nicolosi, I., Speranza, F., Chiappini, M., 2006. Ultra-fast oceanic spreading of the Marsili Basin, southern Tyrrhenian Sea: evidence from magnetic anomaly analysis. Geology 34, 717–720.
Owen, J.P., 2008. Geochemistry of lamprophyres from the Western Alps, Italy: implications for the origin of an enriched isotopic component in the Italian mantle. Contributions to Mineralogy and Petrology 155, 341–362.
Patacca, E., Sartori, R., Scandone, P., 1992. Tyrrhenian basin and Apenninic arcs: kinematic relations since Late Tortonian times. Memorie Società Geologica Italiana 45, 425–451.
Peccerillo, A., 1999. Multiple mantle metasomatism in Central-Southern Italy: geochemical effects, timing and geodynamic implications. Geology 27, 315–318.
Peccerillo, A., 2005. Plio–Quaternary Volcanism in Italy: Petrology, Geochemistry, Geodynamics. Springer-Verlag, Berlin, p. 365.
Peccerillo, A., Taylor, S.R., 1976. Geochemistry of Eocene calc-alkaline volcanic rocks from Kastamonu area, Northern Turkey. Contributions to Mineralogy and Petrology 58, 63–81.
Peccerillo, A., Turco, E., 2004. Petrological and geochemical variations of the Plio–Quaternary volcanism in the Tyrrhenian sea area: regional distribution of magma types, petrogenesis and geodynamic implications. Periodico di Mineralogia 73, 231–251.
Peccerillo, A., Martinotti, G., 2006. The Western Mediterranean lamproitic magmatism: origin and geodynamic significance. Terra Nova 18, 109–117.
Peccerillo, A., Conticelli, S., Manetti, P., 1987. Petrological characteristics and the genesis of the recent magmatism of South Tuscany and North Latium. Periodico di Mineralogia 56, 167–183.
Peccerillo, A., Poli, G., Serri, G., 1988. Petrogenesis of orenditic and kamafugitic rocks from Central Italy. Canadian Mineralogist 26, 45–65.
Perini, G., Conticelli, S., Francalanci, L., Davidson, J.P., 2000. The relationships between potassic and calc-alkaline post-orogenic magmatism at Vico Volcano, Central Italy. Journal of Volcanology and Geothermal Researches 95, 247–272. doi:10.1016/S0377-0273(99)00123-7.
Perini, G., Tepbley III, F.J., Davidson, J.P., Conticelli, S., 2003. The origin of K-feldspar megacrysts hosted in alkaline potassic rocks: track for low pressure processes in primitive magmas. Lithos 66, 223–240. doi:10.1016/S0024-4937(02)00221-9.
Perini, G., Francalanci, L., Davidson, J.P., Conticelli, S., 2004. The petrogenesis of Vico Volcano, Central Italy: an example of low scale mantle heterogeneity. Journal of Petrology 45, 139–182. doi:10.1093/petrology/egg084.
Pinarelli, L., 1991. Geochemical and isotopic (Sr, Pb) evidence of crust–mantle interaction in acidic melts — the Tolfa–Cerveteri–Manziana volcanic complex (Central Italy): a case history. Chemical Geology 92, 177–195.
Piromallo, C., Morelli, A., 2003. P wave tomography of the mantle under the Alpine–Mediterranean area. Journal of Geophysical Research 108. doi:10.1029/2002JB001757 B2, 2065.
Plank, T., 2005. Constraints from thorium/lanthanum on sediment recycling at subduction zones and the evolution of the continents. Journal of Petrology 46, 921–944.
Plank, T., Langmuir, C.H., 1998. The chemical composition of subducting sediments and its consequence for the crust and mantle. Chemical Geology 145, 325–394.
Platt, P., Argles, T.W., Carter, A., Kelley, S.P., Whitehouse, M.J., Lonergan, L., 2003. Exhumation of the Ronda peridotite and its crustal envelope: constraints from thermal modelling of a P–T–time array. Journal of Geological Society 160, 655–676.
Prelević, D., Foley, S.F., 2007. Accretion of arc-oceanic lithospheric mantle in the Mediterranean: evidence from extremely high-Mg olivines and Cr-rich spinel inclusions from lamproites. Earth and Planetary Science Letters 256, 120–135.
Prelević, D., Foley, S.F., Cvetković, V., Romer, R.L., 2004. Origin of minette by mixing of lamproite and dacite magmas in Veliki Majdan Serbia. Journal of Petrology 45, 759–792.
Prelević, D., Foley, S.F., Cvetković, V., Romer, R.L., Downes, H., 2005. Tertiary ultrapotassic volcanism in Serbia: constraints on petrogenesis and mantle source characteristics. Journal of Petrology 46, 1443–1487.
Prelević, D., Foley, S.F., Romer, R.L., Conticelli, S., 2008. Mediterranean Tertiary lamproites: multicomponent melts in post-collisional geodynamics. Geochimica et Cosmochimica Acta 72, 2125–2156.
Principi, G., Treves, B., 1984. Il sistema Corso-Appenninico come prisma di accrezione. Riflessi sul problema generale del limite Alpi-Appennini. Memorie Società Geologica Italiana 28, 549–576.
Rivalenti, G., Mazzuchelli, M., 2000. Interaction of mantle derived magmas and crust in the Ivrea–Verbano zone and the Ivrea mantle peridotites. In: Ranalli, C., Ricci, C.A., Trommsdorff, V. (Eds.), Proceedings of the International School of Earth and Planetary Sciences "Crust–Mantle Interactions", pp. 153–198.
Rosembaum, G., Lister, G.S., Duboz, C., 2002. Reconstruction of the tectonic evolution of the Western Mediterranean since the Oligocene. In: Rosembaum, G., Lister, G.S. (Eds.), Reconstruction of the Evolution of the Alpine–Himalayan Orogeny, 8, pp. 107–130. Journal of Virtual Explorer.
Royden, L., Patacca, E., Scandone, P., 1987. Segmentation and configuration of subducted lithosphere in Italy: an important control on thrust-belt and foredeep-basin evolution. Geology 15, 714–717.
Rudnick, R.L., Fountain, D.M., 1995. Nature and composition of the Continental Crust: a lower crustal perspective. Review of Geophysics 33, 267–309.
Savelli, C., 2002. Time–space distribution of magmatic activity in the Western Mediterranean and peripheral orogens during the past 30 Ma (a stimulus to geodynamic considerations). Journal of Geodynamics 34, 99–126.
Schmid, S.M., Kissling, E., 2000. The arc of the western Alps in the light of geophysical data on deep crustal structure. Tectonics 19 (1), 62–85.
Schmidt, M., Vielzeuf, D., Auzanneau, E., 2004. Melting and dissolution of subducting crust at high pressures: the key role of white mica. Earth and Planetary Science Letters 228, 65–84.
Schreyer, W., Massonne, H.J., Chopin, C., 1987. Continental crust subducted to depths near 100 km implications for magma and fluid genesis in collision zones. In: Mysen, B.O. (Ed.), Magmatic Processes: Physicochemical Principles, The Geochemical Society of America, 1. Special Publication, pp. 155–163.
Selvaggi, G., Amato, A., 1992. Subcrustal earthquakes in the Northern Apennines (Italy): evidence for a still active subduction. Geophysical Research Letters 19, 21, 2127–2130.
Selvaggi, G., Chiarabba, C., 1995. Seismicity and P-wave velocity image of Southern Tyrrhenian subduction zone. Geophysical Journal International 121, 818–826.
Sekine, T., Wyllie, P.J., 1982. Phase relationships in the system $KAlSiO_4$–Mg_2SiO_4–SiO_2–H_2O as a model for hybridization between hydrous siliceous melts and peridotite. Contributions to Mineralogy and Petrology 79, 368–374.
Shaw, C.S.J., Eyzaguirre, J., Fryer, B., Gagnon, J., 2005. Regional variations in the mineralogy of metasomatic assemblages in mantle xenoliths from the West Eifel Volcanic Field, Germany. Journal of Petrology 46, 945–972.
Shimizu, Y., Arai, S., Morishita, T., Yurimoto, H., Gervilla, F., 2004. Petrochemical characteristics of felsic veins in mantle xenoliths from Tallante (SE Spain): an insight into activity of silicic melt within the mantle wedge. Transactions of the Royal Society of Edinburgh: Earth Sciences 95, 265–296.
Spakman, W., Van der Lee, S., Van der Hilst, R., 1993. Travel-time tomography of the European–Mediterranean mantle down to 1,400 km. Physics of the Earth and Planetary Interiors 79, 3–74.
Stampfli, G.M., Mosar, J., Favre, Ph., Pillevuit, A., Vannay, J.C., 2001. Permo–Mesozoic evolution of the Western Tethys realm: the Neo-Tethys East Mediterranean Basin connection. In: Ziegler, P.A. (Ed.), Peri-Tethys Memoir, pp. 51–108. 6. Memories de Museé Historie Naturelle Paris.
Suen, C.J., Frey, F.A., 1987. Origins of the mafic and ultramafic rocks in the Ronda peridotite. Earth and Planetary Science Letters 85, 183–202.
Sun, S.-S., McDonough, W.F., 1989. Chemical and isotopic systematics of Oceanic Basalts: implications for mantle composition and processes. In: Saunders, A.D., Norry, M.J. (Eds.), Magmatism in the Ocean Basins, Geological Society of London, 42. Special Publication, pp. 313–345.
Taylor, S.R., McLennan, S.M., 1985. The Continental Crust: Its Composition and Evolution. Blackwell Scientific Publications, Oxford, pp. 1–312.

Taylor, S.R., McLennan, S.M., 1988. The significance of the Rare Earths in geochemistry and cosmochemistry. In: Gschneidner, K.A., Eyring, L. (Eds.), Handbook on the Physics and Chemistry of Rare Earths, 1. Elsevier, Science Publishers B.V, pp. 485–578.
Thirlwall, M.F., 1991. Long-term reproducibility of multicollector Sr and Nd ratio analyses. Chemical Geology 94, 85–104.
Thompson, R.N., 1977. Primary basalts and magma genesis. III. Alban Hills, Roman Comagmatic Province, Central Italy. Contributions to Mineralogy and Petrology 50, 91–108.
Tilton, G.R., Schreyer, W., Schertl, H.-P., 1989a. Pb, Sr, Nd, isotopic behaviour of deeply subducted crustal rocks from the Dora Maira Massif, Western Alps, Italy—II: what is the age of the ultrahigh-pressure metamorphism? Contributions to Mineralogy and Petrology 108, 22–33.
Tilton, G.R., Schreyer, W., Schertl, H.-P., 1989b. Pb–Sr–Nd isotopic behaviour of deeply subducted crustal rocks from the Dora Maira Massif, Western Alps, Italy. Geochimica et Cosmochimica Acta 53, 1391–1400.
Toscani, L., Venturelli, G., Barbieri, M., Capedri, S., Fernandez-Soler, J.M., Oddone, M., 1990. Geochemistry and petrogenesis of two-pyroxene andesites from Sierra de Gata (SE Spain). Mineralogy and Petrology 51, 199–213.
Toscani, L., Contini, S., Ferrarini, M., 1995. Lamproitic rocks from Cabezo Negro de Zeneta: brown micas as a record of magma mixing. Mineralogy and Petrology 55, 281–292.
Tommasini, S., Heumann, A., Avanzinelli, R., Francalanci, L., 2007. The fate of high-angle dipping slabs in the subduction factory: an integrated trace element and radiogenic isotope (U, Th, Sr, Nd, Pb) study of Stromboli Volcano, Aeolian Arc, Italy. Journal of Petrology 48, 2407–2430. doi:10.1093/petrology/egm066.
Treves, B., 1984. Orogenic belts as accretionary prisms: the example of the Northern Apennines. Ofioliti 9, 577–618.
Turner, S.P., Platt, J.P., George, R.M.M., Kelley, S.P., Pearson, D.G., Nowell, G.M., 1999. Magmatism associated with orogenic collapse of the Betic–Alboran domain, SE Spain. Journal of Petrology 40, 1011–1036.
van Achtenberg, E., Ryan, C.G., Jackson, S.E., Griffin, W., 2001. Data reduction software for LA-ICP-MS. In: Sylvester, P. (Ed.), Laser Ablation-ICPMS in the Earth Science, Mineralogical Association of Canada, 29, pp. 239–243.
van Bergen, M.J., Vroon, P.Z., Varekamp, J.C., Poorter, R.P.E., 1992. The origin of the potassic rock suite from Batu Tara Volcano (East Sunda Arc, Indonesia). Lithos 28, 261–282.
Velde, D., 1967. Sur un lamprophyre hyperalkaline potassique: la minette de Sisco (Ile de Corse). Bulletin Societè Francaise Mineralogique et Cristallographique 90, 214–223.
Venturelli, G., Capedri, S., Di Battistini, G., Crawford, A.J., Kogarko, L.N., Celestini, S., 1984b. The ultrapotassic rocks from southeastern Spain. Lithos 17, 37–54.
Venturelli, G., Thorpe, R.S., Dal Piaz, G.V., Del Moro, A., Potts, P.J., 1984a. Petrogenesis of calc-alkaline, shoshonitic and associated ultrapotassic Oligocene volcanic rocks from Northwestern Alps, Italy. Contributions to Mineralogy and Petrology 86, 209–220.
Venturelli, G., Capedri, S., Barbieri, M., Toscani, L., Salvioli Mariani, E., Zerbi, M., 1991a. The Jumilla lamproite revisited: a petrological oddity. European Journal of Mineralogy 3, 123–145.
Venturelli, G., Toscani, L., Salvioli-Mariani, E., 1991b. Mixing between lamproitic and dacitic components in Miocene Volcanic rocks of S.E. Spain. Mineralogical Magazine 55, 282–285.
Wagner, C., Velde, D., 1986. The mineralogy of K-richterite bearing lamproite. American Mineralogist 71, 17–37.
Watts, A.B., Platt, J.P., Buhl, P., 1993. Tectonic evolution of the Alboran Sea Basin. Basin Researches 5, 153–177.
White, W.M., Dupré, B., 1986. Sediments subduction and magma genesis in the Lesser Antilles: isotopic and trace element constraints. Journal of Geophysical Research 91, 5927–5941.
White, W.M., Dupré, B., Vidal, P., 1985. Isotope and trace element geochemistry of sediments from the Barbados ridge–Demerara plain region, Atlantic Ocean. Geochimica et Cosmochimica Acta 53, 1875–1886.
Woolley, A.R., Church, A.A., 2005. Extrusive carbonatites: a brief review. Lithos 85, 1–14.
Wortel, M.J.R., Spakman, W., 2000. Subduction and slab detachment in the Mediterranean–Carpathian region. Science 290, 1910–1917. doi:10.1126/science.290.5498.1910.
Zanetti, A., Mazzucchelli, M., Vannucci, R., Rivalenti, G., 1999. The Finero phlogopite–peridotite massif: an example of subduction-related metasomatism. Contributions to Mineralogy and Petrology 134, 107 122.